University of Alberta

Study of Non-Covalent Multisubunit Protein-Carbohydrate Interactions by Electrospray Ionization Mass Spectrometry

by

Yixuan Zhang

A thesis submitted to the Faculty of Graduate Studies and Research
in partial fulfillment of the requirements for the degree of

Master of Science

Department of Chemistry

Fall 2013
Edmonton, Alberta

Abstract

This thesis describes the development and application of electrospray ionization mass spectrometry (ESI-MS) based techniques to investigate protein-carbohydrate interactions *in vitro*. A catch-and-release electrospray ionization mass spectrometry (CaR-ESI-MS) assay was developed for the identification of specific interactions between water-soluble multisubunit proteins and glycosphingolipids (GSL). The assay is of high sensitivity and specificity, and demonstrates the potential for discovering biologically relevant protein-GSL interactions.

Collision-induced dissociation (CID) experiments and molecular dynamic simulations were performed to investigate the dissociation pathways of multisubunit protein-ligand complexes in the gas phase. The observation of multiple dissociation pathways suggests that collisional activation of multisubunit protein-ligand complexes in the gas phase is likely to induce significant changes to the nature of the protein-ligand interactions.

Table of Contents

List of Tables

List of Figures

1:12 and (d) 1:400, which correspond to an average of 0.5 and 16.7 molecules of GM1-Cer per ND, respectively. (e) CID mass spectrum acquired for the $(CTB_5 + 5L)^{14-}$ ion, where L ≡ GM1-Cer. (f) IMS arrival time distributions measured for the released L_a^- (solid line) and L_b^- ions (dashed line). (g) CID mass spectrum measured for the L_a^- and L_b^- ions after the IMS cell. Only fragment ions originating from reactant ions with IMS arrival times between 20 to 24 ms are shown. 48-49

Figure 2.4 (a) ESI mass spectrum acquired in negative ion mode for a methanol solution of (40 μM) GM1-Cer. (b) IMS arrival time distributions measured for L_a^- (solid line) and L_b^- ions (dashed line). (c) CID mass spectrum acquired for the L_a^- and L_b^- ions following ion mobility separation. (d) Fragmentation scheme for L_a. 50

Figure 2.5 (a) ESI mass spectrum acquired in negative ion mode for an aqueous ammonium acetate (200 mM) solution of (10 μM) Stx2 (≡ AB_5). (b) CID mass spectrum acquired using an isolation window centered at m/z 5242, which corresponds to $(Stx2 + Gb3\text{-}Cer)^{14-}$. Ions were produced by ESI from an aqueous ammonium acetate (200 mM) solution of (10 μM) Stx2 and (30 μM) Gb3-Cer(+) ND (with a Gb3-Cer:DMPC ratio of 1:100). (c) IMS arrival time distributions measured for the L_e^- (solid line) and L_f^- (dotted line) ions following their release from the $(Stx2 + Gb3\text{-}Cer)^{14-}$ ion. (d) CID mass spectrum acquired using an isolation window centered at

Figure 3.24 (a) Initial structure of the $(CTB_5 + 5GM1)^{15+}$ ion used for MD simulations. (b) Plots of Rg for 12 different charge configurations of $(CTB_5 + 5GM1)^{15+}$ ion calculated from the trajectories at 800 K. (c)-(m) Representative structures taken at ~1.5 ns for charge configurations: (c) B15_12, (d) B15_3, (e) B15_7, (f) B15_1, (g) B15_6 and (h) B15_4, (i) B15_11, (j) B15_2, (k) B15_10, (l) B15_9 and (m) B9_1. 109-112

List of Abbreviations

Ab	Abundance
ACS	Average charge state
ATD	Arrival time distribution
B	Biotin
Btl	1,2-dipalmitoyl-*sn*-glycero-3-phosphoethanolamine-N-(biotinyl)
BIRD	Blackbody infrared radiative dissociation
CaR	Catch and release
CID	Collision induced dissociation
CRM	Charge residue model
CTB_5	Cholera toxin B subunit homopentamer
Da	Dalton
DC	Direct current
DMPC	1,2-dimyristoyl-*sn*-glycero-3-phosphocholine
DMS	Differential-mobility spectrometry
DTIMS	Drift-time ion mobility spectrometry
E_a	Activation energy
ECD	Electron capture dissociation
ESI	Electrospray ionization
ESI-MS	Electrospray ionization mass spectrometry
FAIMS	Field-asymmetric waveform ion mobility spectrometry
FT-ICR	Fourier transform ion cyclotron resonance

GM1	(β-D-Gal*p*-(1→3)-β-D-Gal*p*NAc-(1→4)[α-D-Neu5Ac-(2→3)]-β-D-Gal*p*-(1→4)-β-D-Glc*p*
GM1-Cer	(β-D-Gal*p*-(1→3)-β-D-Gal*p*NAc-(1→4)[α-D-Neu5Ac-(2→3)]-β-D-Gal*p*-(1→4)-β-D-Glc*p*-Cer
GSL	Glycosphingolipid
IEM	Ion evaporation model
IMS	Ion mobility separation
IRMPD	Infrared multiphoton dissociation
ITC	Isothermal titration microcalorimetry
K_a	Binding constant
L	Ligand
MALDI	Matrix-assisted laser desorption ionization
MD	Molecular dynamics
MS	Mass spectrometry
MSP	Membrane scaffold protein
MS/MS	Tandem mass spectrometry
MW	Molecular weight
m/z	Mass-to-charge ratio
ND	nanodisc
nanoESI	Nanoflow electrospray ionization
NMR	Nuclear magnetic resonance
RF	Radio frequency
S_4	Homotetrameric streptavidin

SPR	Surface plasmon resonance
SRIG	Stacked ring ion guide
Stx2	Shiga toxin 2
T-Wave	Travelling wave
TIMS	Trapped ion mobility spectrometry
TOF	Time of flight
TWIMS	Traveling-wave ion mobility spectrometry
ΔH	Solvation enthalpy

Chapter 1

Study of Non-Covalent Multisubunit Protein-Carbohydrate Interactions by Electrospray Ionization Mass Spectrometry

1.1 Introduction

It is well established that the interactions of pathogen-generated proteins, such as toxins or surface lectins (adhesins), with carbohydrates present as glycoproteins or glycolipids on the cell surface are involved in a number of important molecular recognition events, and play critical roles in a wide range of physiological and pathological cell functions, such as inflammation, cell−cell interactions, signal transduction, fertility, development, and cancer metastasis.[1] Hence, the detection and characterization of protein-glycolipid or protein-carbohydrate interactions are of fundamental importance and may facilitate the design of receptor analogues as competitive inhibitors.[2]

Glycolipids are molecules in which an oligosaccharide is linked to a lipid moiety. They reside with their hydrophobic lipid moieties in the external leaflet of the plasma membrane and their hydrophilic oligosaccharides protruding into the aqueous environment. Typically, proteins recognize oligosaccharide moieties through hydrogen bond (H-bond) networks, ionic intereactions and stacking between the side chains of aromatic amino acids and the hydrophobic faces of sugar rings.[3] The interactions for protein-carbohydrate complexes often exhibit low association constants (K_a), in the ~10^3 M^{-1} range.[4] This is compensated by the fact that many carbohydrate-binding proteins possess multiple carbohydrate

binding sites to allow multivalent binding in which a simultaneous association of more than one ligand is involved to give a strong and specific binding required for biological processes.[5]

There are a variety of experimental techniques available to identify and characterize the protein-carbohydrate complexes, each with its own strengths and weaknesses. X-ray crystallography is widely used to establish the higher-order structure of biological complexes and to identify interactions between binding partners.[6, 7] However, not all biomolecules and their complexes are readily crystallized. X-ray does not provide a direct measurement of the strength of the non-covalent interactions. Nuclear magnetic resonance spectroscopy can provide both the structure of the complex and the strength of the interaction.[8-11] However, it usually requires large amounts of sample (~mg), and is generally limited to relatively small proteins or complexes.[8] Surface plasma resonance (SPR) spectroscopy represents one of the most widely used assays for quantifying the interactions of protein-ligand complexes.[12, 13] It is of very high sensitivity, requires a very small amount of sample (~ng), and can measure the K_a as well as the association and dissociation rate constants. A limitation of SPR assay is the immobilization of one of the binding partners, which may affect the nature of binding interaction. Additionally, non-specific adsorption to the surface can lead to false signals. Isothermal titration calorimetry (ITC) is generally considered as the "gold standard" technique for quantifying the binding thermochemistry in solution, and is the only assay that directly provides a measurement of the heat associated with the formation of a complex, i.e., change in enthalpy (ΔH).[14-16]

However, the enthalpy change upon other potential accompanying events such as solvent rearrangement and conformational changes in binding partners may be included in the evaluation of ΔH. A number of other experimental (e.g. atomic force microscopy, small angle scattering, circular dichroism) and computational methods can provide complementary information about interactions and structures of protein-carbohydrate complexes.[17-19]

Recently, electrospray ionization mass spectrometry (ESI-MS) has emerged as an important tool for identifying and characterizing the interactions of protein-ligand complexes.[20] The assay is fast (measurements normally can be completed in less than ~1 min), consumes little sample (typically ~pmol per analysis), provides direct insight into binding stoichiometry, and can be used to measure multiple binding equilibria simultaneously. Furthermore, the assay is extremely versatile as there is no requirement for labeling or immobilization of analyte molecules. While the ESI-MS assay is now well established for detecting and characterizing interactions between water soluble proteins and ligands, its application to interactions between water soluble proteins and insoluble ligands, such as glycolipids, has not been previously demonstrated. Moreover, there were no detailed ESI-MS studies on the changes to the nature of the protein-ligand interactions upon collisional activation. In Chapter 2, a catch-and-release (CaR-ESI-MS) assay for identification of the protein-glycosphingolipid (GSL) interactions is reported. It is achieved by first incubating the target protein with GSL/cell extract, which are incorporated into nanodiscs (ND), in aqueous solution to catch any interaction and then transfer to the gas phase by electrospray

ionization (ESI). The intact protein-GSL complex was detached from ND in the ion source using mild collision induced dissociation (CID). Following their release, the protein-GSL complex ions can be isolated in Quadrupole and subjected to another stage of CID, either in Trap or Transfer region, to break the non-covalent protein-GSL interactions. Accurate mass analysis, fragmentation pattern, together with the IMS results allowed for the positive identification of the released GSL receptor.

The ESI-MS assay has also shown its application in providing insights into the compositions and topology of multiprotein and protein-ligand complexes *in vitro*[21-24] and, in some instances, the identity and location of bound ligands.[25, 26] In Chapter 3, the dissociation pathways of multisubunit protein-ligand complexes in the gas phase were studied based on the results of CID experiments performed on gaseous protonated and deprotonated complex ions and molecular dynamics simulations. Three dissociation pathways: (1) loss of the ligand-unbound protein subunit, (2) loss of subunit-ligand complex and (3) loss of ligand (neutral or charged), were observed upon collisional activation, suggesting that collisional activation of multisubunit protein-ligand complexes in the gas phase is likely to induce significant changes to the nature of the protein-ligand interactions. Consequently, caution must be exercised when using MS and CID (or similar activation methods) to establish the location(s) of ligands bound to multiprotein complexes.

1.2 Mass spectrometry

Mass spectrometry (MS) is an analytical technique that determines the masses of atomic or molecular ions in the gas phase based on the measured mass-to-charge ratios (m/z). Generally, all mass spectrometers consist of three regions: ion source, mass analyzer and ion detector. Samples are first ionized in the ion source by one of the many available ionization methods, and the ions are then transferred to the mass analyzer. In the mass analyzer, ions are sorted and separated by electric or magnetic fields according to their m/z. The number of ions with a particular m/z are recorded and amplified by the ion detector. The mass spectrum is a plot of the detector response as a function of m/z. It should be noted that most MS instruments require a vacuum system of less than 10^{-5} torr[27] to avoid (a) collisional defocusing of ions; (b) electrical discharge and (c) high background signal.

A variety of ionization methods and mass analyzers are currently in use. Based on the nature of the sample and type of information required from the analysis, researchers may choose different combinations. With respect to ionization methods, electron impact ionization (EI) and chemical ionization (CI) are usually used for volatile, low mass molecules. While EI can generate a lot of fragment ions for structural information, CI, which produces the protonated molecules, is good for determining the molecular mass of the compound. Electrospray ionization (ESI) and matrix-assisted laser desorption/ionization (MALDI), often referred to as “soft ionization” techniques, are most suitable for analysis of larger biomolecules. In MALDI, ions are produced from sample

crystals upon exposure to a laser beam, and are usually singly charged.[28, 29] ESI, in contrast, produces a range of charged species for each molecule which is transferred directly from solution by a strong electric field.[30] While both ESI and MALDI allow for the generation of intact macromolecular ions, ESI is usually utilized for mass spectrometric studies of noncovalent protein complexes formed in solution.[31]

There are also a number of different types of mass analyzers including (1) magnetic sector, separating ions based on the radius of arc of ions deflected in the magnetic field[32]; (2) quadrupole, defining specific stable ion trajectories[33]; (3) ion trap, similar as quadruple, trapping ions with stable oscillation[34]; (4) time of flight (TOF), determining m/z based on the time that ions take to move through a field-free region between the source and the detector[35]; (5) Fourier transform ion cyclotron resonance (FT-ICR), measuring the m/z of an ion according to its cyclotron frequency[36] and (6) orbitrap, obtaining m/z using Fourier transform of the ion's axial-oscillation frequency[37]. Among them, TOF has the highest m/z range, up to 10^6.[34]

In the present work, nanoflow ESI (nanoESI), which emits smaller droplets than conventional ESI, combined with TOF was used to investigate the interactions and topologies of protein-ligand complexes.

1.2.1 Electrospray ionization

ESI is one of the techniques used in mass spectrometry to introduce biological molecules into the gas phase. It usually generates intact, multiply charged ions, protonated or deprotonated, i.e., $[M + nH]^{n+}$ or $[M - nH]^{n-}$,

respectively, depending on the ionization mode (positive or negative). The mechanism of ESI[30] involves three steps: (a) production of charged droplets at the ESI capillary tip; (b) the shrinkage of charged ESI droplets due to solvent evaporation and droplet disintegration; and (c) the formation of very small, highly charged droplets from which gas-phase ions are produced.

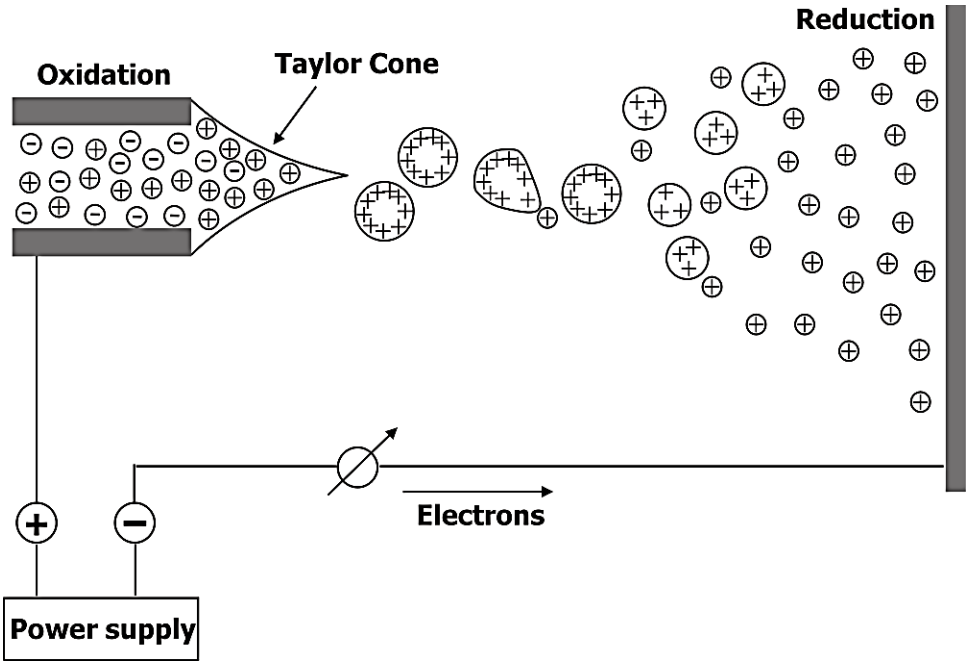

Figure 1.1 Schematic representation of ESI carried out in positive ion mode and the processes that lead to the formation of gas phase ions. Figure is reproduced from reference 30.

Shown in Figure 1.1 is a schematic diagram describing the ESI process in positive ion mode. A voltage of 2-3 kV is applied to the capillary and induces charge separation in solution. The positive ions drift towards liquid surface, leading to the formation of a liquid cone referred to as a Taylor cone – a stable liquid cone exists with competing forces between downfield forces generated by

electric field and resistance by surface tension of the liquid. At a sufficiently high electric field, the liquid cone becomes unstable and emits a thin liquid filament whose surface is enriched in positive ions. Subsequently, it breaks up into small positively charged droplets. Solvent evaporation leads to droplet shrinkage and an increase of electric field normal to the surface of the droplet.[38] As the charge density on the droplet surface increases, the Columbic repulsion of the surface charges overcomes the surface tension of the droplet. This leads the droplet become unstable and undergoing Coulomb fission, forming small, highly charged offspring droplets. The production of gas-phase ions from these droplets follows one of two proposed mechanisms: the ion evaporation model (IEM), and the charge residue model (CRM). IEM, proposed by Iribarne and Thomson, assumes gas-phase ions are emitted directly from very small and highly charged droplets.[39] The escape of the ion to gas phase is initiated by elastic deformation of the droplet, and facilitated by the repulsion between the ion and the charges on the droplet surface. This mechanism does not require the production of extremely small droplets containing only one ion, and is experimentally well-supported for small ions.[40] CRM, proposed by Dole and coworker, postulates that the droplets undergo many fission events and finally produces very small droplets containing a single ion.[41] These droplets undergo solvent evaporation, leading to the production of gas phase ions. It is generally believed that CRM describes the formation of gas phase macromolecule ions based on the observations that (a) the charge acquired by a macromolecule during ESI is dictated by the size of itself, and (b) a number of adducts are present due to the presence of solutes in the final

droplets.

In the present study, gaseous ions were produced by nanoESI whose mechanism is similar to that of ESI. NanoESI was carried out using borosilicate capillaries (1.0 mm o.d., 0.68 mm i.d.) pulled to ~5 μm by a P-97 micropipette puller (Sutter Instruments, Novato, CA). Analyte is filled into the back end of the capillary, and a metal wire is inserted in the back end to apply the spraying potential. A voltage ranging from a few hundred volts to just under 2 kV is typically applied. The advantage of nanoESI is that it operates at very low flow rate of ~20 nL/min and generates small size of droplets, about 100 – 1000 times smaller than conventional ESI.[42] Smaller droplets possess the advantage of higher surface-to-volume ratio, making a larger proportion of analyte molecules available for desorption. In addition, the mild conditions used in nanoESI attenuate effects upon weak bonds in the desolvation process, allowing the detection of noncovalent complexes.

1.2.2 Mass spectrometer

In this work, all experiments were carried out using a Synapt G2-S quadrupole-ion mobility separation-time-of-flight (Q-IMS-TOF) mass spectrometer (Waters, UK), (Figure 1.2), equipped with a nanoESI source. This system combines exact-mass, high resolution mass spectrometry with high-efficiency ion mobility-based separation (IMS).

Gaseous ions are produced by nanoESI. The cone voltage is set to 35-75 V, the source offset voltage is set at 50 V, and the source block temperature is maintained at 60 ℃. Ions first pass through the source sampling orifice and then

enter into the StepWave transfer optic. The focussed ions are then transmitted through a quadrupole mass filter to the ion mobility section of the instrument (Triwave) which contains three traveling wave (T-Wave) ion guides. The Trap T-Wave traps and accumulates ions that will be released in a packet into the IMS T-Wave where the Ion mobility separation is performed. At the front of IMS T-Wave, a high-pressure helium-filled cell is used to minimize scattering and/or fragmentation as ions are introduced into the high N_2 pressure region. The Transfer T-Wave delivers the mobility separated ions to an orthogonal acceleration (oa) - TOF mass analyzer (QuanTof™) equipped with a high field pusher and a dual-stage reflectron.

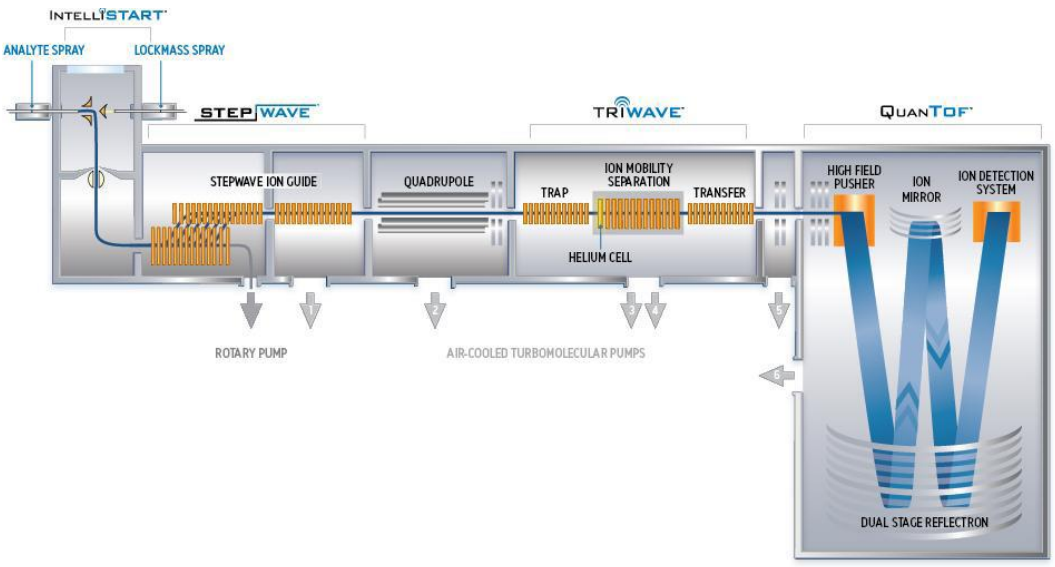

Figure 1.2 A schematic diagram of the Synapt G2-S nanoESI- quadrupole-IMS-TOF mass spectrometer. Figure was adapted with permission from Waters Corporation.

1.2.2.1 StepWave ion guide

The StepWave transfer optics comprise two stages: a conjoined ion guide as the first stage and a narrow bore ion guide as the second one. When sampling ions are generated from an atmospheric pressure ion source, a significant quantity of gas enters the vacuum system. It is essential to remove the accompanying gas from the ions before they enter into the mass analyzer. Moreover, ion beam undergoes expansion when passing through the sampling orifice. The conjoined ion guide (first stage) focuses the ion beam and separates ions from the gas flow by an off-axis configuration (Figure 1.3). Briefly, the ions enter the larger diameter ion guide and are directed into the upper ion guide using a differential voltage. Gas, neutral species, and any non-desolvated material are directed to the rough pump inlet. A reverse travelling wave on the lower guide ensures ions are not swept out with the high gas flow and have time to transfer into the upper guide.[43] The ion beam is then directed to the second stage where it is further focused and propelled into Quadrupole ion guide.

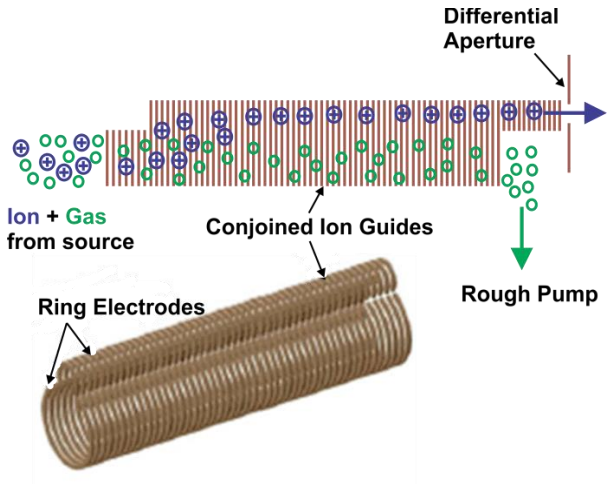

Figure 1.3 Diagram of the conjoined stacked ring ion guides. Figures were reproduced with permission from Waters Corporation.

1.2.2.2 Quadrupole mass filter

Quadrupole mass filters are four cylindrical metal rods that are accurately positioned in a radial array, and the diametrically opposed rods are paired. Each of the rods carries both a direct current (DC) potential and a raiofrequency (RF) potential, with opposing rods being held at identical potentials and polarity, and adjacent rods being identical in potential, but opposite in polarity. Based on this arrangement, a hyperbolic field is created. The filtering action of the quadrupole is obtained by the application of specific voltage and frequency. Ions of a particular m/z ratio can be selected and transmitted down the entire length of the rods while other ions outside the m/z range hit the rods and are expelled. The width of the bandpass region is governed by the ratio of DC-to-RF potentials applied to the rods.[44] By turning off the DC voltages and operating in RF only mode, the quadrupole can also act as a very broad bandpass mass filter that transmits and guides ions over a wide m/z range to other components of the apparatus. In this case, quadrupole is an excellent ion focusing device.

In present study, ions of interest, i.e., precursor ions, were isolated by quadrupole mass filter and transmitted down to the next stage of MS to perform tandem MS.

1.2.2.3 Time of flight mass analyzer

In the TOF mass analyzer, the physical property that is measured during an analysis is the flight time of the ions.[35, 45-47] Mass-to-charge ratios are determined by measuring the time that ions take to move through a field-free region (flight tube) between the source and the detector, according to equation 1.1:

$$(m/z)^{1/2} = t\left(\frac{\sqrt{2eV_s}}{L}\right) \quad (1.1)$$

where m is the mass of the ion, z is the charge state of the ion, e is the elementary charge, V_s is the acceleration potential, t is the flight time and L is the length of the flight tube. This equation shows that m/z can be calculated from a measurement of t^2, provided that all of the ions enter the flight tube at the same time and with the same initial kinetic energy.

There are two types of TOF analyzers, linear TOF analyzer and reflectron TOF analyzer. The linear TOF analyzer suffers from the drawback that ions of the same m/z can reach the detector at different times, due to initial energy distribution, resulting in peak broadening and poor resolution. The reflectron TOF analyzer compensates this energy distribution by using successive sets of electric grids of increasing potential which deflects the ions and reverses their flight direction, sending them back through the flight tube. Depending on their kinetic energy, ions of the same m/z will penetrate the field at different depths; ions with more kinetic energy and hence with more velocity will penetrate the field more deeply than ions with lower kinetic energy. Consequently, the faster ions will spend more time in the reflectron and will reach the detector at the same time as the slower ions with the same m/z. The net effect is improved mass resolution, typically in the range of 10,000-20,000 with minimal losses in sensitivity.

Coupling TOF analyzers with continuous ionization techniques (like ESI) requires the use of the orthogonal acceleration (oa) technique. Ion optics focuses the ions generated from ESI into a parallel beam and directs them to the orthogonal accelerator where the primary ion beam is deflected from its original

direction into a flight tube. Ions gain a new component of velocity which is vectorially independent of their axial velocity. During the time that the ions continue their flight in the flight tube, the orthogonal accelerator is refilled with new ion beam.

In the Synapt G2-S system, a QuanTof technology, which combines a high field pusher and dual-stage refelctron is used to deliver fast, high-resolution, accurate mass and quantitative results simultaneously. Ions are subjected into the dual-stage reflectron twice by high-field pusher and ion mirror, improving the focusing of high energy ions.

1.2.2.4 Ion mobility separation

IMS is a gas-phase electrophoretic technique that separates ions based on their mass, charge and collision cross section (i.e., size and shape).[48-53] Generally, a pulse of ions is injected into a drift region filled with a known inert gas at a known pressure. Under the influence of a static electric field, ions experience electrostatic force pulling them through the region; this force is countered by a number of collisions between ions and the buffer gas. Larger ions with greater collision cross sections experience more collisions than smaller ions and therefore take longer time to traverse the drift tube.[48] Ions can be separated by their characteristic velocity through the gas-filled electric field. The distinct velocity of ions depends on the electric field strength and the ions' mobility (K), which is intrinsic to a particular ion for a specific gas under low electric field conditions[54] and is determined by equation 1.2:

$$K = \frac{d}{t_d E} \tag{1.2}$$

where t_d is the time taken to traverse the drift cell, d is the length of the drift cell and E is the electric field gradient.

In 1960s, McDaniel coupled IMS drift tube to a mass spectrometer, creating the hybrid technique of IMS-MS, to study the separation and reactions of ions and small molecules in the gas phase.[55] In the late 1990s, researchers began to use IMS-MS for simultaneous determination of multiple ions' m/z ratios and mobility.[56] Recently, this technique becomes an important tool for the analysis and conformational determination of biological molecules.[25, 57-59] Moreover, it provides an additional dimension of separation, enabling the separation of structural isomers, i.e., analytes which are isobaric in m/z but different in structure.[60-62]

There are five techniques of IMS that are currently used in mass spectrometry, drift-time ion mobility spectrometry (DTIMS),[63] aspiration ion mobility spectrometry (AIMS),[64] differential-mobility spectrometry (DMS),[65] which is also called field-asymmetric waveform ion mobility spectrometry (FAIMS), trapped ion mobility spectrometry (TIMS) and traveling-wave ion mobility spectrometry (TWIMS).[66] The detail of TWIMS, which is used in this thesis, is outlined briefly below.

The IMS section of the Synapt G2-S system consists of three T-Wave devices (Triwave), Trap T-Wave, IMS T-Wave and Transfer T-Wave, all of which comprise travelling wave-enabled stacked ring ion guides (SRIG) (Fig. 1.4). The SRIG constitutes a series of planar electrodes arranged orthogonally to the ion transmission axis. Opposite phases of a RF voltage are applied to electrodes to

provide a radially confining effective potential barrier. To propel ions, a transient DC voltage is superimposed on the RF applied to a pair of adjacent electrodes in a repeating sequence along the length of the device. A series of potential hills generated are subsequently applied to the next pair of electrodes downstream at regular time intervals, providing a continuous sequence of "travelling waves". The ions within the device are driven away from the potential hills and consequently are carried through the device with the waves, minimizing their transit time. After trapped and accumulated in the Trap region, ions are propelled by the "travelling wave" through the gas in TWIMS where ion species of high mobility slip behind the waves less often than species of low mobility and so are transported through the device more quickly, thus mobility-based separation of ions occurs.[53] The separated ions are then transmitted through the Transfer region and detected by TOF mass analyzer. A particular advantage of the TWIMS device over most drift tubes is that through the use of ion accumulation and radial ion confinement, the sensitivity of the mass spectrometer is not compromised when operating in mobility mode. The use of Trap and Transfer regions furthermore helps to minimize ion loss, allowing investigations on analytically significant levels of sample.[53]

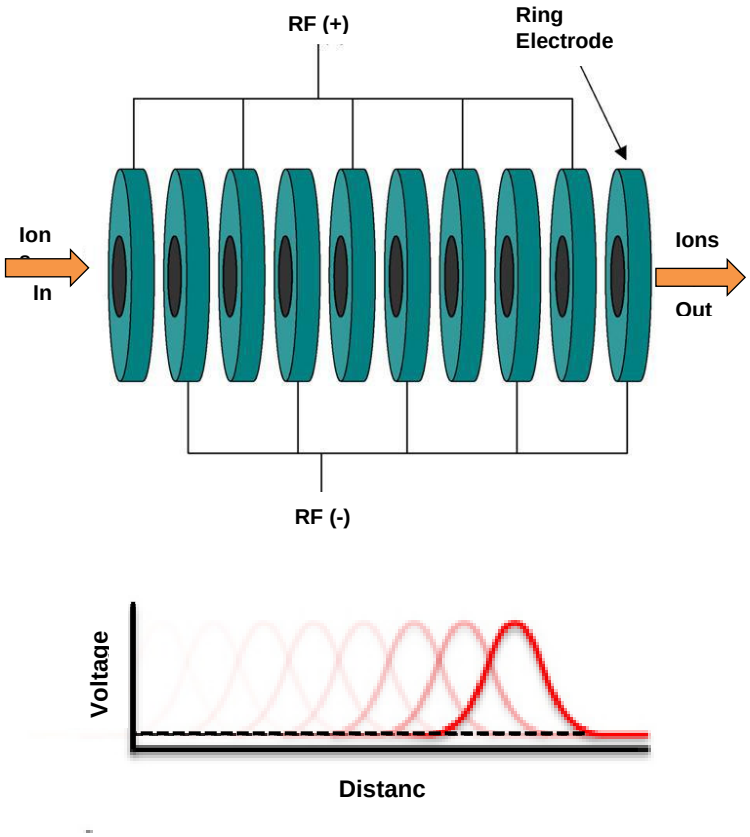

Figure 1.4 Diagram of stacked ring ion guide (SRIG) and its operational principle. Figures were reproduced with permission from Waters Corporation.

In addition, the Trap and Transfer regions can also act as collision cells where CID can be carried out. Under this circumstance, each ring electrode not only has the transient DC voltage used to propel ions to the next stage of the instrument, but also a constant DC offset (collision energy voltage) to increase the kinetic energy of ions. In this study, CID in both Trap and Transfer regions were used for gas-phase dissociation of non-covalent protein complexes which were

first isolated in Quarupole, providing composition and topology information as well as aiding in identification of specific receptors.

1.3 Tandem MS (MS/MS)

Tandem MS, also known as MS/MS, is an MS technique involving multiple sequential stages of mass spectrometry segments where ions are selected, energetically excited and analysed sequentially. Early studies using tandem MS focused on obtaining structural information of a particular ion, the precursor ion, through its fragmentation pattern. Recently, its application in protein complexes study has showed tremendous potential. There are two main categories of instruments that can conduct tandem MS experiments: tandem MS in space and tandem MS in time.[67] In tandem MS in space, the instrument is made up of two or more separate elements, e.g., electric sectors, magnetic sectors, quadrupole, TOF, assembled in tandem. Shown in Figure 1.5a is a representative scheme of mass spectrometer arrangement in tandem MS in space. Analytes are first ionized by one of the ionization methods and then introduced into the first stage of tandem MS, MS^1, where the precursor ion is selected based on its m/z. Fragmentation of the precursor ion occurs in the next stage, MS^2, forming product ions which are consequently subjected to MS^3 for analysis and observed by detector. In tandem MS in time, multiple stages of mass analysis can be achieved by a single mass spectrometer with the MS steps separated in time. Usually, the ion cyclotron resonance (ICR)[68] or the ion trap mass spectrometer is used to store ions, in which the precursor ion can be selected by ejecting all the others. The product ions are produced from fragmentation of the precursor ion during a selected time period

and are analyzed by the same mass spectrometer before detection. As shown in Figure 1.5b, all the processes are implemented sequentially in the same space.

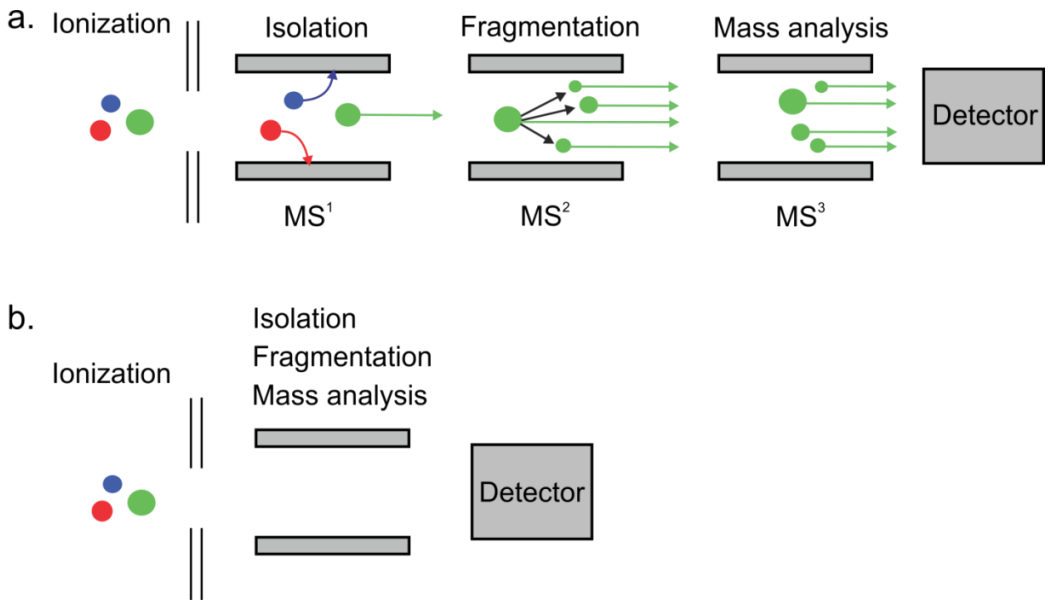

Figure 1.5 Principles of tandem MS in space and in time. (a) A typical arrangement of mass spectrometers in tandem MS in space. Precursor ion is isolated in the first stage, MS^1, and subjected to MS^2 for fragmentation. Ions generated in MS^2 are usually analysed or further selected in MS^3 before going to the detector. (b) A general sequence of events occurs in tandem MS in time. Ions are injected into a mass spectrometer where precursor ion selection, fragmentation and analysis of product ions take place, followed by ion detection.

1.3.1 Activation of gas phase ions by CID

Activation and dissociation of the isolated gaseous ions can be performed by many techniques, including CID or collision-activated dissociation (CAD)[69], surface-induced dissociation (SID)[70], electron transfer and electron capture dissociation (ETD and ECD)[71, 72], infrared radiative multiphoton dissociation (IRMPD)[73] and blackbody infrared radiative dissociation (BIRD)[74]. Among them, CID, which molecular ions are fragmented in the gas phase by colliding with a neutral gas (often helium, nitrogen or argon), is the most commonly used activation method in tandem MS. During the collision, a portion of the ion's kinetic energy is converted into internal energy, resulting in the subsequent fragmentation if sufficient internal energy is accumulated. The increase in internal energy is determined by many factors, including the number of collisions between ions and gas, the amount of time ions spend in the collision cell and the nature of the target ions. Besides its utility in the breakage of covalent bonds for gaining structural information, CID is also the most frequently used method for gas-phase dissociation of non-covalent protein complexes, providing compositional information.[69] In addition, MS combined with CID plays an important role in probing the spatial arrangement of proteins within multiprotein complexes.[75-77]

1.3.2 Application of gas phase dissociation

The transfer of noncovalently bound multiprotein and protein-ligand complexes from solution to gas-phase may lead to change of conformation and interaction due to the removal of solvent. However, numerous reports suggest that some conformational properties of biomolecules in solution are preserved in the

gas phase.[78-81] Thus, gas phase study of desolvated biological complexes represents a promising experimental approach to probe directly the intrinsic (solute-solute) intermolecular interactions and, indirectly, the role of solvent in biological recognition. To elucidate the structure and dynamics of gaseous ions, a variety of ESI-MS based techniques have been developed. Among them, MS/MS is frequently used for the study of protein assembly' composition and topology,[19, 82] identity and location of the bound ligand,[20, 83-85] and characterization of protein-protein or protein-ligand interactions.[26, 86, 87] In the present work, MS combined with CID was used to identify the bound ligand and deliver compositional information of the protein-ligand complex based on the dissociation products and dissociation pathways upon collision.

1.4 Nanodisc technology

Model membrane systems are essential for research on glycolipids and membrane proteins which are naturally embedded in a dynamic lipid bilayer.[88] A variety of systems, including detergent micelles, liposomes and bicelles, have been developed for reconstitution and solubilisation of membrane proteins. Although each of them has its own advantages, they are not perfect for mimicking the biological lipid bilayers. Recently, the Sligar lab established a new model membrane system, the ND system, for rendering membrane proteins or membrane bound ligands soluble in aqueous solution, and, more importantly, in a native-like bilayer environment where they remain active.

1.4.1 Phospholipid bilayer ND

The ND consists of a phospholipid bilayer and two copies of an amphipathic membrane scaffold protein (MSP) (Figure 1.5), which is derived from apolipoprotein A-I (apoA-I).[89] ApoA-I is a major protein component of high-density lipoprotein (HDL). In *vivo*, two molecules of ApoA-I wrap around the edges of the lipid bilayer to form nascent discoidal HDL particles. The ND is assembled in a similar way: phospholipids are first transiently solubilized by a detergent in the presence of MSPs; and a self-assembly process is initiated when the detergent is removed, either by dialysis or adsorption to hydrophobic beads. Due to the amphipathic characteristic of MSPs, they shield the hydrophobic acyl chain from the aqueous solution, making the ND water-soluble.[90] The resulting ND contains approximately 130-260 phospholipids and is 9.5-13 nm in diameter, and about 5.5 nm in thick based on small-angle X-ray scattering.[91] To ensure a production of homogenous size of NDs, the self-assembly should be performed at the phase transition temperature of the chosen lipid so that a homogeneous phospholipid/detergent micellar phase is present before assembly starts. After detergent removal, the NDs are purified by size exclusion chromatography (SEC) to remove any excess lipids or proteins.

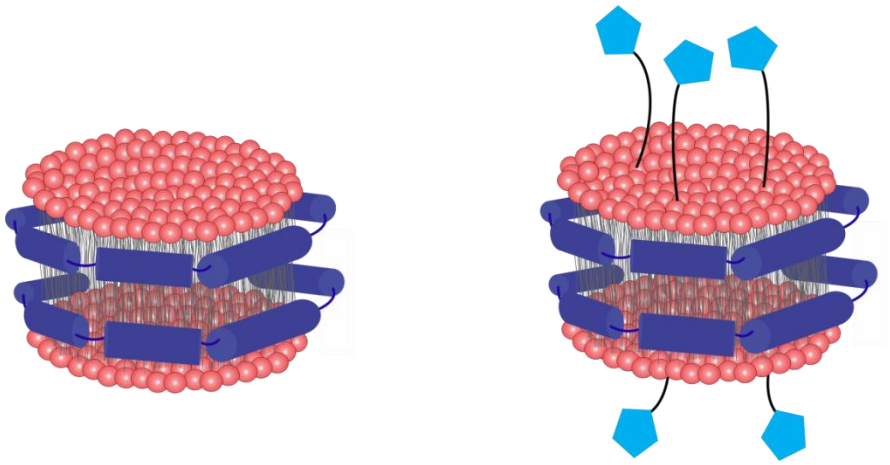

Figure 1.6 Cartoon of nanodisc. Blue belts represent two copies of MSP which surround the lipid bilayer with (right) or without (left) receptors incorporated.

Table 1.1 Optimal ratios of phospholipids to MSPs, diameters and incubation temperature for nanodisc assembly. The diameter of nanodisc is determined by the length of MSP, while the incubation temperature is the phase transition temperature of the chosen lipid.[89, 92]

Optimal Ratios	MSP1D1	MSP1E1	MSP1E1D1	MSP1E2D1	MSP1E3D1	Incubation Temperature
POPC	61	79	79	103	125	4 °C
DPPC	82	106	106	134	167	37 °C
DMPC	77	N/A	102	122	148	23 °C
Diameter of Nanodisc (Å)	98	105	106	119	129	

Data from references 89 and 92.

1.4.2 Membrane proteins or receptors assembled into ND

Membrane proteins or membrane-bound receptors are usually pre-solubilized with a compatible detergent and mixed with phospholipids and MSPs. The proteins or receptors will self-assemble into ND upon the removal of detergent. By using different length of MSPs, ND size can be changed to accommodate a range of membrane proteins, such as cytochrome P450[93-95], phosphoinositides[96], bacteriorhodopsin[97], G-protein coupled receptors[98] and SecYEG[99]. Also, uniform size of protein/receptor incorporated NDs can be produced by optimizing the lipid : MSP : protein/receptor stoichiometry during the self-assembly process.[100] Thus, ND possesses the advantages of self-assembly, solubility, size-control, stability, and the ability to provide a native-like environment for membrane proteins and membrane-bound receptors.

DMPC and MSP1E1 were used for the present study. The optimal ratio, 100:1, was determined based on SEC profile. NDs with varying degrees of GSL or 1,2-dipalmitoyl-*sn*-glycero-3-phosphoethanolamine-N-(biotinyl) (Btc), the receptors in this work, were prepared by mixing the desired ratios of DMPC and GSL or Btc, keeping the total GSL/Btc + DMPC molar amount constant.

1.4.3 Applications of ND

The distinct characteristics of ND offer diverse biochemical applications. To date, it has been applied to receptor studies, enzyme studies, ligand binding, channels and transporters, and structural investigations.[96, 98, 99, 101-103] A variety of analytical techniques, including surface plasmon resonance spectroscopy[104], nuclear magnetic resonance spectroscopy[96], fluorescence polarization

measurements[91], Raman spectroscopy[95], atomic force microscopy[105], and MALDI-TOF MS[106] have been used. In the present study, ND was used to solubilize membrane-bound receptors for revealing their interactions with water-soluble proteins and investigating gas-phase dissociation of multisubunit protein-ligand complexes by ESI-MS.

1.5 Literature cited

1. Lopez, P. H. H.; Schnaar, R. L. *Curr. Opin. Struct. Biol.* **2009,** *19* (5), 549-557.

2. Beachey, E. H. *J. Infect. Dis.* **1981,** *143* (3), 325-345.

3. Evans, S. V.; MacKenzie, C. R. *J. Mol. Recognit.* **1999,** *12* (3), 155-168.

4. Weis, W. I.; Drickamer, K. *Annu. Rev. Biochem.* **1996,** *65*, 441-473.

5. Sacchettini, J. C.; Baum, L. G.; Brewer, C. F. *Biochemistry* **2001,** *40* (10), 3009-3015.

6. Greco, A.; Ho, J. G. S.; Lin, S. J.; Palcic, M. M.; Rupnik, M.; Ng, K. K. S. *Nat. Struct. Mol. Biol.* **2006,** *13* (5), 460-461.

7. Ho, J. G. S.; Greco, A.; Rupnik, M.; Ng, K. K. S. *Proc. Natl. Acad. Sci. U. S. A.* **2005,** *102* (51), 18373-18378.

8. Wishart, D. *Curr. Pharm. Biotechnol.* **2005,** *6* (2), 105-120.

9. Angulo, J.; Rademacher, C.; Biet, T.; Benie, A. J.; Blume, A.; Peters, H.; Palcic, M.; Parra, F.; Peters, T. *Glycomics*. **2006,** *416*, 12-30.

10. Shuker, S. B.; Hajduk, P. J.; Meadows, R. P.; Fesik, S. W. *Science* **1996,** *274* (5292), 1531-1534.

11. Zech, S. G.; Olejniczak, E.; Hajduk, P.; Mack, J.; McDermot, A. E. *J. Am. Chem. Soc.* **2004,** *126* (43), 13948-13953.

12. Campbell, C. T.; Kim, G. *Biomaterials* **2007,** *28* (15), 2380-2392.

13. Pattnaik, P. *Appl. Biochem. Biotechnol.* **2005,** *126* (2), 79-92.

14. Ladbury, J. E. *Biochem. Soc. Trans.* **2010,** *38*, 888-893.

15. Wiseman, T.; Williston, S.; Brandts, J. F.; Lin, L. N. *Anal. Biochem.* **1989,** *179* (1), 131-137.

16. Ladbury, J. E.; Chowdhry, B. Z. *Chem. Biol.* **1996,** *3* (10), 791-801.

17. Lee, C. K.; Wang, Y. M.; Huang, L. S.; Lin, S. M. *Micron* **2007,** *38* (5), 446-461.

18. Ghosh, K. S.; Sen, S.; Sahoo, B. K.; Dasgupta, S. *Biopolymers* **2009,** *91* (9), 737-744.

19. Baird, N. J.; Ferre-D'Amare, A. R. *RNA-Publ. RNA Soc.* **2013,** *19* (2), 167-176.

20. El-Hawiet, A.; Shoemaker, G. K.; Daneshfar, R.; Kitova, E. N.; Klassen, J. S. *Anal. Chem.* **2012,** *84* (1), 50-58.

21. Loo, J. A. *Int. J. Mass Spectrom.* **2000,** *200* (1-3), 175-186.

22. Benesch, J. L.; Robinson, C. V. *Curr. Opin. Struct. Biol.* **2006,** *16* (2), 245-251.

23. Uetrecht, C.; Heck, A. J. R. *Angew. Chem.-Int. Edit.* **2011,** *50* (36), 8248-8262.

24. Felitsyn, N.; Kitova, E. N.; Klassen, J. S. *Anal. Chem.* **2001,** *73* (19), 4647-4661.

25. Hall, Z.; Politis, A.; Robinson, C. V. *Structure* **2012,** *20* (9), 1596-1609.

26. McCammon, M. G.; Hernandez, H.; Sobott, F.; Robinson, C. V. *J. Am. Chem. Soc.* **2004,** *126* (19), 5950-5951.

27. Barber, M.; Bordoli, R. S.; Elliott, G. J.; Tyler, A. N.; Bill, J. C.; Green, B. N. *Biomedical Mass Spectrometry* **1984,** *11* (4), 182-186.

28. Zenobi, R.; Knochenmuss, R. *Mass Spectrom. Rev.* **1998,** *17* (5), 337-366.

29. Karas, M.; Kruger, R. *Chem. Rev.* **2003,** *103* (2), 427-439.

30. Kebarle, P.; Tang, L. *Anal. Chem.* **1993,** *65* (22), A972-A986.

31. Loo, J. A. *Mass Spectrom. Rev.* **1997,** *16* (1), 1-23.

32. Bateman, R. H.; Brown, J.; Lefevere, M.; Flammang, R.; Vanhaverbeke, Y. *Int. J. Mass Spectrom.* **1992,** *115* (2-3), 205-218.

33. De Hoffmann, E. S., V. *Mass Spectrometry Principles and Applications 3th Ed.* **2007,** *New York: John Wiley & Sons.*

34. Wong, P. S. H. C., R.G. *Current Separations* **1997,** *16* (3).

35. Wollnik, H. *Mass Spectrom. Rev.* **1993,** *12*, 89-114.

36. Amster, I. J. *J. Mass Spectrom.* **1996,** *31* (12), 1325-1337.

37. Makarov, A. *Anal. Chem.* **2000,** *72* (6), 1156-1162.

38. Kebarle, P.; Verkerk, U. H. *Mass Spectrom. Rev.* **2009,** *28* (6), 898-917.

39. Iribarne, J. V.; Thomson, B. A. *J. Chem. Phys.* **1976,** *64* (6), 2287-2294.

40. Sakairi, M.; Yergey, A. L.; Siu, K. W. M.; Leblanc, J. C. Y.; Guevremont, R.; Berman, S. S. *Anal. Chem.* **1991,** *63* (14), 1488-1490.

41. Dole, M.; Mack, L. L.; Hines, R. L. *J. Chem. Phys.* **1968,** *49* (5), 2240-&.

42. Wilm, M.; Mann, M. *Anal. Chem.* **1996,** *68* (1), 1-8.

43. Waters Application Note, Literature No.720003964EN.

44. Miller, P. E. D., M.B. *J Chem Education* **1986,** *63*, 617-622.

45. Weickhardt, C. M., F.; Grotemeyer, J. *Mass Spectrom.Rev.* **1996,** *15*, 139-162.

46. Mamyrin, B. A. *Int. J. Mass spectrom.* **2001,** *206*, 251-266.

47. El-Aneed, A. C., A.; Banoub, J. *Appl Spectrosc Rev.* **2009,** *44*, 210-230.

48. Creaser, C. S. G., J. R.; Bramwell, C. J.; Noreen, S.; Hill, C. A.; Paul Thomas, C. L. *Analyst* **2004,** *129*, 984-994.

49. Karasek, F. W. *Anal.Chem.* **1974,** *46*, 710A.

50. McDaniel, E. W. M., E. A. *The Mobility and Diffusion of Ions in Gases, John Wiley & Sons, New York, USA* **1973**.

51. Kanu, A. B. D., P.; Tam, M.; Matz, L.; Hill, H. H. *J. Mass Spectrom.* **2008,** *43*, 1-22.

52. Pringle, S. D. G., K.; Wildgoose, J. L.; Williams, J. P.; Slade, S. E.; Thalassinos, K.; Bateman, R. H.; Bowers, M. T.; Scrivens, J. H. *Int. J. Mass spectrom.* **2007,** *261*, 1-12.

53. Sergio, A. M., A..; Marcelo, B. *Anal. Chim. Acta.* **2011,** *703*, 114-123.

54. Kliman, M. M., J.C.; McLean, J.A. *Biochimica et Biophysica Acta.* **2011**, 935-945.

55. McDaniel, E. W.; Barnes, W. S.; Martin, D. W. *Rev. Sci. Instrum.* **1962,** *33* (1), 2-5.

56. Hoaglund, C. S.; Valentine, S. J.; Sporleder, C. R.; Reilly, J. P.; Clemmer, D. E. *Anal. Chem.* **1998,** *70* (11), 2236-2242.

57. Ruotolo, B. T.; Giles, K.; Campuzano, I.; Sandercock, A. M.; Bateman, R. H.; Robinson, C. V. *Science* **2005,** *310* (5754), 1658-1661.

58. Clemmer, D. E.; Hudgins, R. R.; Jarrold, M. F. *J. Am. Chem. Soc.* **1995,** *117* (40), 10141-10142.

59. Williams, J. P.; Lough, J. A.; Campuzano, I.; Richardson, K.; Sadler, P. J. *Rapid Commun. Mass Spectrom.* **2009,** *23* (22), 3563-3569.

60. Jin, L.; Barran, P. E.; Deakin, J. A.; Lyon, M.; Uhrin, D. *Phys. Chem. Chem. Phys.* **2005,** *7* (19), 3464-3471.

61. Dwivedi, P.; Wu, P.; Klopsch, S. J.; Puzon, G. J.; Xun, L.; Hill, H. H. *Metabolomics* **2008,** *4* (1), 63-80.

62. Seo, Y.; Andaya, A.; Bleiholder, C.; Leary, J. A. *J. Am. Chem. Soc.* **2013,** *135* (11), 4325-32.

63. Cohen, M. J. K., F. W. *J. Chromatogr. Sci.* **1970,** *8*, 330-339.

64. Sacristan, E. S., A. A. *IEEE Trans. Instrum. Meas.* **1998,** *47*, 769-777.

65. Buryakov, I. A. K., E. V.; Nazarov, E. G.; Rasulev, U. K. *Int. J. Mass Spectrom.* **1993,** *128*, 143-152.

66. Giles, K. P., S. D.; Worthington, K. R.; Little, D.; Wildgoose, J. L.; Bateman, R. H. *Rapid Commun. Mass Spectrom.* **2004,** *18*, 2401-2406.

67. Johnson, J. V.; Yost, R. A.; Kelley, P. E.; Bradford, D. C. *Anal. Chem.* **1990,** *62* (20), 2162-2172.

68. Beu, S. C.; Laude, D. A. *Anal. Chem.* **1992,** *64* (2), 177-180.

69. Benesch, J. L. P.; Ruotolo, B. T.; Simmons, D. A.; Robinson, C. V. *Chem. Rev.* **2007,** *107* (8), 3544-3567.

70. Jones, C. M.; Beardsley, R. L.; Galhena, A. S.; Dagan, S.; Cheng, G. L.; Wysocki, V. H. *J. Am. Chem. Soc.* **2006,** *128* (47), 15044-15045.

71. Tang, X. J.; Brewer, C. F.; Saha, S.; Chernushevich, I.; Ens, W.; Standing, K. G. *Rapid Commun. Mass Spectrom.* **1994,** *8* (9), 750-754.

72. Myers, S. A.; Daou, S.; Affar, E. B.; Burlingame, A. *Proteomics* **2013,** *13* (6), 982-91.

73. McLafferty, F. W.; Guan, Z. Q.; Haupts, U.; Wood, T. D.; Kelleher, N. L. *J. Am. Chem. Soc.* **1998,** *120* (19), 4732-4740.

74. Price, W. D.; Schnier, P. D.; Williams, E. R. *Anal. Chem.* **1996,** *68* (5), 859-866.

75. Lorenzen, K.; Vannini, A.; Crarner, P.; Heck, A. J. R. *Structure* **2007,** *15* (10), 1237-1245.

76. Sharon, M.; Taverner, T.; Ambroggio, X. I.; Deshaies, R. J.; Robinson, C. V. *PLoS. Biol.* **2006,** *4* (8), 1314-1323.

77. Damoc, E.; Fraser, C. S.; Zhou, M.; Videler, H.; Mayeur, G. L.; Hershey, J. W. B.; Doudna, J. A.; Robinson, C. V.; Leary, J. A. *Mol. Cell. Proteomics* **2007,** *6* (7), 1135-1146.

78. Cubrilovic, D.; Biela, A.; Sielaff, F.; Steinmetzer, T.; Klebe, G.; Zenobi, R. *J. Am. Soc. Mass Spectrom.* **2012,** *23* (10), 1768-1777.

79. Kitova, E. N.; El-Hawiet, A.; Schnier, P. D.; Klassen, J. S. *J. Am. Soc. Mass Spectrom.* **2012,** *23* (3), 431-441.

80. Erba, E. B.; Barylyuk, K.; Yang, Y.; Zenobi, R. *Anal. Chem.* **2011,** *83* (24), 9251-9259.

81. Liu, L.; Bagal, D.; Kitova, E. N.; Schnier, P. D.; Klassen, J. S. *J. Am. Chem. Soc.* **2009,** *131* (44), 15980-+.

82. Benesch, J. L. P.; Aquilina, J. A.; Ruotolo, B. T.; Sobott, F.; Robinson, C. V. *Chem. Biol.* **2006,** *13* (6), 597-605.

83. Borch, J.; Jorgensen, T. J. D.; Roepstorff, P. *Curr. Opin. Chem. Biol.* **2005,** *9* (5), 509-516.

84. Ilag, L. L.; Ubarretxena-Belandia, I.; Tate, C. G.; Robinson, C. V. *J. Am. Chem. Soc.* **2004,** *126* (44), 14362-14363.

85. Heath, B. L.; Jockusch, R. A. *J. Am. Soc. Mass Spectrom.* **2012,** *23* (11), 1911-1920.

86. Versluis, C.; Heck, A. J. R. *Int. J. Mass Spectrom.* **2001,** *210* (1-3), 637-649.

87. Tesic, M.; Wicki, J.; Poon, D. K. Y.; Withers, S. G.; Douglas, D. J. *J. Am. Soc. Mass Spectrom.* **2007,** *18* (1), 64-73.

88. Chan, Y. H. M.; Boxer, S. G. *Curr. Opin. Chem. Biol.* **2007,** *11* (6), 581-587.

89. Bayburt, T. H.; Sligar, S. G. *FEBS Lett.* **2010,** *584* (9), 1721-1727.

90. Shaw, A. W. M., M.A.; Sligar, S.G. *FEBS Lett.* **2004,** *556*, 260-264.

91. Nath, A.; Atkins, W. M.; Sligar, S. G. *Biochemistry* **2007,** *46* (8), 2059-2069.

92. Denisov, I. G.; Grinkova, Y. V.; Lazarides, A. A.; Sligar, S. G. *J. Am. Chem. Soc.* **2004,** *126* (11), 3477-3487.

93. Das, A.; Grinkova, Y. V.; Sligar, S. G. *J. Am. Chem. Soc.* **2007,** *129* (45), 13778-+.

94. Denisov, I. G.; Shih, A. Y.; Sligar, S. G. *J. Inorg. Biochem.* **2012,** *108*, 150-158.

95. Mak, P. J.; Denisov, I. G.; Grinkova, Y. V.; Sligar, S. G.; Kincaid, J. R. *J. Am. Chem. Soc.* **2011,** *133* (5), 1357-1366.

96. Kobashigawa, Y.; Harada, K.; Yoshida, N.; Ogura, K.; Inagaki, F. *Anal. Biochem.* **2011,** *410* (1), 77-83.

97. Shenkarev, Z. O.; Lyukmanova, E. N.; Butenko, I. O.; Petrovskaya, L. E.; Paramonov, A. S.; Shulepko, M. A.; Nekrasova, O. V.; Kirpichnikov, M. P.; Arseniev, A. S. *Biochimica et biophysica acta* **2013,** *1828* (2), 776-84.

98. Leitz, A. J.; Bayburt, T. H.; Barnakov, A. N.; Springer, B. A.; Sligar, S. G. *Biotechniques* **2006,** *40* (5), 601-602.

99. Alami, M.; Dalal, K.; Lelj-Garolla, B.; Sligar, S. G.; Duong, F. *Embo J.* **2007,** *26* (8), 1995-2004.

100. Boldog, T.; Li, M. S.; Hazelbauer, G. L. *Methods in Enzymology*. **2007,** *423*, 317-335.

101. Borch, J.; Hamann, T. *Biol. Chem.* **2009,** *390* (8), 805-814.

102. Schwall, C. T.; Greenwood, V. L.; Alder, N. N. *Biochim. Biophys. Acta-Bioenerg.* **2012,** *1817* (9), 1588-1596.

103. Choi, W. S.; Rice, W. J.; Negri, A.; Filizola, M.; Stokes, D. L.; Coller, B. S. *Blood* **2012,** *120* (21).

104. Borch, J.; Torta, F.; Sligar, S. G.; Roepstorff, P. *Anal. Chem.* **2008,** *80* (16), 6245-6252.

105. Blanchette, C. D.; Cappuccio, J. A.; Kuhn, E. A.; Segelke, B. W.; Benner, W. H.; Chromy, B. A.; Coleman, M. A.; Bench, G.; Hoeprich, P. D.; Sulchek, T. A. *Biochim. Biophys. Acta-Biomembr.* **2009,** *1788* (3), 724-731.

106. Marty, M. T.; Das, A.; Sligar, S. G. *Anal. Bioanal. Chem.* **2012,** *402* (2), 721-729.

Chapter 2

Protein-Glycosphingolipid Interactions Revealed using Catch-and-Release Mass Spectrometry*

2.1 Introduction

Interactions between pathogen-generated proteins, such as toxins and surface lectins, with glycosphingolipids (GSL) in the membrane of epithelial cells are critical events in the progression of many infectious diseases.[1] The development of receptor analogs as competitive inhibitors of cell adherence and invasion by pathogens represents an attractive therapeutic strategy.[2] For this strategy to be effective the natural receptors must first be identified and their interactions with pathogen-generated proteins characterized. While human receptors have been established for some bacterial and viral proteins, the identification and characterization of the functional GSL receptors is a significant challenge, one that demands new, and more sensitive, experimental methods.[3] Recently, electrospray ionization mass spectrometry (ESI-MS) has emerged as a powerful tool for detecting and quantifying protein-ligand complexes *in vitro*,[4] and is extensively used in the analysis of protein-carbohydrate interactions.[5] The application of ESI-MS to the analysis of membrane proteins and their complexes has also been reported.[6] These measurements are typically carried out on aqueous solutions containing high concentrations of detergents, which are needed to solubilize the membrane proteins. However, the ESI-MS assay is not readily

* A version of this chapter has been published: Zhang, Y.; Liu, L.; Daneshfar, R.; Kitova, E. N.; Li, C.; Jia, F.; Cairo, C. W.; Klassen, J. S. *Anal. Chem.* **2012**, *84*(18), 7618-21.

amenable to analysis of interactions between water-soluble proteins and insoluble ligands, such as GSL. The common practice of using water-soluble receptor analogs for structural and quantitative binding studies is of questionable value since the structural and functional properties of the receptors may change upon removal from the cell membrane.[7] Thus, it is essential to develop an experimental method to characterize the protein-GSL interactions.

Nanodiscs (ND) consist of a discoidal phospholipid bilayer surrounded by two copies of an amphipathic helical scaffold protein (called membrane scaffold protein, MSP) that stabilize and solubilize the lipid bilayer by shielding the hydrophobic region from the aqueous environment. These bilayer packets have been used to solubilize a variety of membrane-bound receptors, including GSL, for structural and binding studies.[8-14] However, to the best of our knowledge, they have not been previously used in conjunction with direct ESI-MS binding measurements. As highlighted below, direct ESI-MS detection of the intact protein-GSL-ND complexes is not straightforward. Therefore, a novel catch-and-release (CaR) ESI-MS assay is established for detecting specific interactions between proteins or protein complexes and their cellular GSL receptors.

2.2 Materials and methods

2.2.1 Reagents

Cholera toxin (CT) B subunit (monomer MW 11 604 Da) was purchased from Sigma Aldrich (Oakville, ON). Shiga toxin 2 (Stx2) (MW 72 260 Da) was a gift from Prof. G. Armstrong (University of Calgary). To prepare stock solutions of CTB_5 and Stx2 for the ESI-MS measurements, samples were concentrated and

dialyzed against 200 mM ammonium acetate (pH 7.0) using microconcentrators (Millipore Corp., Bedford, MA) with a molecular weight cutoff (MWCO) of 10 kDa and stored at -20 ℃ until needed. 1,2-dimyristoyl-s*n*-glycero-3-phosphocholine (DMPC, MW 677.9 Da) dissolved in chloroform was purchased from Avanti Polar Lipids (Alabaster, AL). Globotriaosylceramide (Gal(αl-4)Gal(βl-4)Glc(β1)-ceramide, Gb3-Cer) was purchased from Matreya LLC (Pleasant Gap, PA) and bovine monosialotetrahexosylganglioside (Gal(βl-3)GalNac(βl-4)[Neu5Ac(α2-3)]Gal(βl-4)Glc(β1)-ceramide, GM1-Cer) was purchased from Axxora LLC (San Diego, CA). All detergents and other chemicals were purchased from Thermo Fisher Scientific Inc. (Toronto, Canada) or Sigma-Aldrich Canada (Oakville, Canada).

2.2.2 Glycolipid extraction

The A549 cell line was obtained from ATCC (Manassas, VA) and cultured according the manufacturer's directions (DMEM, supplemented with 10% FBS, grown at 37 ℃ in a humidified incubator with 5% CO_2). Wash steps were performed in a desktop centrifuge at 1200 rpm for 2 min. Control cells were grown in a 75 cm^2 flask to about 80-90% confluency. The culture medium was removed by aspiration, and the cell monolayer was washed twice with phosphate buffered saline (PBS). Fresh PBS (3 mL) was then added to the flask, and the cells were scraped and transferred to a 15 mL centrifuge tube. The suspension was spun at 1200 rpm for 2 min, and the pellet was resuspended in 1 mL of fresh PBS. The suspension was then loaded into 1.5 mL centrifuge tubes, spun at 1200 rpm for 2 min and washed 3 times with PBS. The pellet was then re-suspended in 60

μL water and sonicated in a water bath for 30 s. A solution of 1:1 chloroform-methanol (400 μL) was added and the sample was incubated at room temperature for 10 min. The sample was spun at 10,000 rpm for 10 min, and the supernatant was transferred to a glass sample vial. The solution was reduced by drying with N_2. An additional aliquot of 1:1 chloroform-methanol solution (1.4 mL) was added at -20 ℃ for 4 hr. The cleared solution was then transferred to a 1.5 mL centrifuge tube and spun at 10,000 rpm for 10 min. The remaining sample was dried over N_2 in a glass vial and stored at -20 ℃.

2.2.3 Expression and purification of MSP1E1

Recombinant membrane scaffold protein MSP1E1 (MW 27 494 Da) was prepared using plasmid pMSP1E1 acquired from Addgene (Cambridge, MA). Protein expression and purification was carried out using the procedure described at http://sligarlab.life.uiuc.edu/nanodisc.html. Briefly, protein was expressed using the pET 28a system (Novagen, Madison, WI) with the E.coli BL-21 (DE3) strain as a host. Liquid LB medium containing 30 μg/mL kanamycin was inoculated with the biggest colony from a plate and shaked at 37 ℃ until OD_{600} reached 0.6-0.8. 40 mL of this starter culture was transferred to 1 L scale-up culture, shaking at 200 rpm, 37 ℃, until OD_{600} reached 2.5-3.0 after 2.5-3 hr. 1 mM IPTG was added to induce expression. One hour after induction, the temperature was lowered to 28 ℃. After another 3-3.5 hr, cells were collected by centrifugation at 8 000 g for 20 min and stored at - 80 ℃ for up to several months.

For purification, about 15 grams of cells were resuspended in 100 mL 20 mM sodium phosphate (pH 7.4) and disrupted in the presence 1% Triton X-100,

inhibitor and RNase by sonication. The lysate was cleared by centrifugation at 36,000 rpm for 60 min at 4 ℃. The supernatant was passed through a 2.5x6 cm column containing Chelating Sepharose Fast Flow (Amersham Biosciences, Piscataway, NJ) charged with Ni^{2+} according to manufacturer's instruction. MSP1E1 fractions were collected and checked for purity by both sodium dodecyl sulfate polyacrylamide gel electrophoresis (SDS-PAGE) and mass spectrometry, then dialyzed against ND buffer (20 mM Tris, 0.1 M NaCl, 0.5mM EDTA, pH 7.4), 8 hr x 3 times, stored at -80 ℃. The MSP1E1 concentration was determined by absorbance at 280 nm using calculated extinction coefficient.

2.2.4 Preparation of nanodiscs

Nanodiscs composed of DMPC alone or DMPC and GSL, or lipids extracted from cells were prepared using procedures described previously[15,16] and only brief description is given here. To prepare ND containing only DMPC, the chloroform was removed under a gentle stream of nitrogen and replaced with Tris buffer (20 mM Tris pH 7.4, 0.1 M NaCl, 0.5 mM EDTA) containing 25 mM sodium cholate. To prepare the ND containing GM1-Cer or Gb3-Cer, DMPC (in chloroform) and either GM1-Cer or Gb3-Cer (in a 2:1 chloroform-methanol solution) were mixed at the desired molar ratio; the procedure for solvent removal and addition of buffer was the same as above. To prepare the ND containing the lipids extracted from the A549 cells, the lipids were first dissolved in a 2:1 chloroform-methanol mixture; the procedure for solvent removal and addition of buffer was the same as above. MSP1E1 at a concentration of 0.3 to 0.4 mM was added to the cholate-solubilized lipid and GSL mixture at the desired ratios. After

30 min incubation at 23 ℃, the self-assembly process was initiated by adding equal volume of pre-washed biobeads SM-2 (Bio-Rad) followed by gentle agitation at 23 ℃, 4 hr. Beads were removed by sedimentation and the supernatant was then loaded onto a Superdex 200 HR 10/300 GL column (GE Healthcare). ND fractions were collected, concentrated and dialyzed against 200 mM ammonium acetate (pH 7.0) using an Amicon microconcentrator with a MW cut-off of 30 kDa, then stored at -80 ℃. The concentration of the ND solutions was determined by absorbance at 280 nm using the extinction coefficient of MSP1E1.

2.2.5 Mass spectrometry

All experiments were carried out using a Synapt G2-S quadrupole-ion mobility separation-time-of-flight (Q-IMS-TOF) mass spectrometer (Waters, UK), equipped with a nanoflow ESI source. To perform nanoESI, tips were produced from borosilicate capillaries (1.0 mm o.d., 0.68 mm i.d.) and pulled to ~5 μm using a P-97 micropipette puller (Sutter Instruments, Novato, CA). A platinum wire was inserted into the nanoESI tip, and a capillary voltage of 1.0−1.3 kV was applied to carry out ESI. Given below are representative instrumental conditions. Cone voltage and source offset voltage were both set at 50 V, and the source block temperature was maintained at 60 ℃. The Trap CE and Transfer CE were maintained at 5 V and 2 V, respectively. The bias on Trap DC was 45 V. Argon was used in the Trap and Transfer ion guides at a pressure of 1.42×10^{-2} mbar and 1.74×10^{-2} mbar, respectively. The helium chamber preceding the traveling wave ion mobility (TWIMS) device was operated with a He flow rate of 151 mL

min^{-1}. All traveling-wave ion mobility measurements were carried out using N_2 as the mobility gas at a flow rate of 40 mL min^{-1}. Data acquisition and processing were carried out using MassLynx (v 4.1).

To confirm the identity of the bound GSL, ions of the protein−GSL complex of interest were isolated using the quadrupole mass filter and then subjected to CID. The bound GSL were released from the protein by increasing the collision energy in the Trap ion guide from to 5 V to between 40 and 70 V. The released GSL ions were subjected to MS analysis, allowing for accurate MW determinations. The released GSL ions were also subjected to IMS, and the corresponding arrival time distributions (ATD) were compared to ATDs measured for the GSL in the commercial samples. The uncertainty in the average ATDs for the GSL ions was found to be less than 2% under the experimental conditions used. Following IMS, the GSL ions were fragmented by increasing the collision energy in the Transfer ion guide from 2 V to between 50 and 100 V. The resulting CID mass spectra were compared to CID mass spectra measured for GSL from commercial samples.

2.3 Results and discussion

2.3.1 Overview of catch-and-release (CaR) ESI-MS assay

The assay, which is outlined in Figure 2.1, involves direct ESI-MS analysis of carbohydrate-binding proteins and GSL, which are incorporated into ND, in aqueous solution.[17] Briefly, GSL-ND were incubated with protein of interest to catch any interaction and then transferred to the gas phase by ESI. Identification of the protein-GSL interactions is achieved by first detaching the

intact protein-receptor complex from the ND in the ion source using mild collision-induced dissociation (CID), which breaks the lipid-lipid interactions involving the GSL and phospholipids. Following their release, the protein-GSL complex ions can be isolated and subjected to another stage of CID to break the stabilizing protein-GSL interactions. Accurate mass analysis of the released GSL receptor ions is usually sufficient for positive identification. However, in cases where there is the possibility of isomeric GSL being present, analysis of the arrival time distributions measured using ion mobility separation (IMS), and fragmentation spectra produced by CID, can aid in identifying receptors.[5]

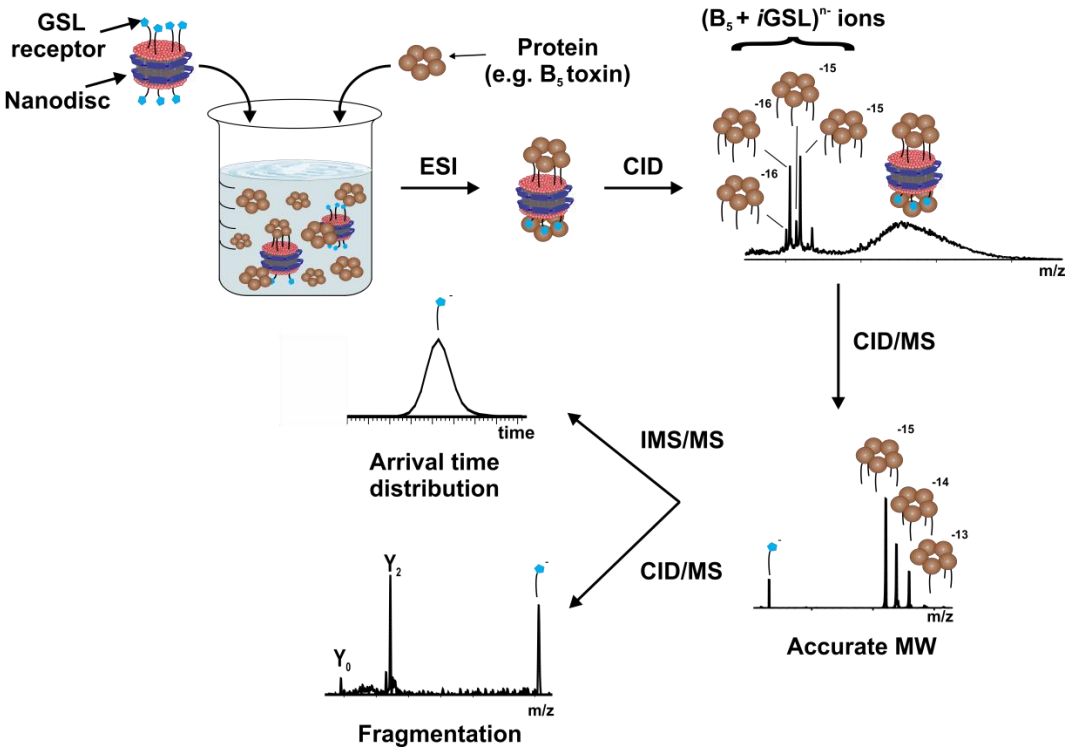

Figure 2.1 Schematic overview of the catch-and-release electrospray ionization mass spectrometry (CaR-ESI-MS) assay for detecting protein-glycosphingolipid interactions in solution. The soluble carbohydrate-binding protein (shown here as a hompentameric protein complex, B_5) is incubated with nanodiscs (ND) containing the glycosphingolipid (GSL) receptors and the resulting ND-bound (B_5 + *i*GSL) complexes are transferred to the gas phase by ESI. Mild collision-induced dissociation (CID) conditions in the ion source of the mass spectrometer allow for the detachment of the intact (B_5 + *i*GSL) complexes from the ND. Isolation of the gas phase ions corresponding to the (B_5 + *i*GSL) complexes is followed by CID to release the bound GSL. GSL released as ions are analyzed by ion mobility separation (IMS), followed by CID and mass analysis.

2.3.2 Revealing protein-GSL interactions using ND of defined composition

Interactions between the cholera toxin (CT) and Shiga toxin type 2 (Stx2) and their native GSL receptors, the ganglioside GM1-Cer and the globotriaosylceramide Gb3-Cer (Figure 2.2), respectively, served as model systems. Both CT and Stx2 belong to the family of AB_5 bacterial toxins and are composed of five B subunits, which are responsible for host recognition, and an A subunit, which is catalytically active and responsible for toxicity. While the Stx2 holotoxin was used in the present study, only the B_5 homopentamer of CT (which is non-toxic) was employed due to safety concerns. Each B subunit of CT and Stx2 possess a single, dominant, carbohydrate binding site.[18,19] The affinities of CTB_5 for Gal(βl-3)GalNAc(βl-4)[Neu5Ac(α2-3)]Gal(βl-4)Glc and Stx2 for Gal(αl-4)Gal(βl-4)Glc are reported to be $2x10^7$ M^{-1} and $<10^3$ M^{-1}, respectively.[20,21]

(a)

L_c^-: d16:1-18:0 (MW 1517.8 Da)

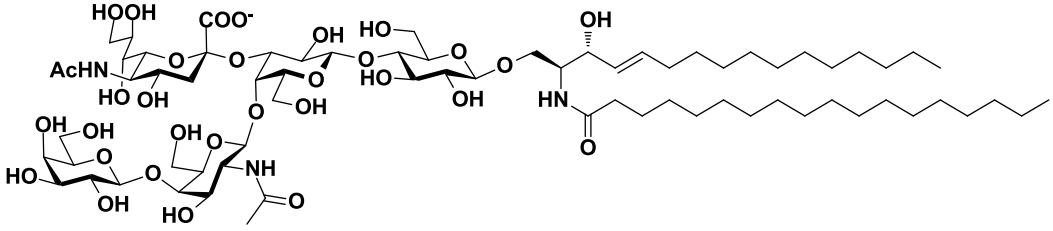

L_c^-: d18:1-16:0 (MW 1517.8 Da)

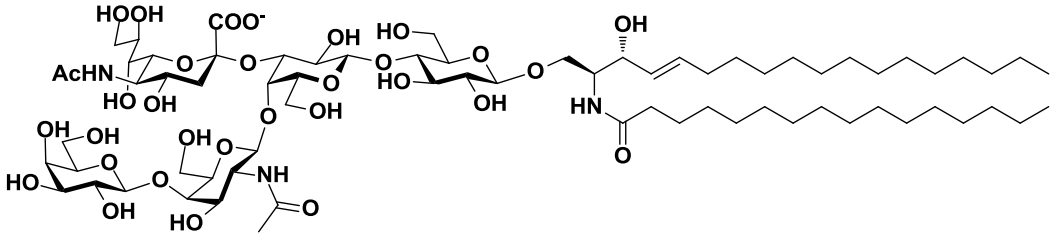

L_a^-: *d*18:1-18:0 (MW 1545.8 Da)

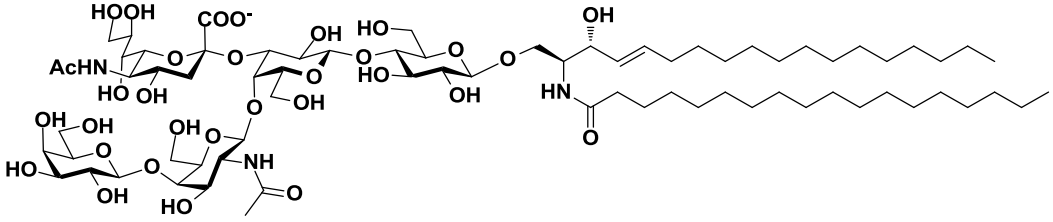

L_b^-: *d*20:1-18:0 (MW 1573.9 Da)

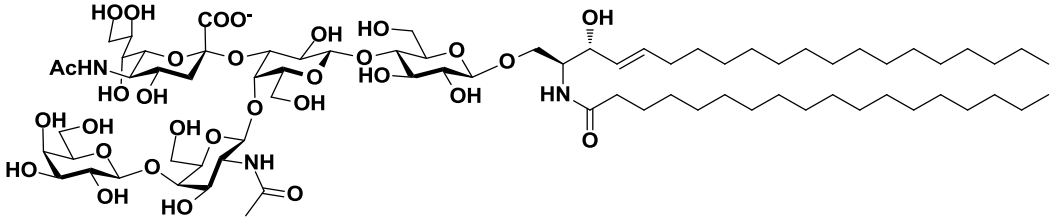

Figure 2.2 Isoforms of the glycosphingolipids GM1-Cer and Gb3-Cer. (a) GM1-Cer, L_c^- (*d*16:1-18:0, *d*18:1-16:0), L_a^- (*d*18:1-18:0) and L_b^- (*d*20:1-18:0).

L_d^-: *d*20:1-22:0 (MW 1629.9 Da)

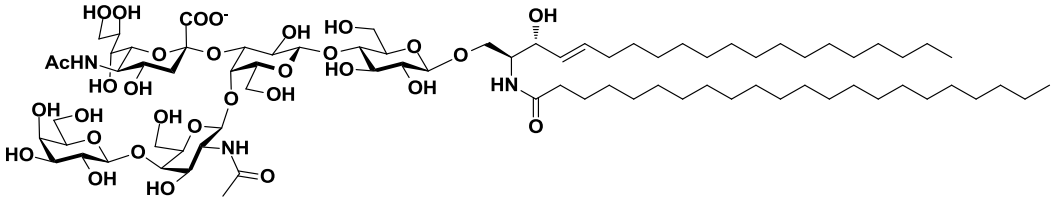

L_d^-: *d*18:1-24:0 (MW 1629.9 Da)

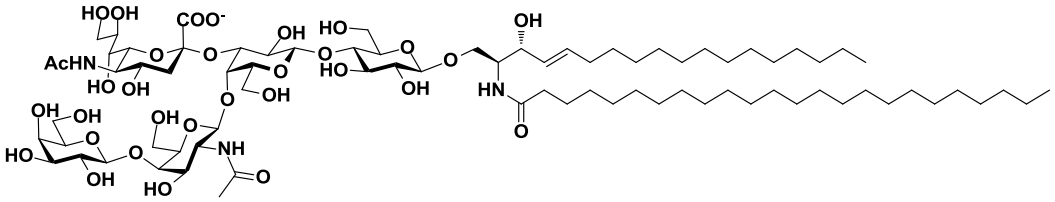

(b)

L_e^-: *d*18:1-22:0 (MW 1107.8 Da)

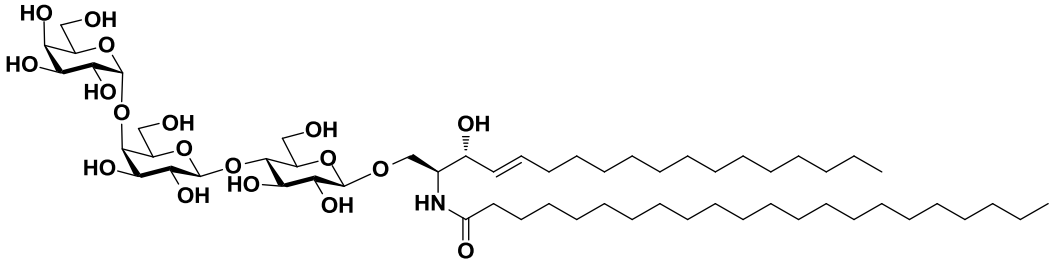

L_f^-: *d*18:1-24:0 (MW 1135.8 Da)

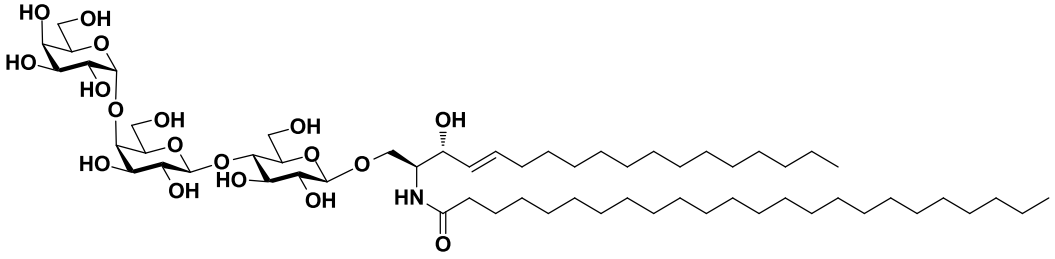

Figure 2.2 Continued. GM1-Cer, L_d^- (*d*20:1-22:0 and *d*18:1-24:0). (b) Gb3-Cer, L_e^-(*d*18:1-22:0) and L_f^- (*d*18:1-24:0); the structure of the L_g^- (C42:2-OH, MW 1150.8 Da) isoform has not been reported.

Shown in Figure 2.3 are ESI mass spectra acquired in negative ion mode for aqueous neutral solutions of CTB_5 alone, in the presence of GM1-Cer(-) ND (containing only DMPC) and GM1-Cer(+) ND (containing GM1-Cer and DMPC). The major CTB_5 ions detected by ESI-MS correspond to the deprotonated homodecamer ions, i.e., $(B_5)_2^{n-}$, was also detected (Figure 2.3a). The latter are likely nonspecific in nature and formed during the ESI process.[22] Upon addition of GM1-Cer(-) ND to the solution, a broad peak centered at mass-to-charge ratio (*m/z*) ~9000 was observed (Figure 2.3b). This spectral feature is attributed to the gaseous ions of intact ND. The ND ions are, presumably, unresolved due to their heterogeneity and the associated charge-state distributions resulting from the ESI process. The introduction of GM1-Cer(+) ND (at a GM1-Cer:DMPC ratio of 1:12) resulted in the complete disappearance of the B_5^{n-} ions and the appearance of putative $(CTB_5 + i\text{GM1-Cer})^{n-}$ ions, where i = 4 or 5 (Figure 2.3c). Reduction of the GM1-Cer:DMPC ratio resulted in a decrease in the number of bound GM1-Cer molecules; a maximum of one bound GM1-Cer was observed at a GM1-Cer:DMPC ratio of 1:400 (Figure 2.3d). To confirm the presence of bound GM1-Cer, the $(CTB_5 + 5\text{GM1-Cer})^{14-}$ ion was isolated and CID was performed to release the deprotonated GM1-Cer receptor. In addition to the loss of deprotonated subunit, i.e., B^{n-}, CID of the $(CTB_5 + 5\text{GM1-Cer})^{14-}$ ion resulted in the sequential loss of deprotonated ligands, L_a^- and L_b^-, which appeared at *m/z* 1545 and 1573, respectively (Figure 2.3e). According to the measured *m/z* values, L_a^- and L_b^- correspond to the deprotonated ions of the two major forms of GM1-Cer (*d*18:1-18:0 and *d*20:1-18:0, respectively) that were detected in the GM1-Cer

sample that was added to the ND (Figure 2.4).[23] The identity of L_a^- and L_b^- could be further confirmed by their IMS arrival times, 21.37 and 21.92 ms, respectively (Figure 2.3f), which agree with those measured (under identical conditions) for the ions produced directly from the GM1-Cer sample (Figure 2.4). CID of the L_a^- and L_b^- ions following IMS produced a number of diagnostic fragment ions, notably the $(B_0 - H_2)^-$, Y_0^- and Y_2- NeuAc$^-$ ions, which are formed by cleavage of the pentasaccharide (Figure 2.3g).[24] These same ions are observed in the CID spectra measured for the L_a^- and L_b^- ions (using the same collision energies) obtained directly from the GM1-Cer sample (Figure 2.4).

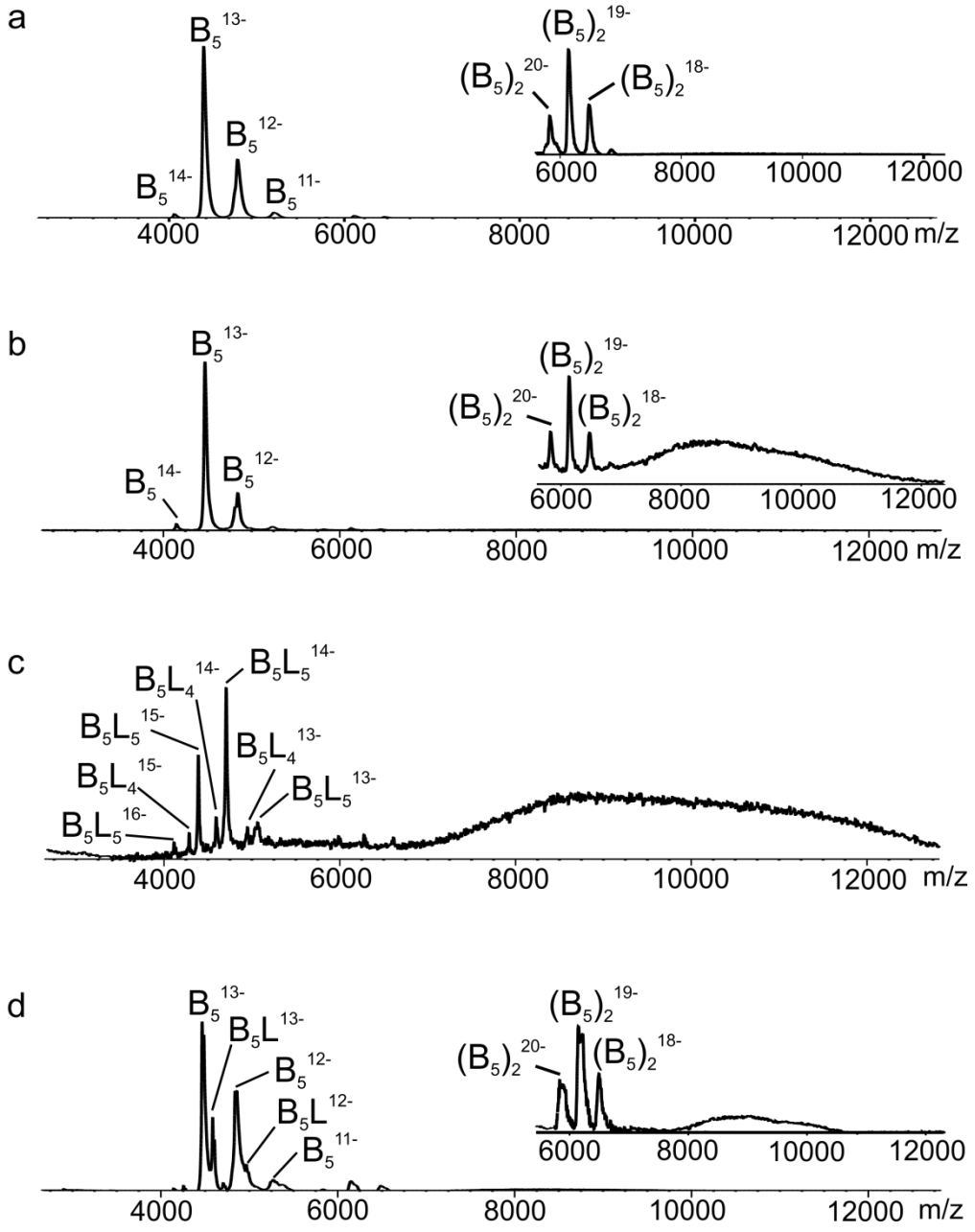

Figure 2.3 ESI mass spectra acquired in negative ion mode for aqueous ammonium acetate (200 mM) solutions of (6 μM) CTB subunit (a) alone or in presence of (10 μM) ND containing (b) only DMPC (GM1-Cer(-)) or GM1-Cer(+) ND in GM1-Cer:DMPC ratios of (c) 1:12 and (d) 1:400, which correspond to an average of 0.5 and 16.7 molecules of GM1-Cer per ND, respectively.

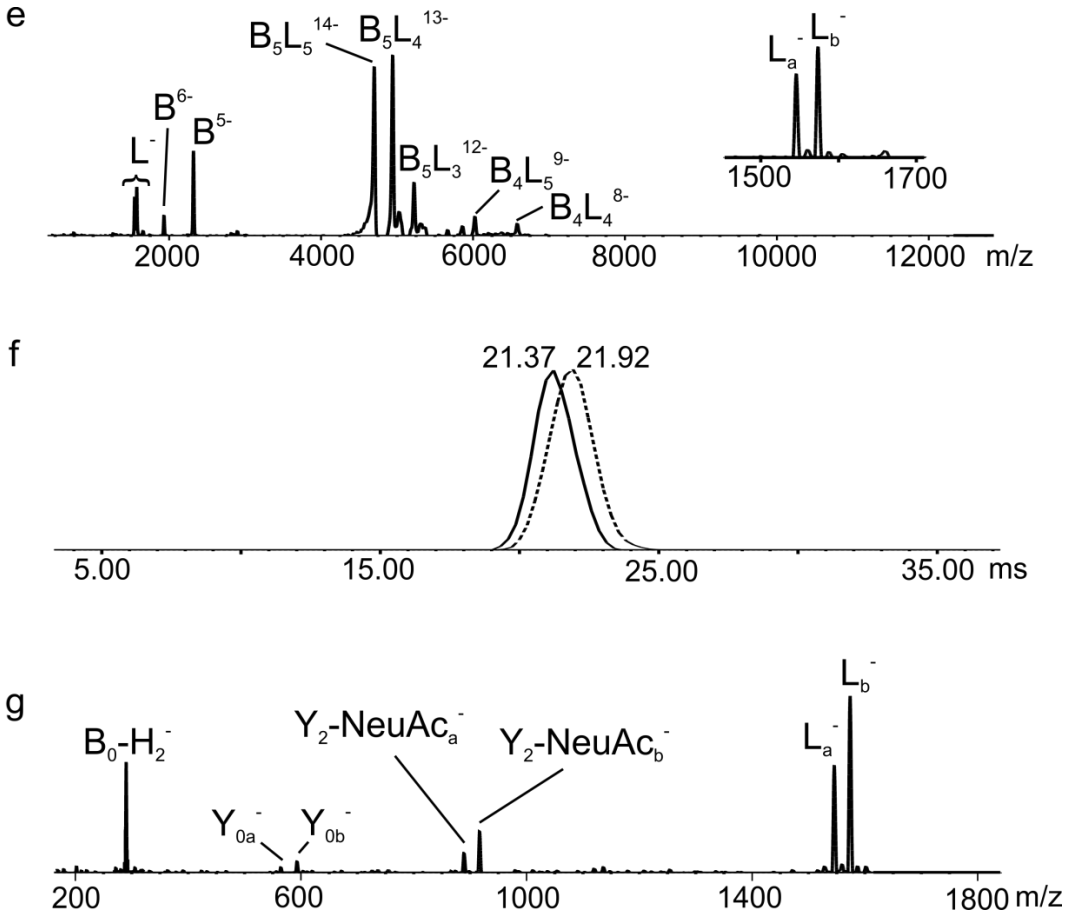

Figure 2.3 continued (e) CID mass spectrum acquired for the $(CTB_5 + 5L)^{14-}$ ion, where L ≡ GM1-Cer. (f) IMS arrival time distributions measured for the released L_a^- (solid line) and L_b^- ions (dashed line). (g) CID mass spectrum measured for the L_a^- and L_b^- ions after the IMS cell. Only fragment ions originating from reactant ions with IMS arrival times between 20 to 24 ms are shown.

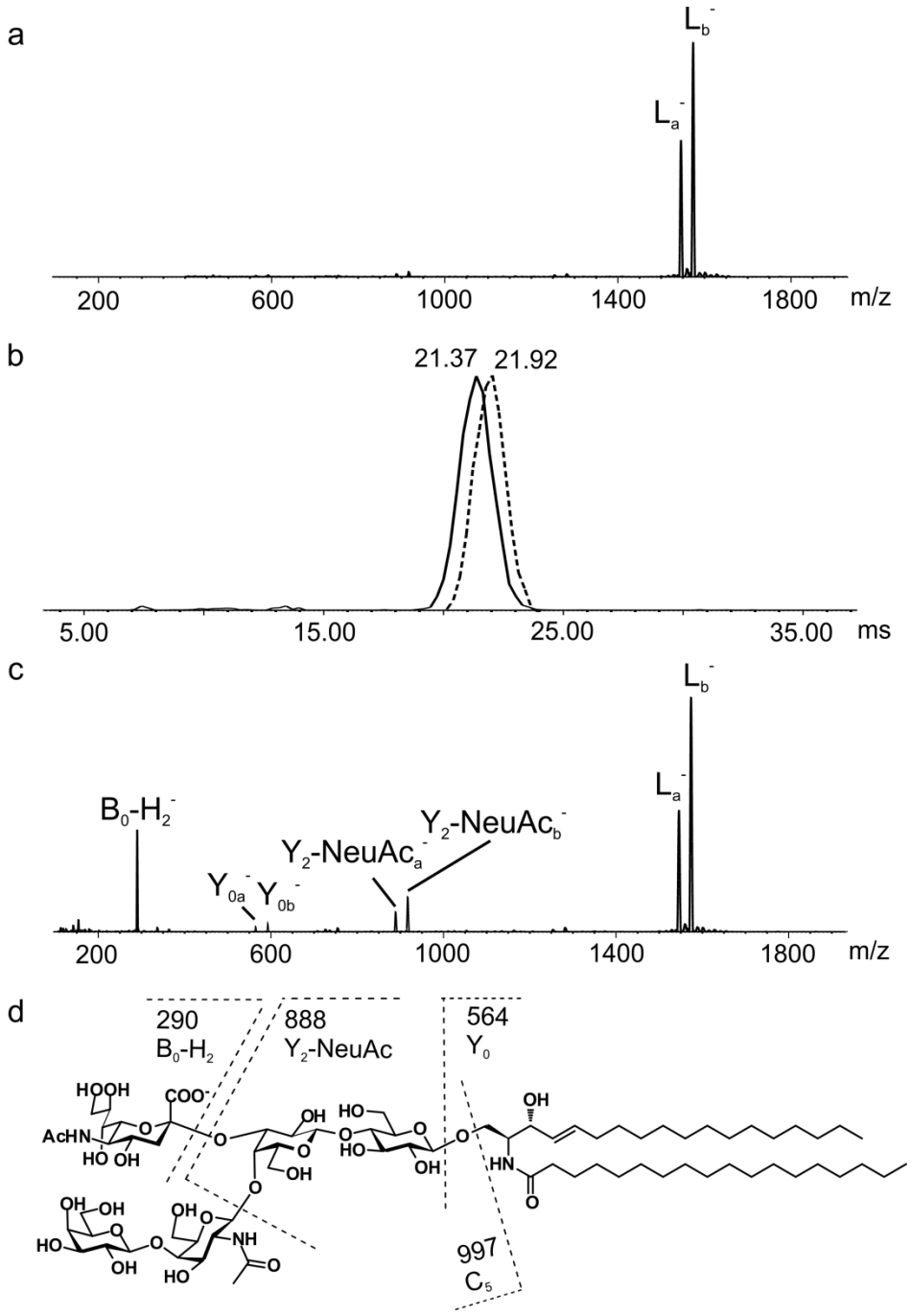

Figure 2.4 (a) ESI mass spectrum acquired in negative ion mode for a methanol solution of (40 μM) GM1-Cer. (b) IMS arrival time distributions measured for L_a^- (solid line) and L_b^- ions (dashed line). (c) CID mass spectrum acquired for the L_a^- and L_b^- ions following ion mobility separation. (d) Fragmentation scheme for L_a (*d*18:1-18:0).

The interactions in CT B subunit-GM1-Cer complex are quite strong compared to most protein-carbohydrate interactions, which often exhibit affinities in the 10^3 M^{-1} range.[25] However, as illustrated by the results obtained for the Stx2-Gb3-Cer complex, the utility of the CaR-ESI-MS assay is not limited to only high affinity interactions. Shown in Figures 2.5a and 2.5b are ESI mass spectra acquired in negative ion mode for aqueous neutral solutions of Stx2 alone and in the presence of Gb3-Cer(+) ND, respectively. Although the exact Gb3-Cer:DMPC ratio could not be accurately determined due to the presence of impurities in the commercial sample, it was estimated to be 1% based on the relative signal of Gb3-Cer ions in ESI mass spectrum acquired for the sample alone (c.a. 3%, Figure 2.6a). In contrast to the CTB_5/GM1-Cer system, ESI-MS analysis (with mild collisional activation in the ion source) failed to detect evidence of ions corresponding to distinct (Stx2 + *i*Gb3-Cer) complexes. However, following isolation of a narrow *m/z* window centered at 5242 (which corresponds to the *m/z* of the expected $(Stx2 + Gb3\text{-}Cer)^{14-}$ ion composed of the *d*18:1-24:0 form of Gb3-Cer), CID resulted in the appearance of free B subunits ions and ions corresponding to Gb3-Cer (Figure 2.5b). The dominant form of Gb3-Cer detected was *d*18:1-22:0 (*m/z* 1107); the *d*18:1-24:0 form (*m/z* 1135) was also detected but at lower abundance.[26] The measured arrival times (Figure 2.5c) were consistent with those measured for the ions of Gb3-Cer produced directly from the Gb3-Cer sample (Figure 2.6b). Notably, in the absence of Stx2 in solution, isolation of the same *m/z* window, followed by CID did not result in the appearance of any Gb3-Cer ions (Figure 2.5d). To test for false positives, which could result from

nonspecific GSL-protein binding, measurements were also performed on solutions of CTB_5 with Gb3-Cer(+) ND (at a Gb3-Cer:DMPC ratio of 1:100) and Stx2 with GM1-Cer(+) ND (at a GM1-Cer:DMPC ratio of 1:12). Importantly, these control experiments failed to produce any evidence of interactions between CTB_5 or Stx2 with the non-native GSL (Figure 2.7).

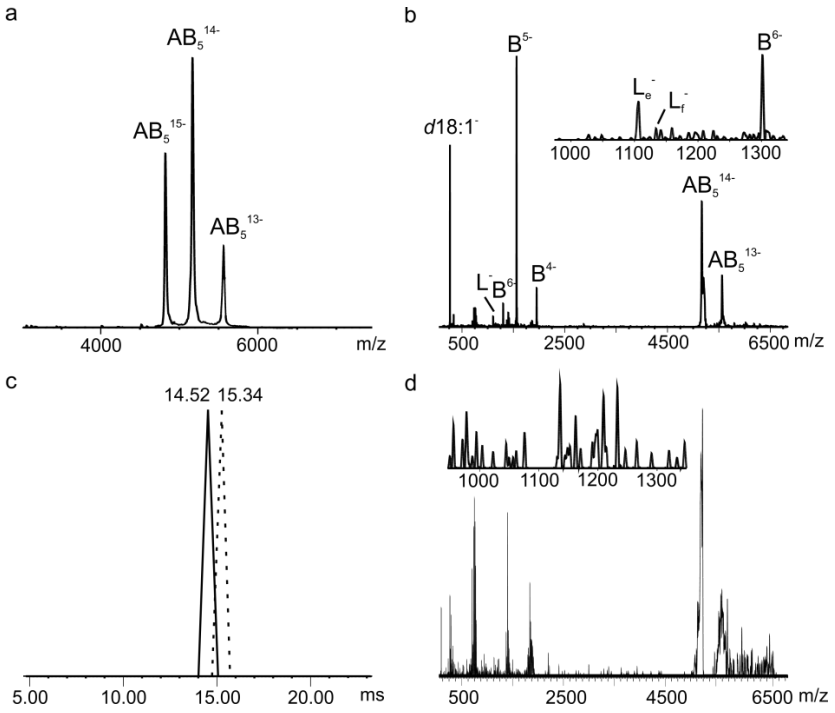

Figure 2.5 (a) ESI mass spectrum acquired in negative ion mode for an aqueous ammonium acetate (200 mM) solution of (10 μM) Stx2 (≡ AB_5). (b) CID mass spectrum acquired using an isolation window centered at m/z 5242, which corresponds to $(Stx2 + Gb3\text{-}Cer)^{14-}$. Ions were produced by ESI from an aqueous ammonium acetate (200 mM) solution of (10 μM) Stx2 and (30 μM) Gb3-Cer(+) ND (with a Gb3-Cer:DMPC ratio of 1:100). (c) IMS arrival time distributions measured for the L_e^- (solid line) and L_f^- (dotted line) ions following their release from the $(Stx2 + Gb3\text{-}Cer)^{14-}$ ion. (d) CID mass spectrum acquired using an isolation window centered at m/z 5242. Ions were produced by ESI from an aqueous ammonium acetate (200 mM) solution of (30 μM) Gb3-Cer(-) ND (DMPC only). The maximum signal intensity of the portion of the mass spectrum shown in the inset is 1/50 that of the inset shown in Figure 2.5b.

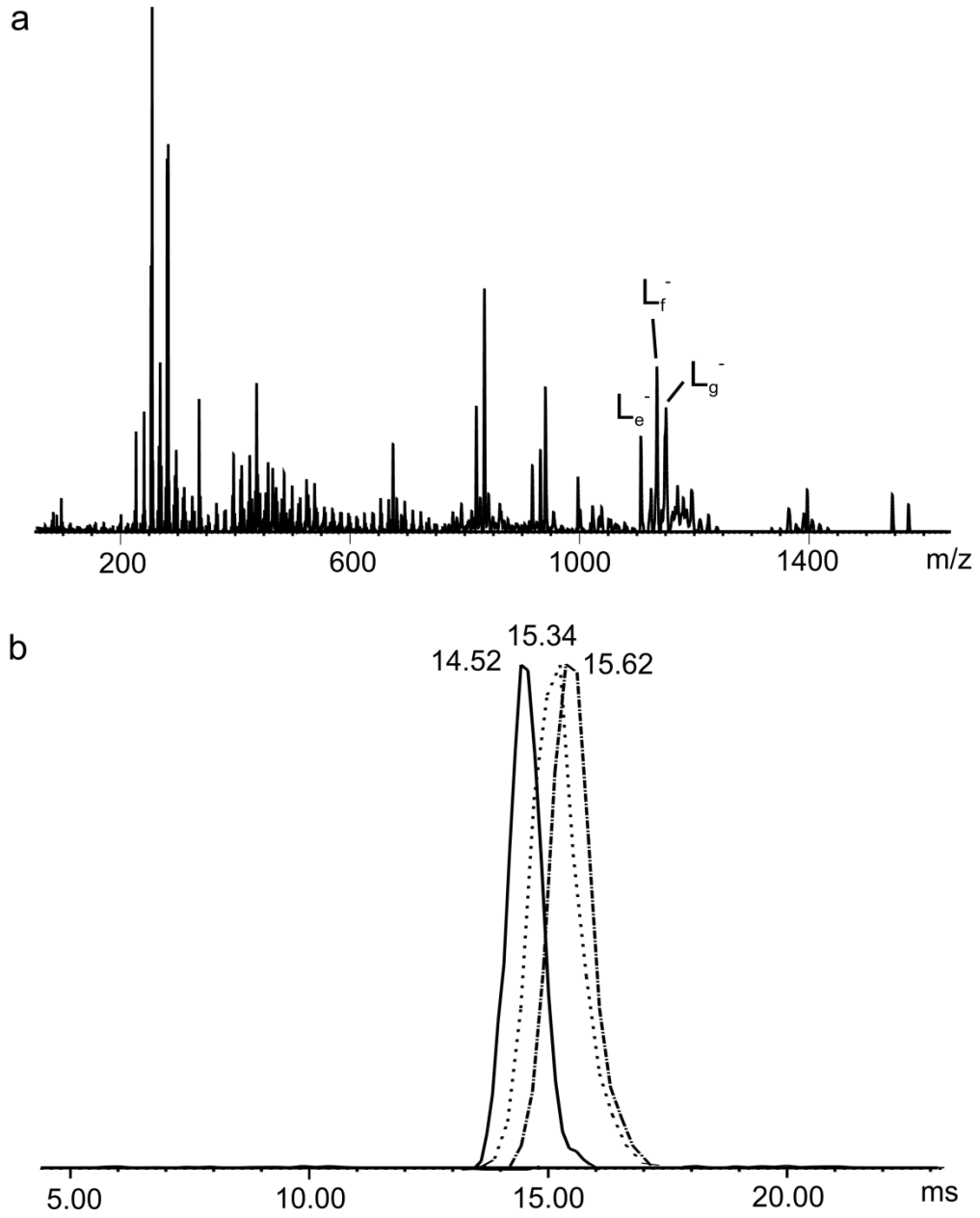

Figure 2.6 (a) ESI mass spectrum acquired in negative ion mode for a methanol solution of (35 μM) Gb3-Cer. (b) IMS arrival time distributions measured for three Gb3-Cer isoforms, L_e^- (——), L_f^- (- - -) and L_g^-(—·—) ions.

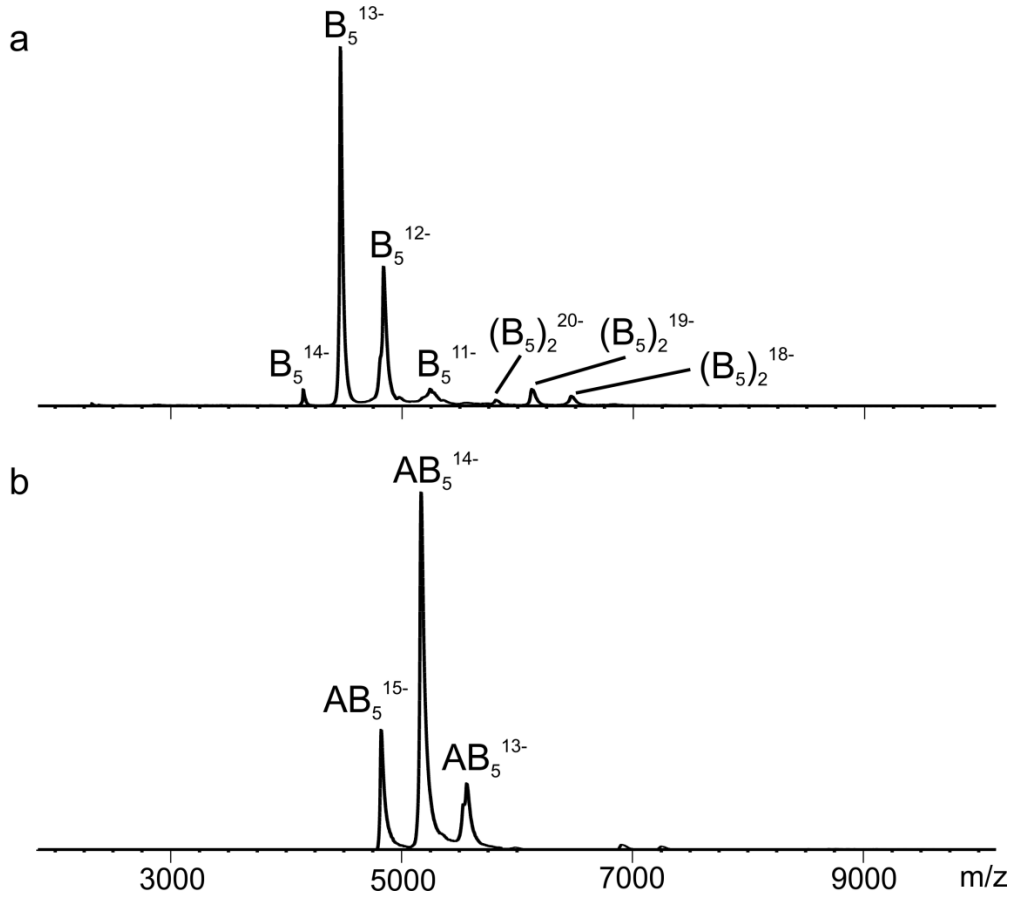

Figure 2.7 ESI mass spectra acquired in negative ion mode for aqueous ammonium acetate (200 mM) solutions of (a) (6 μM) CTB and (10 μM) Gb3-Cer(+) ND with a Gb3-Cer:DMPC ratio of 1:100 and (b) (10 μM) Stx2 and (30 μM) GM1-Cer(+) ND with a GM1-Cer:DMPC ratio of 1:12.

2.3.3 Discovering receptors using ND of a complex mixture

The results described above illustrate the application of the CaR-ESI-MS strategy for detecting specific protein-GSL interactions using ND of well-defined composition. This experimental strategy requires foreknowledge of the specific GSL receptor(s) to be loaded into the ND. However, an alternative approach would be to use the CaR-ESI MS assay for the discovery of unknown receptors from a complex mixture. Along these lines, we envisioned ND could be used as "surrogate cells" by allowing the transfer of packets of the plasma membrane into the gas phase, while preserving the specific protein interactions. To demonstrate this capability, measurements were performed on solutions of CTB_5 and ND produced using lipids extracted from a human epithelial cell-line (A549, lung adenocarcinoma) known to contain GM1-Cer.[27] Weak signals corresponding to $(CTB_5 + GM1\text{-}Cer)^{n-}$ ions are evident, suggesting that GM1-Cer is in low abundance (Figure 2.8a). CID of $(CTB_5 + GM1\text{-}Cer)^{13-}$ produced free B^{n-} ions, the L_a^- and L_b^- ions (confirmed by IMS and CID), and two other ions, L_c^- at *m/z* 1517 and L_d^- at *m/z* 1629, which correspond to the *d*16:1-18:0 (or *d*18:1-16:0) and *d*20:1-22:0 (or *d*18:1-24:0) forms of GM1-Cer, respectively (Figure 2.8b).[23] These ganglioside isoforms are not found in appreciable abundance in the commercial GM1-Cer sample, which was derived from bovine brain (Figure 2.4). But they are detected in the methanol solution of A549 cell extract (Figure 2.9a). The CID

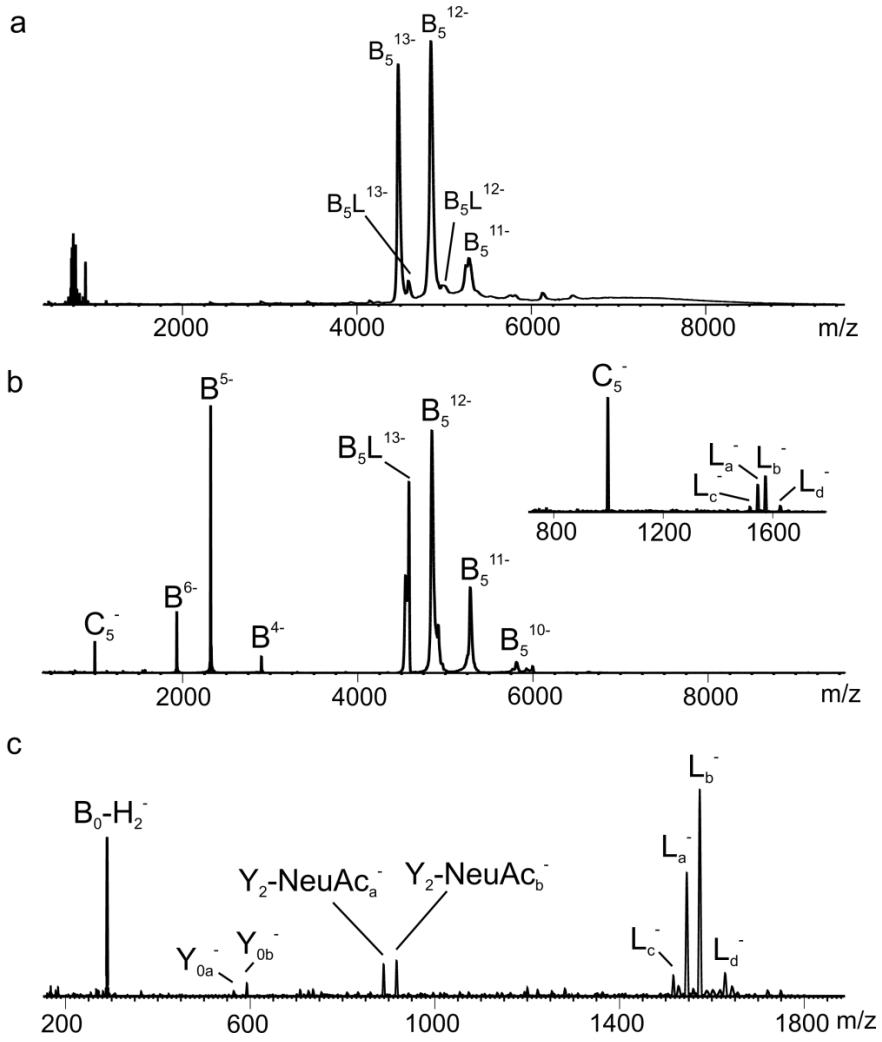

Figure 2.8 (a) ESI mass spectrum acquired in negative ion mode for aqueous ammonium acetate (200 mM) solution of (6 μM) CT B subunit and (20 μM) ND prepared using lipids extracted from A549 cells. (b) CID mass spectrum of the $(CTB_5 + L)^{13-}$ ion, where L ≡ GM1-Cer. The inset shows an expanded view of the mass spectrum in the region from m/z 700 to 1800. (c) CID mass spectrum measured for the L_a^-, L_b^-, L_c^- and L_d^- ions after the IMS cell. Only fragment ions originating from reactant ions with IMS arrival times between 20 to 24 ms are shown.

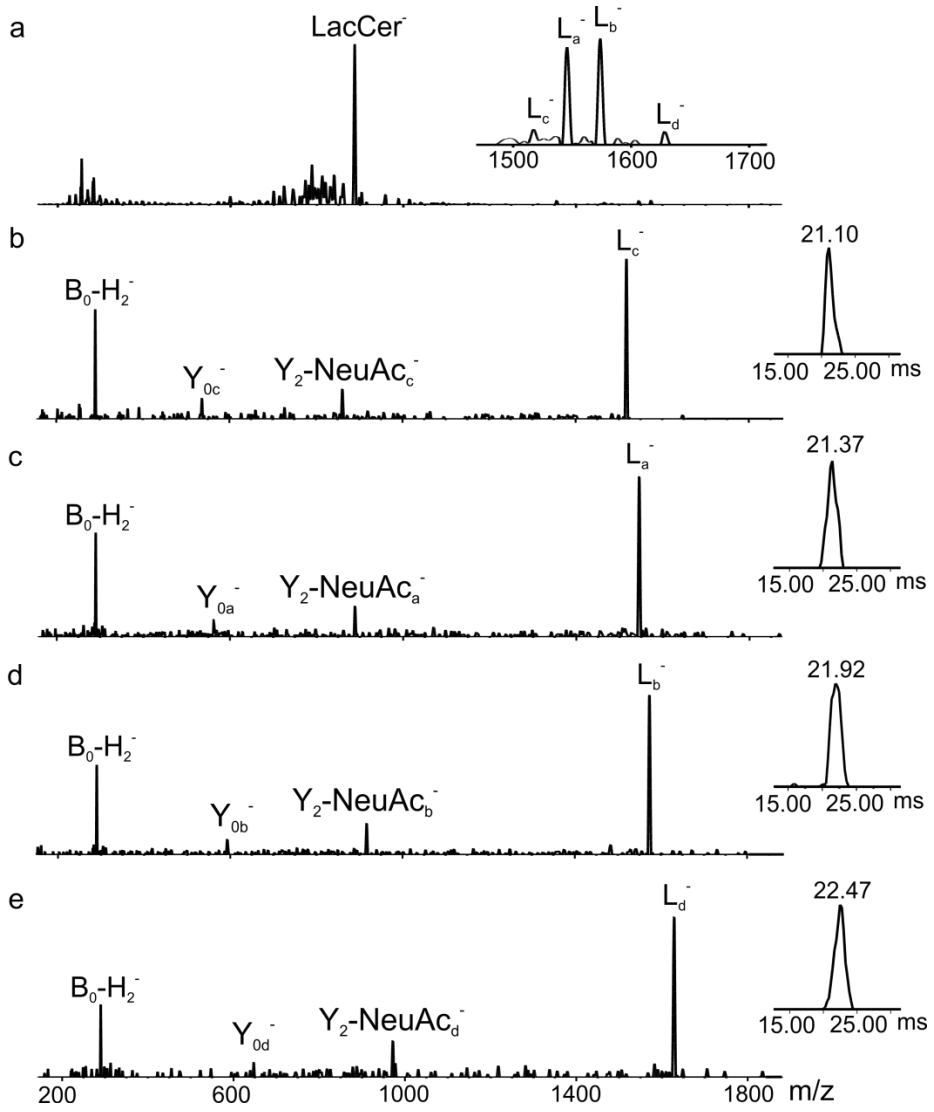

Figure 2.9 (a) ESI mass spectrum acquired in negative ion mode for a methanol solution of A549 cell extract. The major ion corresponds to depronated lactosylceramide (LacCer). The inset shows an expanded view of the mass spectrum in the region from m/z 1470 to 1720 that corresponds to ions with arrival times of between 20 and 24 ms. CID mass spectrum acquired for (b) L_c^-, (c) L_a^-, (d) L_b^- and (e) L_d^- after isolation. Shown in the insets are the corresponding arrival time distributions.

mass spectrum and corresponding arrival time distributions of L_a^-, L_b^-, L_c^- and L_d^- provide more information for comfirmation (Figure 2.9b, c, d, e). Signal corresponding to the deprotonated pentasaccharide, i.e., the C_5^- ion (Figure 2.8b), which in principle could come from the fragmentation of GM1-Cer ions, was also detected (Figure 2.4d). However, it can be shown, based on an analysis of arrival times, that the C_5^- ion is not produced by CID of the GM1-Cer ions following IMS (Figure 2.8c).

2.4 Conclusions

In summary, the CaR-ESI-MS assay represents an important addition to the arsenal of tools available for identifying and characterizing protein-GSL receptor interactions. The assay can be applied to ND of known GSL composition in order to test for specific interactions. The assay may also prove useful for evaluating relative affinities for different GSL, although this application remains to be demonstrated. Significantly, the assay can be applied to ND composed entirely of lipids extracted from tissue or cell cultures and, therefore, holds tremendous potential as a tool for the discovery of native GSL receptors within the complex milieu of the plasma membrane.

2.5 Literature cited

1. Varki, A.; Cummings, R. D.; Esko, J. D.; Freeze, H. H.; Stanley, P.; Marth, J. D.; Bertozzi, C. R.; Hart, G. W.; Etzler, M. E., *Proteomics* **2009,** *9* (24), 5398-5399.
2. Hartmann, M.; Lindhorst, T. K., *Eur. J. Org. Chem.* **2011,** (20-21), 3583-3609.
3. Song, X. Z.; Lasanajak, Y.; Xia, B. Y.; Heimburg-Molinaro, J.; Rhea, J. M.; Ju, H.; Zhao, C. M.; Molinaro, R. J.; Cummings, R. D.; Smith, D. F., *Nat. Methods* **2011,** *8* (1), 85-U125.
4. Kitova, E. N.; El-Hawiet, A.; Schnier, P. D.; Klassen, J. S., *J. Am. Soc. Mass Spectrom.* **2012,** *23* (3), 431-441.
5. El-Hawiet, A.; Shoemaker, G. K.; Daneshfar, R.; Kitova, E. N.; Klassen, J. S., *Anal. Chem.* **2012,** *84* (1), 50-58.
6. Barrera, N. P.; Di Bartolo, N.; Booth, P. J.; Robinson, C. V., *Science* **2008,** *321* (5886), 243-246.
7. Kobashigawa, Y.; Harada, K.; Yoshida, N.; Ogura, K.; Inagaki, F., *Anal. Biochem.* **2011,** *410* (1), 77-83.
8. Bayburt, T.H.; Sligar, S.G. *FEBS Letters* **2010**, *584*, 1721-1727.
9. Borch, J.; Torta, F.; Sligar, S.G.; Roepstorff, P. *Anal. Chem*. **2008**, 80, 6245-6252.
10. Nath, A.; Grinkova, Y.V.; Sligar, S.G.; Atkins, W.M. *J. Biol. Chem.* **2007**, *282*, 28309-28320.

11. Mak, P.J.; Denisov, I.G.; Grinkova, Y.V.; Sligar, S.G.; Kincaid, J.R. *J. Am. Chem. Soc.* **2011**, *133*, 1357-1366.

12. Marty, M.T.; Das, A.; Sligar, S.G. *Anal. Bioanal. Chem.* **2012**, *402*, 721-729.

13. Hebling, C.M.; Morgan, C.R.; Stafford, D.W.; Jorgenson, J.W.; Rand, K.D.; Engen, J.R. *Anal. Chem.* **2010**, *82*, 5415-5419.

14. Marin, V.L.; Bayburt, T.H.; Sligar, S.G.; Mrksich, M. *Angew. Chem. Int. Ed. Engl.* **2007**, *46*, 8796-8798.

15. Ritchie, T.K.; Grinkova, Y.V.; Bayburt, T.H.; Denisov, I.G.; Zolnerciks, J.K.; Atkins, W.M., Sligar, S.G. *Methods Enzymol*. **2009**, *464*, 211-31.

16. Bayburt, T.H.; Grinkova, Y.V.; Sligar, S.G. *Nanoletters* **2002**, *2*, 853-856.

17. Nath, A.; Atkins, W.M.; Sligar, S.G. *Biochemistry* **2007**, *46*, 2059-2069.

18. Merritt, E.A.; Sarfaty, S.; Van Den Akker, F.; L'Hoir, C.; Martial, J.A.; Hol, W.G.J. *Protein Sci.* **1994**, *3*, 166-175.

19. Flagler, M.J.; Mahajan, S.S.; Kulkarni, A.A.; Iyer, S.S.; Weiss, A.A. *Biochemistry.* **2010,** *49*, 1649-1657.

20. Turnbull, W.B.; Precious, B.L.; Homans, S.W. *J. Am. Chem. Soc.* **2004**, *126*, 1047-1054.

21. Kitova, E.N.; Kitov, P.I.; Armstrong, G.D.; Bundle, D.R.; Klassen, J.S. *Glycobiology*. **2007**, *17*, 1127-1137.

22. Sun, J.; Kitova, E.N.; Sun, N.; Klassen, J.S. *Anal. Chem.* **2007**, *79*, 8301-8311.

23. Ikeda, K.; Taguchi, R. *Rapid Commun. Mass Spectrom.* **2010**, *24*, 2957–2965.

24. Whitfield, P.; Johnson, A.W.; Dunn, K.A.; Delauche, A.J.N; Winchester, B.G.; Franklin, R.J.M. *Acta Neuropathol* **2000**, *100*, 409-414.

25. Weis, W.I.; Drickamer, K. *Annu. Rev. Biochem.* **1996**, *65*, 441-473.

26. Touboul, D.; Roy, S.; Germain, D.P.; Baillet, A; Brion, F.; Prognon, P.; Chaminade, P.; Laprévote, O. *Anal. Bioanal. Chem.* **2005**, *382*, 1209-1216.

27. Garcia-Alvarz, I.; Egido-Gabas, M.; Romero-Ramirez, L.; Doncel-Perez, E.; Nieto-Sampedro, M.; Casas, J.; Fernandez-Mayoralas, A. *Mol. BioSyst*. **2011**, *7*, 129-138.

Chapter 3

Dissociation of Multisubunit Protein-Ligand Complexes in the Gas Phase. Evidence for Ligand Migration*

3.1 Introduction

Investigations into the assembly and organization of proteins into complexes and their interactions with other biomolecules (e.g. DNA, RNA, peptides, carbohydrates) and small molecules is stimulated by the critical importance of protein complexes and multiprotein assemblies in cellular processes.[1-3] There are a variety of experimental techniques available to probe the structures of protein complexes. High resolution structural data have been generated using X-ray crystallography and solution and solid state nuclear magnetic resonance spectroscopy.[4, 5] A number of other experimental (e.g. electron microscopy, small angle scattering, circular dichroism) and computational methods can provide complementary structural information on protein complexes.[6-9]

In recent years electrospray ionization mass spectrometry (ESI-MS) has emerged as an important tool for characterizing the composition and structure of multiprotein and protein-ligand complexes *in vitro* and, in some instances, it can provide insights into topology and connectivity and the identity and location of bound ligands.[10-35] The disruption of the non-covalent interactions within multiprotein complexes, either in solution or the gas phase, followed by the MS

* A version of this chapter has been accepted for publication: Zhang, Y.; Deng, L.; Kitova, E.N.; Klassen, J.S. *J. Am. Soc. Mass. Spectrom.*

analysis of the monomeric/multimeric products can provide information about composition. The dissociation/disassembly of multiprotein complexes in solution can be achieved by altering the solution pH, temperature or ionic strength.[15, 16] In the gas phase, energetic collisions with neutral gases (collision-induced dissociation, CID) are commonly used to cause the dissociation of multiply charged ions of intact protein complexes.[16, 17] The use of CID, as well as other slow heating methods, such as infrared radiative multiphoton dissociation (IRMPD)[18] and blackbody infrared radiative dissociation (BIRD)[19-21], to establish the composition of multiprotein complexes is somewhat limited by the tendency of the complexes to dissociate by the loss of a single, highly charged subunit, with the remaining complex resisting further dissociation. This phenomenon is believed to involve the asymmetric unfolding of the leaving subunit (relative to the other subunits in the complex); unfolding enhances the gas phase acidity/basicity of the subunit and promotes charge transfer.[22-24] In contrast, nearly complete disassembly of multiprotein complexes into monomers can be achieved with surface induced dissociation (SID), for which heating occurs on a much shorter timescale.[25, 26] In addition to composition, MS combined with gas-phase activation methods such as CID can be used to probe the spatial arrangement of proteins within multiprotein complexes.[27-30] For example, it has been shown that subunits located on the periphery of the large multiprotein assemblies of the intact ribosome[27], RNA polymerase[28], 19S proteasome lid[29] and human eukaryotic initiation factor 3 protein complex[30] are preferentially lost upon collisional activation.

To date, there have been relatively few studies of the gas-phase dissociation of ligand-bound multiprotein/multisubunit complexes[31-35] and it remains unclear to what extent the location and nature of ligand binding can be probed in the gas phase. CID performed on the fully ligand-bound 24-mer of tryptophan RNA-binding attenuation protein (TRAP) resulted in the loss of the TRAP monomer, as well as the successive loss of ligands (Trp).[31] Based on differences in the relative stabilities of the bound ligands, an asymmetric structure of the $TRAP_{24}$ assembly bound to 22 Trp molecules was suggested.[31] The results of both CID and SID of the heterotetrameric hemoglobin complex have been reported. SID resulted predominantly in the formation of α and β subunits, free of heme.[32] In contrast, CID proceeded by multiple pathways involving the loss of α and β subunits, heme, heme dimer and α and β subunits bound to heme[33], Surprisingly, CID also produced $\alpha\beta_2$ trimers bound to four heme groups.[32,33] The loss of an α subunit, in its apo-form, from the intact holo-tetramer necessarily requires the migration of a heme group from one subunit to another. The process of ligand migration is, presumably, induced by collisional activation of the gaseous complex.

In the present study, the possibility of ligand migration within multisubunit protein complexes in the gas phase is examined in more detail. To this end, CID was performed on the complexes of two different multisubunit proteins, cholera toxin B subunit homopentamer (CTB_5) bound to its native ganglioside receptor β-D-Gal*p*-(1→3)-β-D-Gal*p*NAc-(1→4)[α-D-Neu5Ac-(2→3)]-β-D-Gal*p*-(1→4)-β-D-Glc*p*-Cer (GM1-Cer) and the soluble

pentasaccharide β-D-Gal*p*-(1→3)-β-D-Gal*p*NAc-(1→4)[α-D-Neu5Ac-(2→3)]-β-D-Gal*p*-(1→4)-β-D-Glc*p* (GM1) and the homotetramer streptavidin (S_4) with its high affinity ligand biotin (B) and biotin bound to a phosphatidylethanolamine group (PE), 1,2-dipalmitoyl-*sn*-glycero-3-phosphoethanolamine-N-(biotinyl) (Btl). CTB_5 possesses five identical binding sites for GM1 (and GM1-Cer) and the intrinsic affinity (K_a) is reported to be between 10^5 and 10^7 M^{-1}.[36-38] According to the crystal structure of the the (CTB_5 + 5GM1) complex (PDB id 3CHB), the GM1 binding site is made up primarily from a single B subunit, with 18 direct or solvent mediated H-bonds between GM1 and amino acid residues located within the subunit and one H-bond with residue Gly33 from an adjacent subunit.[39] The S_4 homotetramer possesses four identical binding sites for B and the streptavidin-biotin interaction ($K_a \approx 10^{14}$ M^{-1}) is one of the strongest known.[40] Each B is stabilized primarily through intermolecular H-bonds and van-der-Waals interactions within a single subunit. Additionally, there is a contact between B and the aromatic ring of the Trp120 in an adjacent subunit.[41] CID was performed on the protonated and deprotonated ions of the (CTB_5 + 5GM1), (CTB_5 + 5GM1-Cer), (S_4 + 4B) and (S_4 + 4Btl) complexes. The influence of charge state and collision energy on the dissociation pathways was assessed. Molecular dynamics (MD) simulations were performed on the protonated $(CTB_5 + 5GM1)^{15+}$ and deprotonated $(CTB_5 + 5GM1)^{14-}$ ions in an effort to elucidate the molecular details of the ligand migration and dissociation reactions.

3.2 Materials and methods

3.2.1 Proteins and ligands

The pentasaccharide β-D-Gal*p*-(1→3)-β-D-Gal*p*NAc-(1→4)[α-D-Neu5Ac-(2→3)]-β-D-Gal*p*-(1→4)-β-D-Glc*p* (GM1, MW 998.34 Da), was obtained from Elicityl (Crolles, France) and bovine monosialotetrahexosylganglioside β-D-Gal*p*-(1→3)-β-D-Gal*p*NAc-(1→4)[α-D-Neu5Ac-(2→3)]-β-D-Gal*p*-(1→4)-β-D-Glc*p*-Cer (GM1-Cer) was purchased from Axxora LLC (San Diego, CA). The GM1-Cer sample was composed predominantly of two isoforms, *d*18:1-18:0 (MW 1545.88 Da) and *d*20:1-18:0 (MW 1573.91 Da). 1,2-dipalmitoyl-*sn*-glycero-3-phosphoethanolamine-N-(biotinyl) (Btl, MW 917.59 Da) and 1,2-dimyristoyl-*sn*-glycero-3-phosphocholine (DMPC, MW 677.50 Da) were purchased from Avanti Polar Lipids (Alabaster, AL). Recombinant membrane scaffold protein MSP1E1 (MW 27 494 Da), used in the preparation of nanodiscs (ND), was produced using plasmid pMSP1E1 acquired from Addgene (Cambridge, MA). Protein expression and purification was carried out using the procedure described at http://sligarlab.life.uiuc.edu/nanodisc.html. Cholera toxin B subunit (CTB, monomer MW 11 604 Da) and biotin (B, MW 244.09 Da) were purchased from Sigma-Aldrich Canada (Oakville, Canada). A recombinant, truncated form (containing residues 13-139) of wild type streptavidin (S, monomer MW 13 271 Da) was used in this study; the plasmid was a gift from Prof. Stayton (University of Washington). The protein was expressed in *E. coli* and purified using procedures described elsewhere.[42] The solutions of S_4 and CTB_5 were exchanged into 200 mM aqueous ammonium acetate using an Amicon microconcentrator

with a MW cut-off of 10 kDa, concentrated to 100 μM and stored at -20 ℃ and 4 ℃, respectively, until needed.

3.2.2 Nanodiscs

Nanodiscs (NDs) composed of DMPC and GM1-Cer or Btl were prepared using procedures reported elsewhere[43, 44] and only brief description is given here. DMPC (in chloroform) was mixed with either GM1-Cer or Btl (in a 2:1 chloroform-methanol solution) at a 12:1 ratio; the solvent was removed under a gentle stream of nitrogen and replaced with Tris buffer containing 25 mM sodium cholate. MSP1E1 at a concentration of 0.3 to 0.4 mM was added to the cholate-solubilized lipid and GM1-Cer or Btl mixture at the desired ratios. After 30 min incubation at 23 ℃, the self-assembly process was initiated by adding an equal volume of pre-washed biobeads SM-2 (Bio-Rad), followed by gentle agitation for 4 hr at 23 ℃. The beads were removed by sedimentation and the supernatant was then loaded onto a Superdex 200 HR 10/300 GL column (GE Healthcare). GM1-Cer-ND or Btl-ND fractions were collected, concentrated and dialyzed against 200 mM ammonium acetate (pH 7.0) using an Amicon microconcentrator with a MW cut-off of 30 kDa, then stored at -80 ℃. The concentration of the ND solutions was determined by absorbance at 280 nm using the extinction coefficient of MSP1E1.

3.2.3 Mass spectrometry

All experiments were carried out using a Synapt G2-S quadrupole-ion mobility separation-time-of-flight (Q-IMS-TOF) mass spectrometer (Waters, UK), equipped with a nanoflow ESI (nanoESI) source. To perform nanoESI, tips

were produced from borosilicate capillaries (1.0 mm o.d.; 0.68 mm i.d.) and pulled to ~5 μm using a P-97 micropipette puller (Sutter Instruments, Novato, CA). A platinum wire was inserted into the nanoESI tip, and a capillary voltage of 1.0−1.2 kV was applied to carry out ESI. Given below are representative instrumental conditions used in positive ion mode. A cone voltage of 35-50 V was used, and the source block temperature was maintained at 60 ℃. The Trap and Transfer collision energies were maintained at 5 V and 2 V, respectively, for detection of the complexes. For the energy-resolved CID experiments, ions of interest were isolated using the quadrupole mass filter and then subjected to CID by increasing the collision energy in the Trap ion guide from 10 to 120 V for the $(CTB_5 + 5GM1)^{n+}$ and $(CTB_5 + 5GM1\text{-}Cer)^{n+}$ ions or from 3 to 70 V for the $(S_4 + 4B)^{n+}$ and $(S_4 + 4Btl)^{n+}$ ions, using steps of 2 or 3 V. Argon was used in the Trap and Transfer ion guides at a pressure of 1.42×10^{-2} mbar and 1.74×10^{-2} mbar, respectively. Helium, at a flow rate of 151 mL min^{-1}, was introduced into the He chamber preceding the traveling wave ion mobility (TWIMS) device. Data acquisition and processing were carried out using MassLynx (v 4.1).

To produce gaseous ions of the protein complexes containing the water soluble ligands (GM1 or B), ESI was performed on aqueous 200 mM ammonium acetate solutions containing 6 μM of CTB_5 and 38 μM GM1, or 5 μM S_4 and 20 μM B. To produce gaseous ions of the protein complexes containing the insoluble GM1-Cer or Btl ligands, ESI was performed on aqueous 200 mM ammonium acetate solutions containing 6 μM of CTB_5 and 10 μM ND with 8% GM1-Cer or 5 μM S_4 and 10 μM ND with 8% Btl. Mild in-source dissociation was used to

release the $(CTB_5 + 5GM1\text{-}Cer)^{n+/-}$ and $(S_4 + 4Btl)^{n+/-}$ ions from the gaseous ND complexes.[45] Shown in Figures 3.1 and 3.2 are representative mass spectra measured in positive and negative ion mode, respectively.

The average charge states (*ACS*) of the subunit product ions (i.e. $CTB^{x+/-}$ and $S^{x+/-}$) were calculated from the CID mass spectra using eq 1:

$$ACS = \frac{\sum_{x} xAb_x}{\sum_{x} Ab_x} \quad (1)$$

where Ab_x and x are the relative abundance and the charge state of each $CTB^{x+/-}$ or $S^{x+/-}$ ion. The *ACS* values of the $(CTB + GM1)^{y+/-}$, $(CTB + GM1\text{-}Cer)^{y+/-}$ and $(S+Btl)^{y+/-}$ product ions were calculated in a similar manner.

3.2.4 Computational methods

MD simulations were performed using the Amber 11 program suite[46] (Accelrys, San Diego, CA). Currently with Amber atomic charges and atom type parameters are available only for the charged forms of the Arg, N-terminal Thr (NThr) and C-terminal Asn (CAsn) residues. Consequently, it was necessary to develop charges and parameters for the neutral form of Arg, NThr and CAsn. The charges and parameters for the neutral form of Arg were established in a previous study.[47] The charges for the neutral form of NThr and CAsn, incorporated into dipeptides (NThr-Gly-NME and ACE-Gly-CAsn, respectively), were parameterized using the RESP ESP Charge Derive server[48, 49] and Gaussian C.01[50], enforcing net neutrality across the residues. The crystal structure of the CTB_5 subunit complexed with five GM1 (PDB ID: 3CHB) has been reported.[51] The initial geometry of the CTB_5 was generated by converting all of the charged

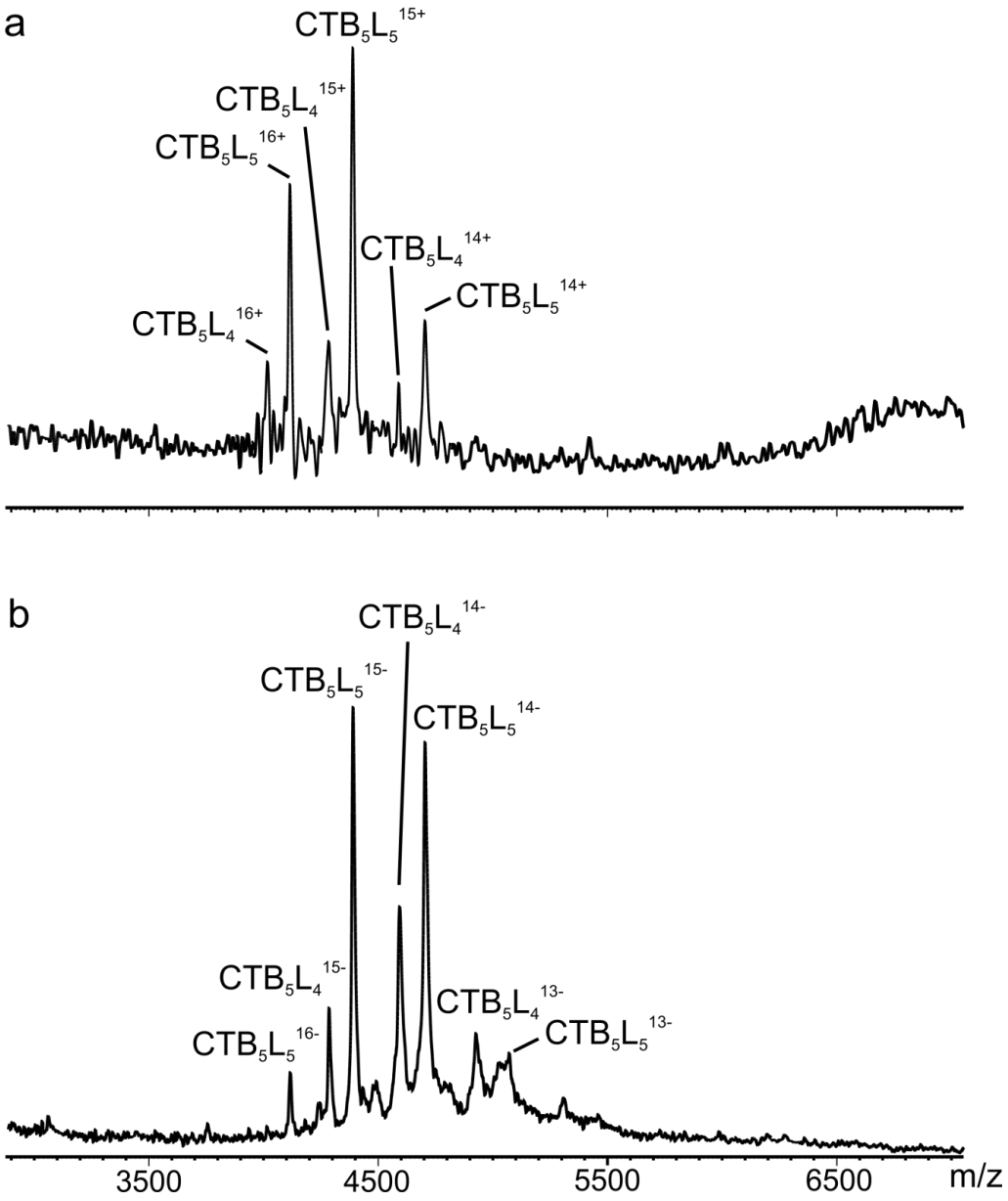

Figure 3.1 ESI mass spectra acquired in (a) positive and (b) negative ion mode for aqueous ammonium acetate (200 mM) solution of (6 μM) CTB_5 subunit and (10 μM) ND containing 8% GM1-Cer (≡ L).

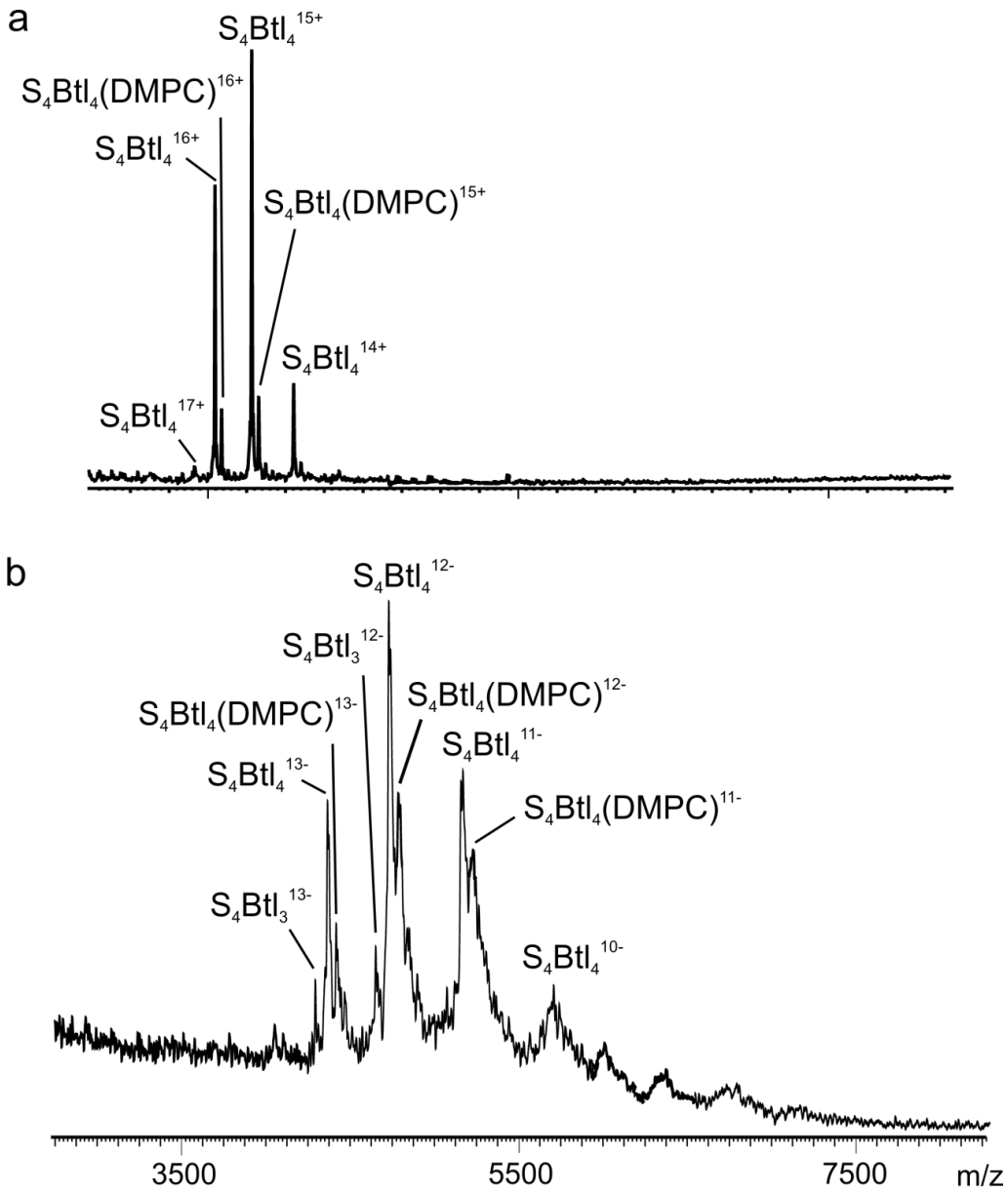

Figure 3.2 ESI mass spectra acquired in (a) positive and (b) negative ion mode for aqueous ammonium acetate (200 mM) solution of (5 μM) streptavidin and (10 μM) ND containing 8% Btl. Nonspecific binding between DMPC and Btl is likely responsible for the appearance of the $S_4Btl_4(DMPC)^{n+/-}$ ions.

acidic and basic amino acid residues to their neutral forms. Incomplete GM1 structures found in the crystal structure were corrected by aligning each incomplete ligand to the complete ligand structure and grafting the missing atoms onto each ligand using Open Babel 2.0[52, 53].

The (CTB_5 + 5GM1) complex at charge state +15 and -14 were chosen for investigation. For the $(CTB_5 + 5GM1)^{15+}$ ion, only the basic residues (Lys, Arg and His) on the surface of CTB_5 (<5 Å from the surface) and N-Thr were considered as possible protonation sites.[54] To mimic the dissociation pathways observed in the CID experiments, seven of the fifteen charges were placed on subunit D and the other eight were distributed evenly on other four subunits (E, F, G, H). The twelve different charge configurations considered are listed in Table 3.1. Topology and coordinate files for the simulations of each charge configuration were created using the Antechamber module of the AmberTools (version 11)[55]. For the $(CTB_5 + 5GM1)^{14-}$ ion, all five GM1 ligands were deprotonated (at the sialic acid residue); the other nine charges were distributed asymmetrically among the five subunits (five charges on subunit D and one charge on each of the other four subunits). Only Glu and Asp residues on the surface of CTB_5 (<5 Å from the surface) were considered as possible deprotonation sites (Table 3.1). The MD simulations were performed using the Amber 03 force field[56] for CTB_5 and a general Amber force field (GAFF)[57] for GM1. The MD integration time step was 1 fs; bonds involving hydrogen atoms were constrained with SHAKE. Following 1000 steps of minimization, the system was heated from 300K to 800 K within 20,000 steps (0.02 ns). The temperature

was then held constant at 800 K and 3 ns of dynamics were performed. Trajectory analysis and the calculation of the radius of gyration (Rg) were performed using the Visual Molecular Dynamics package.[58]

Table 3.1 Charge configurations considered for the MD simulations performed on the $(CTB_5 + 5GM1)^{15+}$ and $(CTB_5 + 5GM1)^{14-}$ ions.

Configuration	Subunit	Protonated residues
B15_1	D	NThr 01, Lys 23,34, 62, 91, His 13, 18
	E, F, G and H	His 13, Lys 43
B15_2	D	NThr 01, Lys 23, 34, 63, 91, His 13, 18
	E, F, G and H	His 13, Lys 43
B15_3	D	NThr 01, Lys 43,34, 62, 91, His 13, 18
	E, F, G and H	His 13, Lys 43
B15_4	D	NThr 01, Lys 43, 34, 63, 91, His 13, 18
	E, F, G and H	His 13, Lys 43
B15_5	D	NThr 01, Lys 81,34, 62, 91, His 13, 18
	E, F, G and H	His 13, Lys 43
B15_6	D	NThr 01, Lys 81, 34, 63, 91, His 13, 18
	E, F, G and H	His 13, Lys 43
B15_7	D	NThr 01, Lys 43, 34, 63, Arg 94, His 13, 18
	E, F, G and H	His 13, Lys 43
B15_8	D	NThr 01, Lys 43, 34, 62, Arg 94, His 13, 18
	E, F, G and H	His 13, Lys 43
B15_9	D	NThr 01, Lys 23, 34, 63, Arg 94, His 13, 18
	E, F, G and H	His 13, Lys 43
B15_10	D	NThr 01, Lys 23, 34, 62, Arg 94, His 13, 18
	E, F, G and H	His 13, Lys 43
B15_11	D	NThr 01, Lys 81, 34, 63, Arg 94, His 13, 18
	E, F, G and H	His 13, Lys 43
B15_12	D	NThr 01, Lys 81, 34, 62, Arg 94, His 13, 18
	E, F, G and H	His 13, Lys 43
		Deprotonated residues
B9_1	D	Glu 11, 51, 79, 83, Asp 59
	E, F, G and H	Asp 22

3.3 Results and discussion

3.3.1 CID of $(CTB_5 + 5GM1)^{n+/-}$ and $(CTB_5 + 5GM1\text{-}Cer)^{n+/-}$ ions

Representative ESI mass spectra acquired in both positive and negative ion mode for an aqueous ammonium acetate (200 mM) solution of CTB_5 (6 μM) and GM1 (38 μM) are shown in Figure 3.3. The major protein ions detected correspond to protonated (+ mode) or deprotonated (- mode) homopentamer bound to three, four or five GM1 ligands, i.e.; $(CTB_5 + iGM1)^{n+}$ ions where i = 3, 4 and 5, at charge states +13, +14, +15 (Figure 3.3a) and $(CTB_5 + iGM1)^{n-}$ ions where i = 3, 4 and 5, at charge states -12, -13, -14 (Figure 3.3b). Control ESI-MS measurements, employing the reference protein method[59], were performed in order to confirm that observed ions were formed from the specific $(CTB_5 + iGM1)$ complexes in solution, with no contribution from nonspecific ligand binding during the ESI process (data not shown).[60] Energy-resolved CID of the protonated $(CTB_5 + 5GM1)^{n+}$ ions, at charge states +14 and +15, and deprotonated $(CTB_5 + 5GM1)^{n-}$ ions, at charge states -12, -13 and -14, was carried out as described in the Experimental section. A summary of the dissociation pathways observed for the $(CTB_5 + 5GM1)^{n+}$ and $(CTB_5 + 5GM1)^{n-}$ ions is given in Scheme 3.1.

a. $(CTB_5 + 5GM1)^{n+} \longrightarrow (CTB_4 + 5GM1)^{(n-x)+} + CTB^{x+}$

$\longrightarrow (CTB_4 + 4GM1)^{(n-y)+} + (CTB + GM1)^{y+}$

$(CTB_5 + 5GM1\text{-}Cer)^{n+} \longrightarrow (CTB_4 + 5GM1\text{-}Cer)^{(n-x)+} + CTB^{x+}$

$\longrightarrow (CTB_4 + 4GM1\text{-}Cer)^{(n-y)+} + (CTB + GM1\text{-}Cer)^{y+}$

b. $(CTB_5 + 5GM1)^{n-} \longrightarrow (CTB_5 + 4GM1)^{(n-1)-} + GM1^{-}$

$\longrightarrow (CTB_4 + 4GM1)^{(n-y)-} + (CTB + GM1)^{y-}$

$\longrightarrow (CTB_4 + 5GM1)^{(n-x)-} + CTB^{x-}$

$(CTB_5 + 5GM1\text{-}Cer)^{n-} \longrightarrow (CTB_5 + 4GM1\text{-}Cer)^{(n-1)-} + GM1\text{-}Cer^{-}$

$\longrightarrow (CTB_4 + 4GM1\text{-}Cer)^{(n-y)-} + (CTB + GM1\text{-}Cer)^{y-}$

$\longrightarrow (CTB_4 + 5GM1\text{-}Cer)^{(n-x)-} + CTB^{x-}$

c. $(S_4 + 4B)^{n+} \longrightarrow (S_4 + 3B)^{n+} + B$

$\longrightarrow (S_4 + 3B)^{(n-1)+} + B^{+}$

$\longrightarrow (S_3 + 4B)^{(n-x)+} + S^{x+}$

$(S_4+4Btl)^{n+} \longrightarrow (S_3+4Btl)^{(n-x)+} + S^{x+}$

$\longrightarrow (S_3+3Btl)^{(n-y)+} + (S+Btl)^{y+}$

d. $(S_4+4B)^{n-} \longrightarrow (S_4+3B)^{n-} + B$

$\longrightarrow (S_4+3B)^{(n-1)-} + B^{-}$

$(S_4+4Btl)^{n-} \longrightarrow (S_4+3Btl)^{(n-1)-} + Btl^{-}$

Scheme 3.1 Summary of CID pathways observed for (a) $(CTB_5 + 5GM1)^{n+}$, n = 14 and 15, and $(CTB_5 + 5GM1\text{-}Cer)^{n+}$, n = 14 – 16; (b) $(CTB_5 + 5GM1)^{n-}$, n = 12 – 14, and $(CTB_5 + 5GM1\text{-}Cer)^{n-}$, n = 13 – 15; (c) $(S_4 + 4B)^{n+}$ and $(S_4 + Btl)^{n+}$, n = 15 and 16; and (d) $(S_4+4B)^{n-}$, n = 12 and 13, and $(S_4+4Btl)^{n-}$, n = 11 – 13.

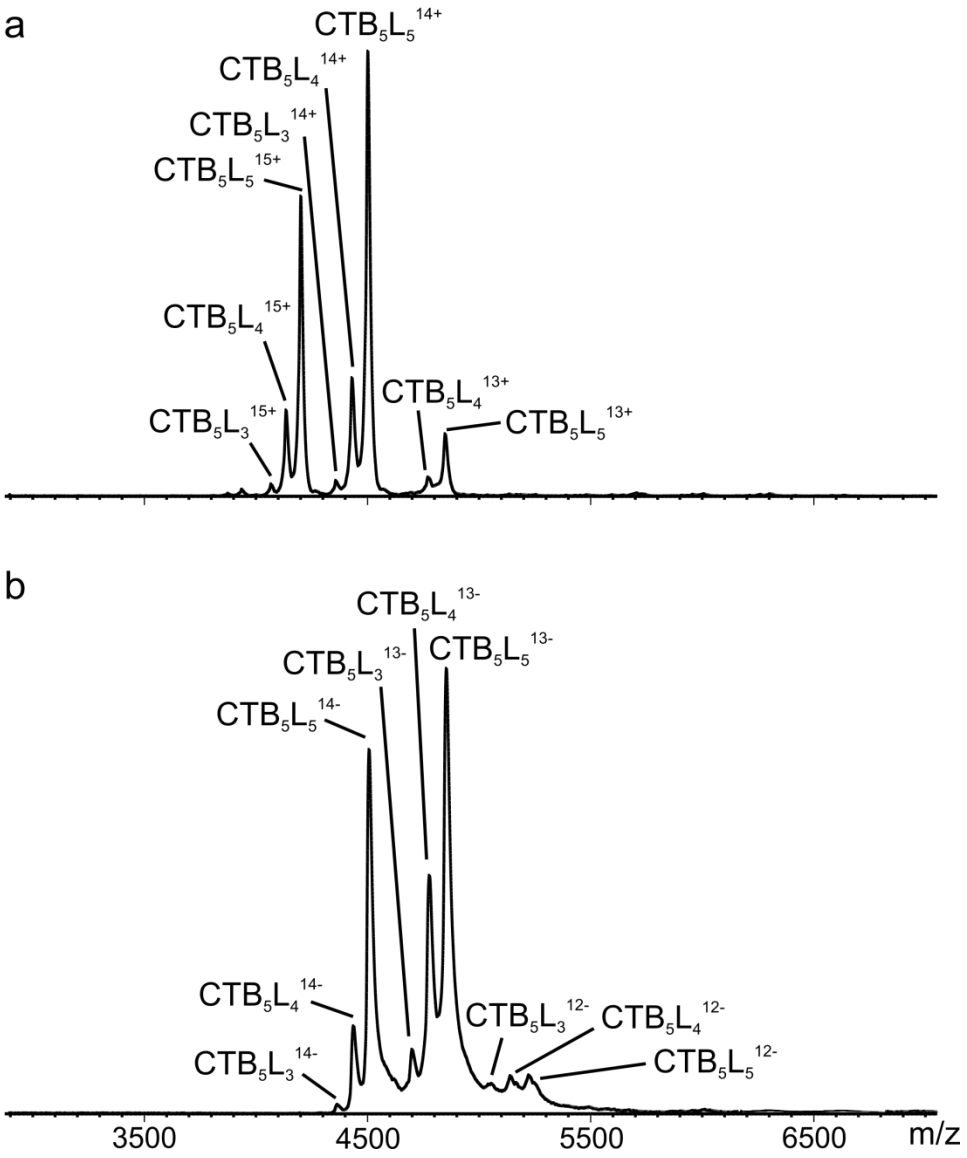

Figure 3.3 ESI mass spectra acquired in (a) positive and (b) negative ion mode for an aqueous ammonium acetate (200 mM) solution of (6 μM) CTB_5 subunit and (38 μM) GM1 (≡ L).

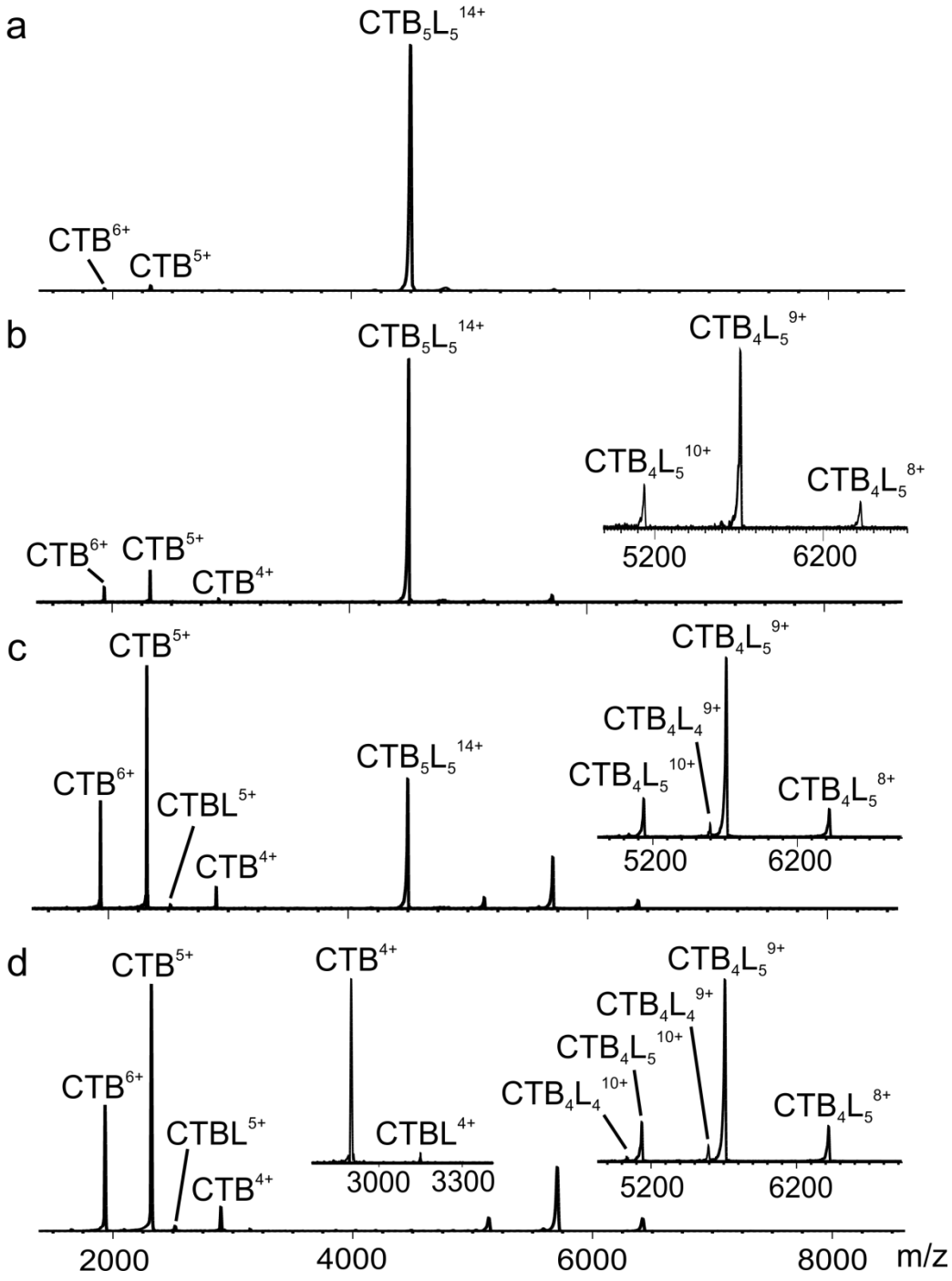

Figure 3.4 CID mass spectra of the $(CTB_5 + 5L)^{14+}$ ion, where L ≡ GM1, at a collision energy of (a) 30 V, (b) 40 V, (c) 50 V and (d) 60 V.

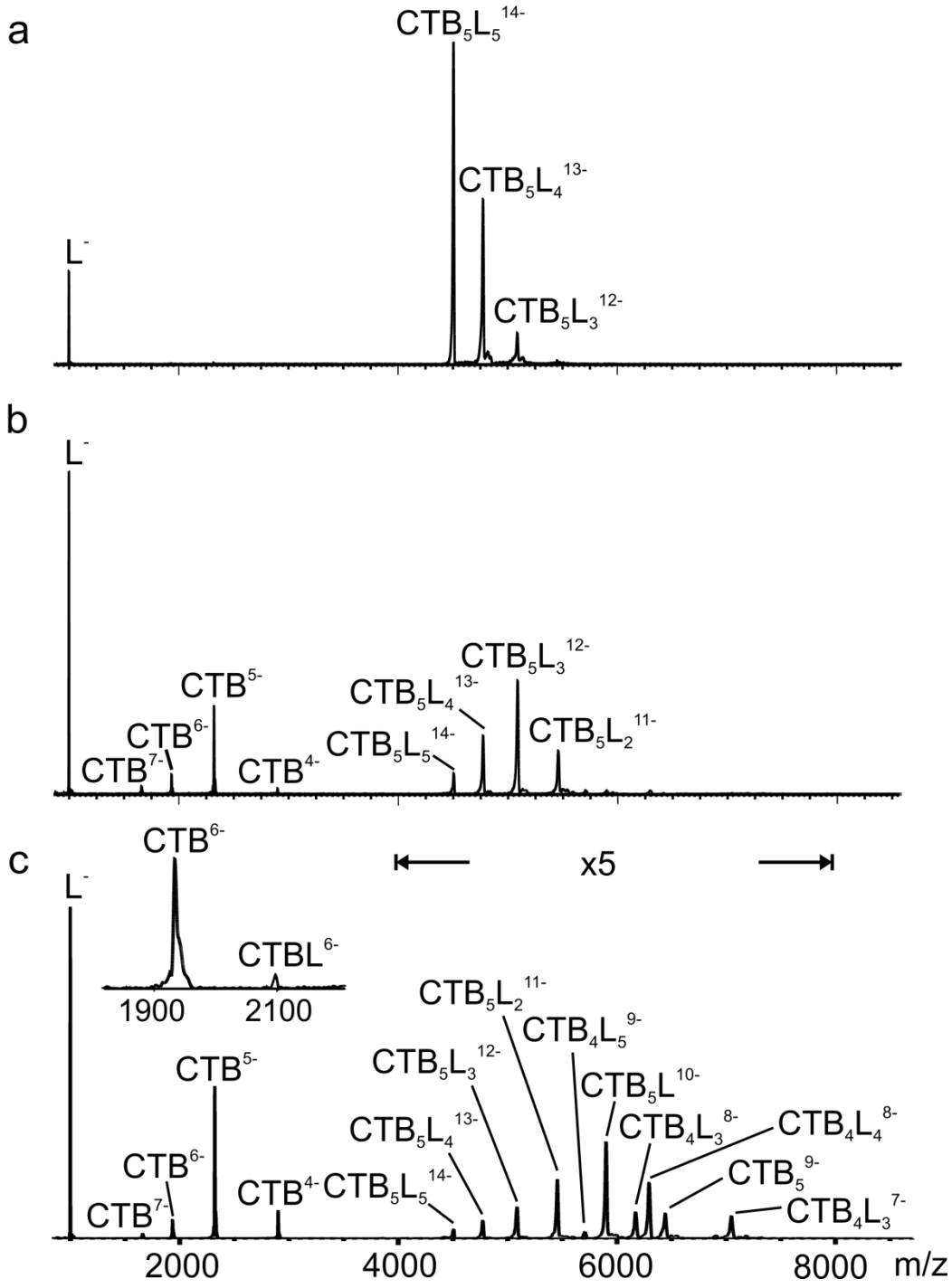

Figure 3.5 CID mass spectra of the $(CTB_5 + 5L)^{14-}$ ion, where L ≡ GM1, at a collision energy of (a) 10 V, (b) 30 V and (c) 50 V.

Shown in Figures 3.4 and 3.5 are representative CID mass spectra acquired for the $(CTB_5 + 5GM1)^{14+}$ and $(CTB_5 + 5GM1)^{14-}$ ions, respectively; CID mass spectra measured for the $(CTB_5 + 5GM1)^{15+}$, $(CTB_5 + 5GM1)^{13-}$ and $(CTB_5 + 5GM1)^{12-}$ ions are shown in Figures 3.6 – 3.8. At all collision energies investigated, the major dissociation pathway observed for the protonated $(CTB_5 + 5GM1)^{n+}$ ions was the loss of a single subunit, i.e.; CTB^{x+}, where x = 4 – 6 (for +14 parent ion) and x = 4 – 7 (+15) and the formation of the complementary $(CTB_4 + 5GM1)^{(n-x)+}$ ions, where (n-x) = 8 – 10 (+14) and (n-x) = 8 – 11 (+15). The *ACS* (Table 3.2) of the CTB^{x+} product ions (5.3 ± 0.1 for +14 and 5.9 ± 0.1 for +15) was found to be independent of collision energy. A second (minor) pathway, observed at higher collision energies (>40 V), was the simultaneous loss of CTB subunit and GM1, i.e.; $(CTB + GM1)^{y+}$ ions, where y = 4 and 5 (for +14) and y = 5 and 6 (for +15), and the formation of the complementary $(CTB_4 + 4GM1)^{10+}$ and $(CTB_4 + 4GM1)^{9+}$ ions. Notably, the loss of GM1 (charged or neutral) was not observed at any collision energy.

The dominant dissociation pathway observed for the $(CTB_5 + 5GM1)^{n-}$ ions, at charge states -12, -13 and -14, (Figures 3.8, 3.7 and 3.5) was the sequential loss of the deprotonated GM1, leading to abundant $(CTB_5 + iGM1)^{[n-(5-i)]-}$ product ions, where i = 0 – 4. Subunit loss, which resulted in CTB^{x-} ions (*ACS* of 4.8 ± 0.1 (-12), 4.9 ± 0.1 (-13) and 5.2 ± 0.1 (-14), Table 3.2) and the complementary $(CTB_4 + 5GM1)^{(n-x)-}$ ions, was a minor pathway. The collision energy was found to have little influence on the CID mass spectra, although a second minor pathway, involving the loss of $(CTB + GM1)^{5-}$ and $(CTB + GM1)^{6-}$

ions, was observed for charge states -13 and -14 at higher collision energies (Figures 3.7 and 3.5).

The native receptor of CTB_5 is the ganglioside GM1-Cer, which possesses ceramide at the reducing end of the pentasaccharide.[61] To assess whether the presence of ceramide influences the dissociation pathways, CID was performed on $(CTB_5 + 5GM1\text{-}Cer)^{n+}$ ions at charge states +14, +15 and +16, and $(CTB_5 + 5GM1\text{-}Cer)^{n-}$ ions at charge states -13, -14, and -15. Representative CID spectra for the $(CTB_5 + 5GM1\text{-}Cer)^{14+}$ and $(CTB_5 + 5GM1\text{-}Cer)^{14-}$ ions are shown in Figure 3.9 and Figure 3.10, respectively. CID mass spectra for the other charge states investigated are shown in Figures 3.11 – 3.14. Dissociation of the $(CTB_5 + 5GM1\text{-}Cer)^{n+}$ ions proceeded by the loss of a single CTB subunit and by the simultaneous loss of CTB subunit and GM1-Cer. This is similar to what was observed for the $(CTB_5 + 5GM1)^{n+}$ ions. However, the presence of ceramide measurably enhanced (by ~6%) the latter pathway. The *ACS* of the ejected subunit (5.2 ± 0.1 (+14), 5.9 ± 0.1 (+15) and 6.5 ± 0.1 (+16) are similar to those of the $(CTB + GM1\text{-}Cer)^{x+}$ product ions and those of subunits ejected from $CTB_5{}^{n+}$ ions (Table 3.2). CID of $(CTB_5 + 5GM1\text{-}Cer)^{n-}$ ions proceeded by two major pathways, the loss of deprotonated GM1-Cer and the loss of subunit. The enhancement of the subunit loss pathway (compared to that for the corresponding $(CTB_5 + 5GM1)^{n-}$ ions) was particularly significant for the -13 charge state (Figure 3.13). The *ACS* of the ejected subunits (4.8 ± 0.1 (-13), 5.0 ± 0.1 (-14), and 5.4 ± 0.2 (-15)) are similar to those found for the corresponding $(CTB_5 + 5GM1)^{n-}$ ions (Table 3.2).

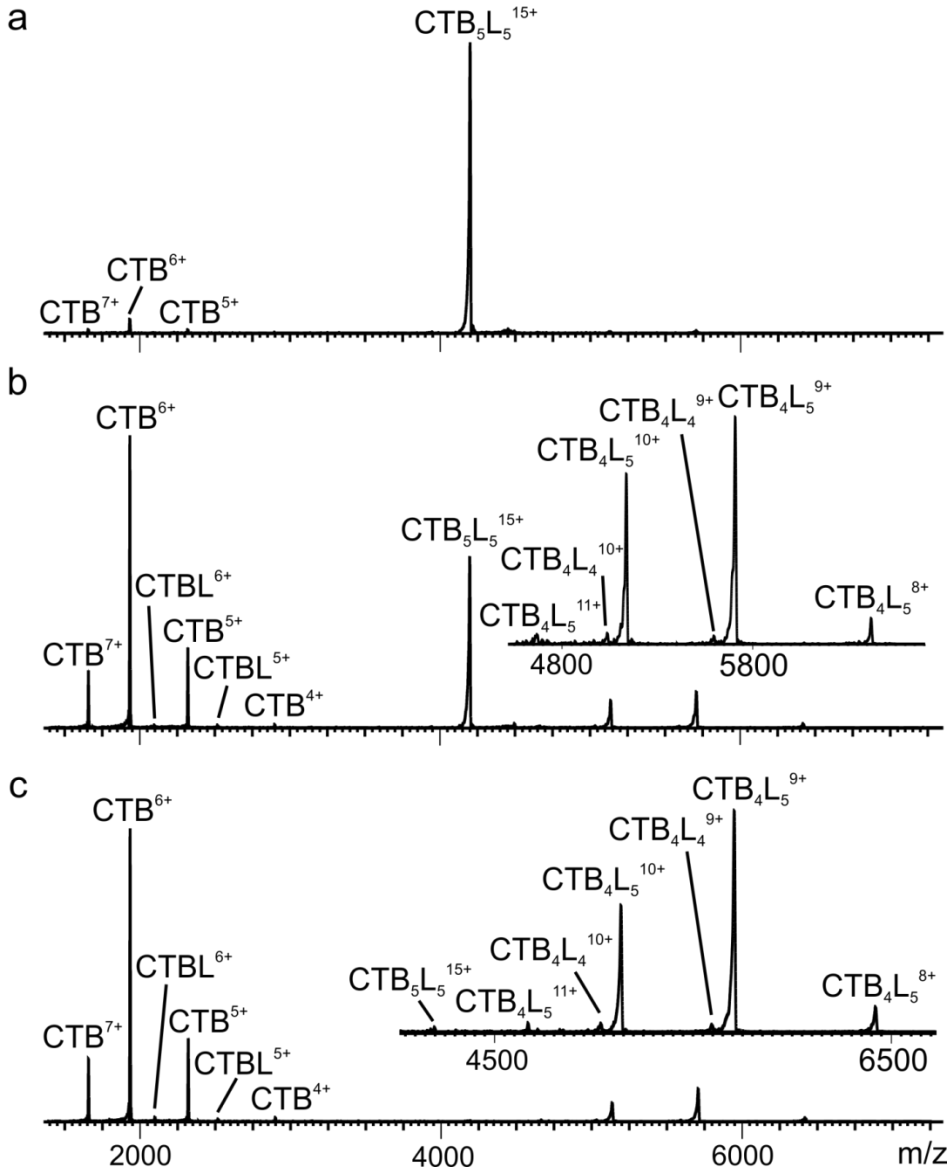

Figure 3.6 CID mass spectra in positive mode of the $(CTB_5 + 5L)^{15+}$ ion (where L = GM1) at a collision energy of (a) 20 V, (b) 40 V and (c) 50 V.

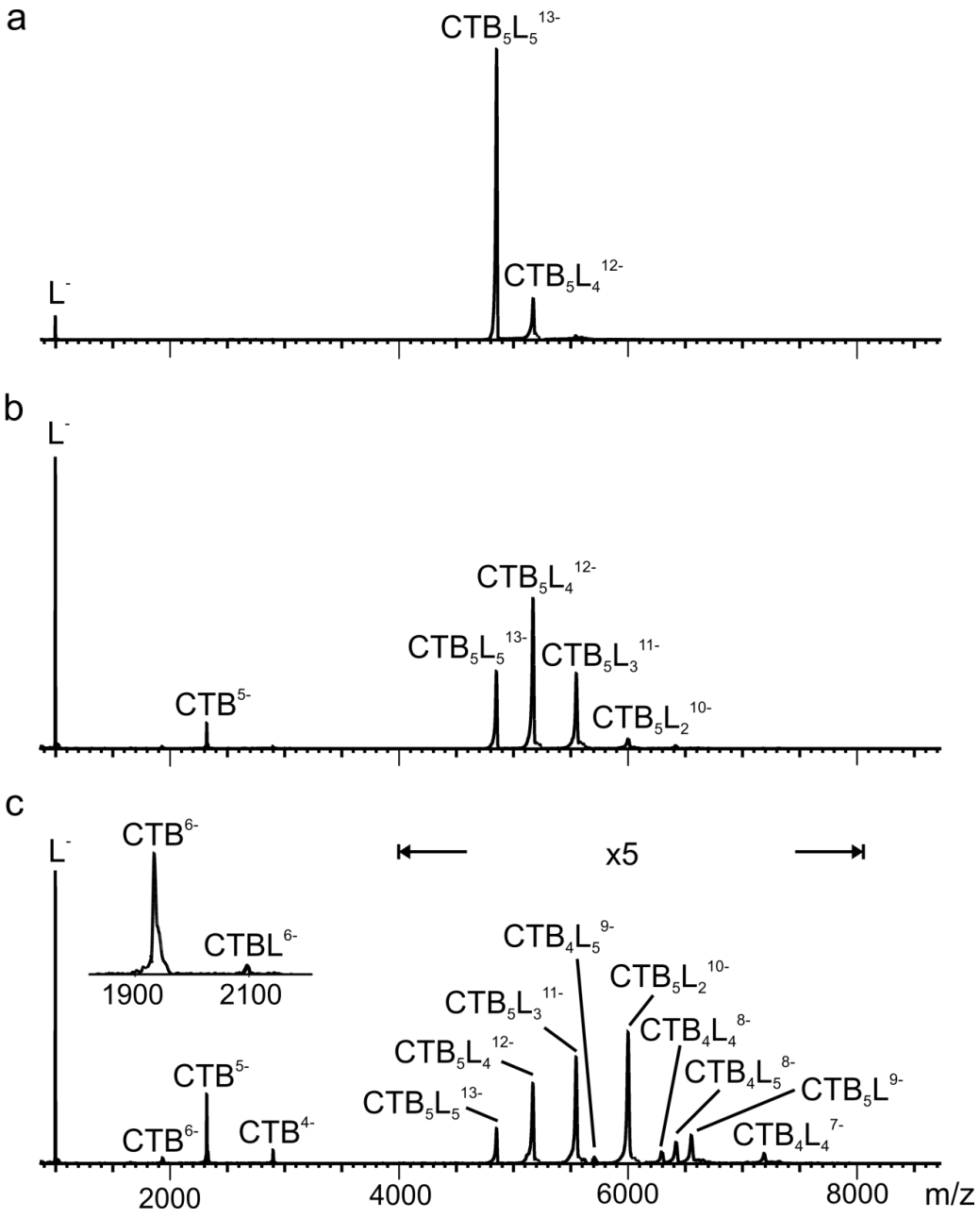

Figure 3.7 CID mass spectra in negative mode of the $(CTB_5 + 5L)^{13-}$ ion (where L = GM1), at a collision energy of (a) 10 V, (b) 30 V and (c) 50 V. The intensities in the m/z range 4000 – 8000 (c) were magnified x5.

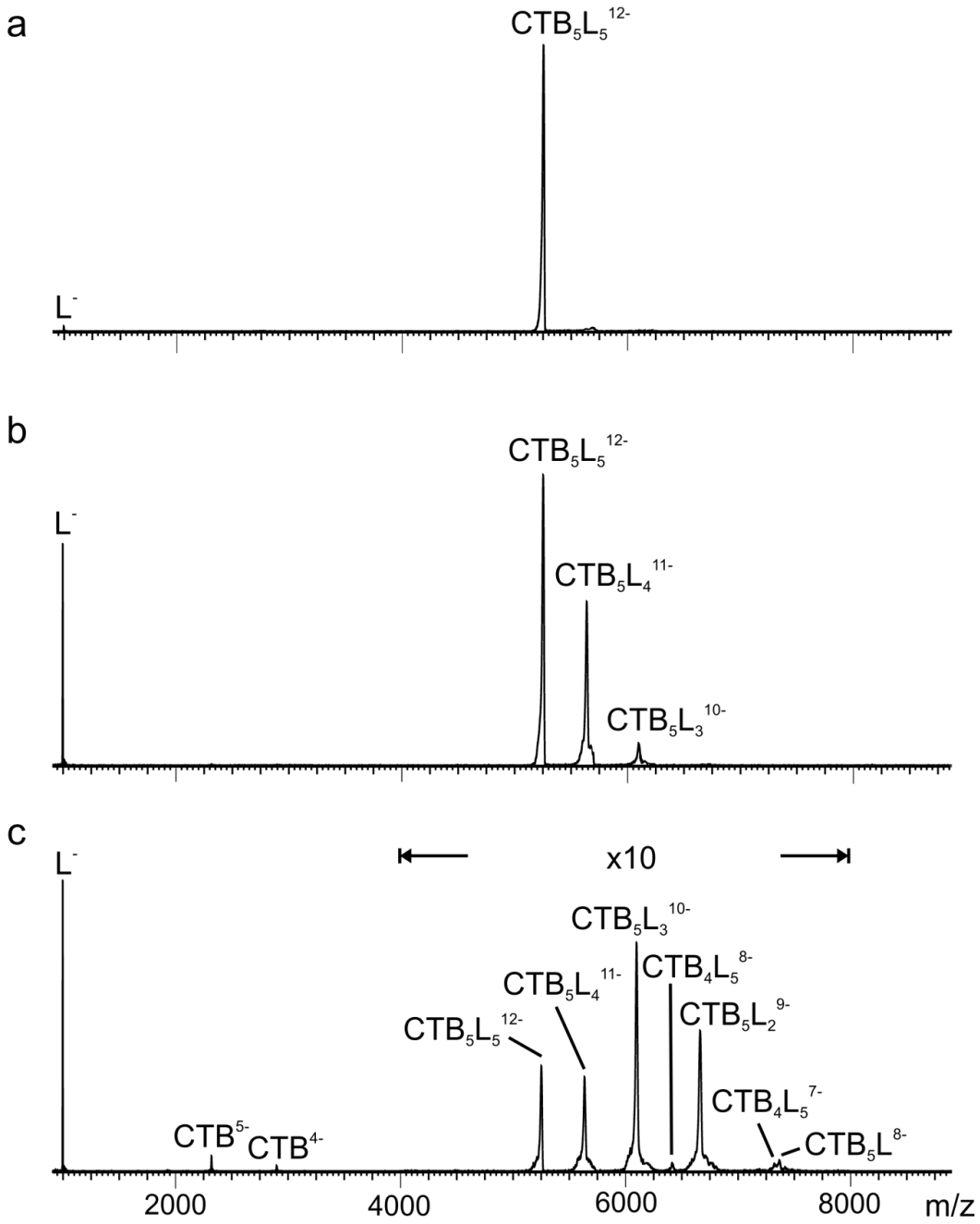

Figure 3.8 CID mass spectra in negative mode of the $(CTB_5 + 5L)^{12-}$ ion (where L = GM1) at a collision energy of (a) 10 V, (b) 30 V and (c) 60 V. The intensities in the m/z range 4000 – 8000 (c) were magnified x10.

The CID results obtained for protonated and deprotonated ions of the (CTB_5 + 5GM1) and (CTB_5 + 5GM1-Cer) complexes are intriguing. The loss of a single subunit, free of ligand, necessarily requires that the ligand originally bound to the ejected subunit migrate to another subunit. The migration process is, presumably, induced upon collisional heating of the gaseous complex. It is also possible that migration occurs prior to CID (i.e.; during or after desolvation the complex). However, this possibility is viewed as unlikely given that the intermolecular interactions in a number of protein-ligand complexes have been shown to be preserved upon transfer of the complexes from solution to the gas phase.[47, 62-67] The observation of ligand migration between subunits is, perhaps, a surprising finding given that it is generally accepted that the loss of a charge-enriched subunit requires unfolding.[22-24, 34, 68-70] Subunit unfolding would, in turn, be expected to result in the loss of intermolecular protein-ligand interactions and, consequently, the loss of the ligand from the complex. However, for the protonated complexes, GM1 loss is not observed under any conditions. The absence of this pathway would seem to suggest a high kinetic barrier to the cleavage of the intermolecular interactions. However, these same interactions are necessarily lost during the migration process (to a neighbouring subunit). While the exact mechanisms of ligand migration cannot be established from the CID results alone, the experimental observations can be reasonably explained in terms of a multistep mechanism involving bond (intermolecular) cleavage and formation of protein-ligand interactions. According to this view, the energetic penalty associated with the cleavage of the intermolecular interactions (presumably H-

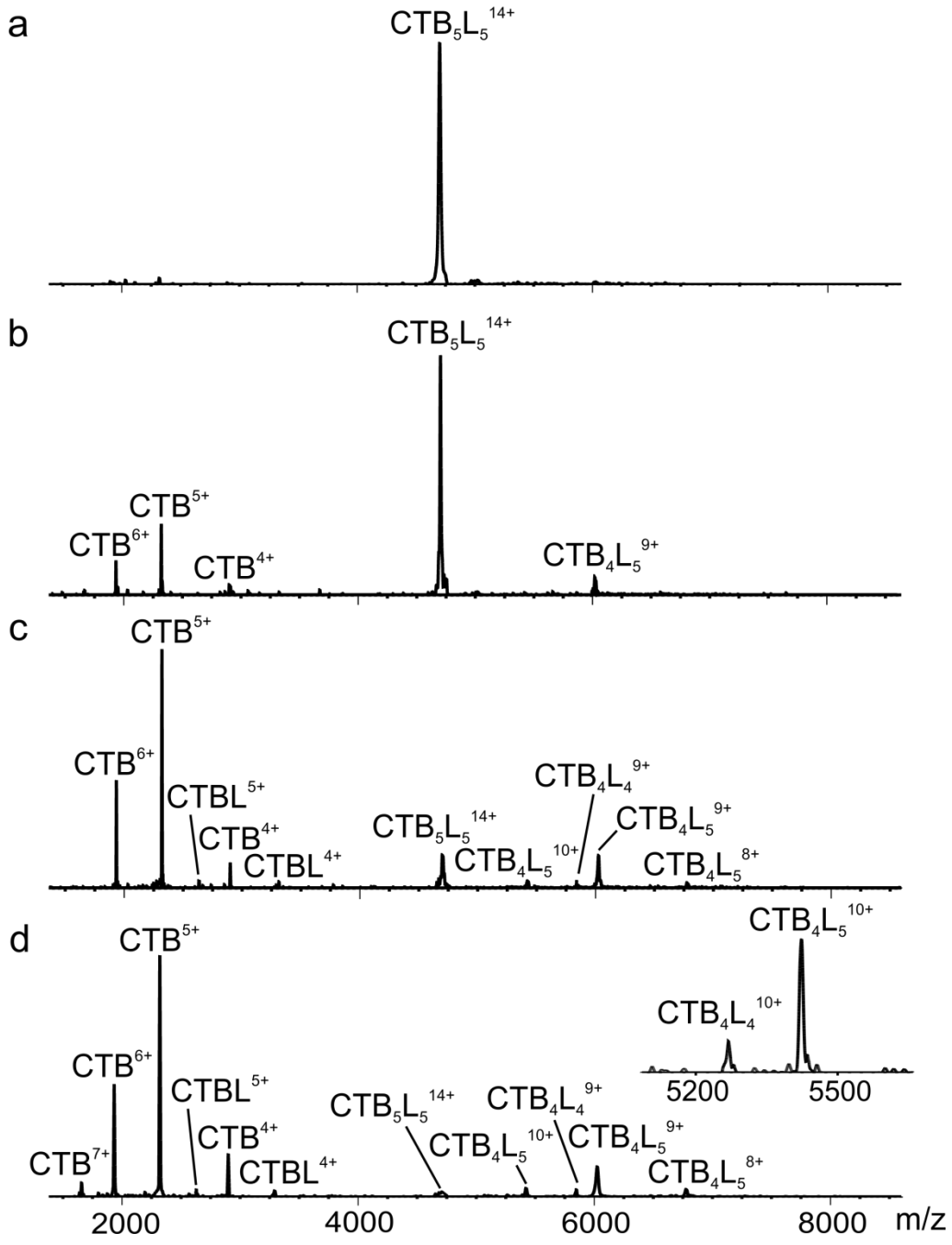

Figure 3.9 CID mass spectra of the $(CTB_5 + 5L)^{14+}$ ion, where L ≡ GM1-Cer, at a collision energy of (a) 30 V, (b) 40 V, (c) 50 V, and (d) 60V.

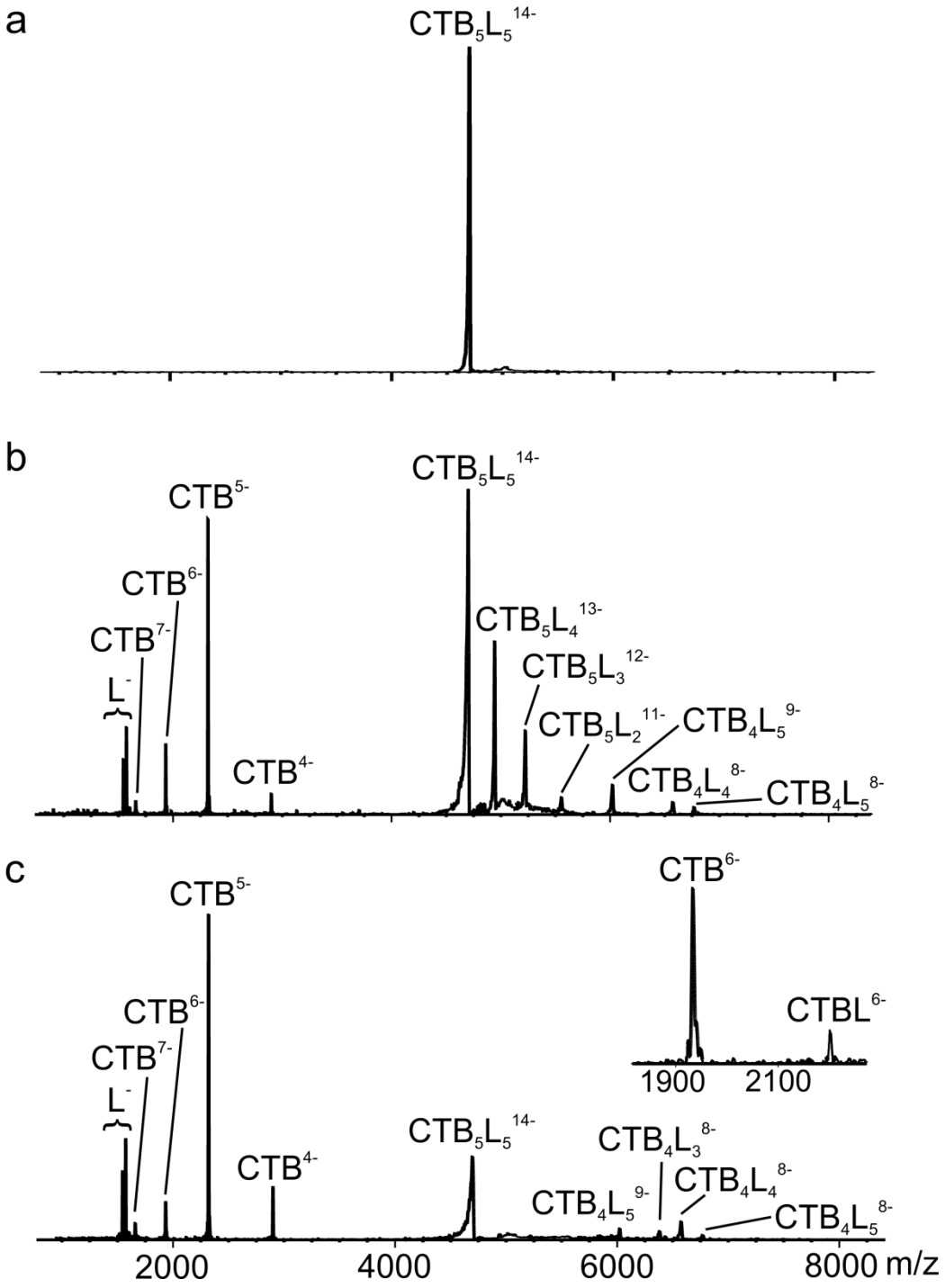

Figure 3.10 CID mass spectra of the $(CTB_5 + 5L)^{14-}$ ion, where L ≡ GM1-Cer, at a collision energy of (a) 10 V, (b) 30 V and (c) 55 V.

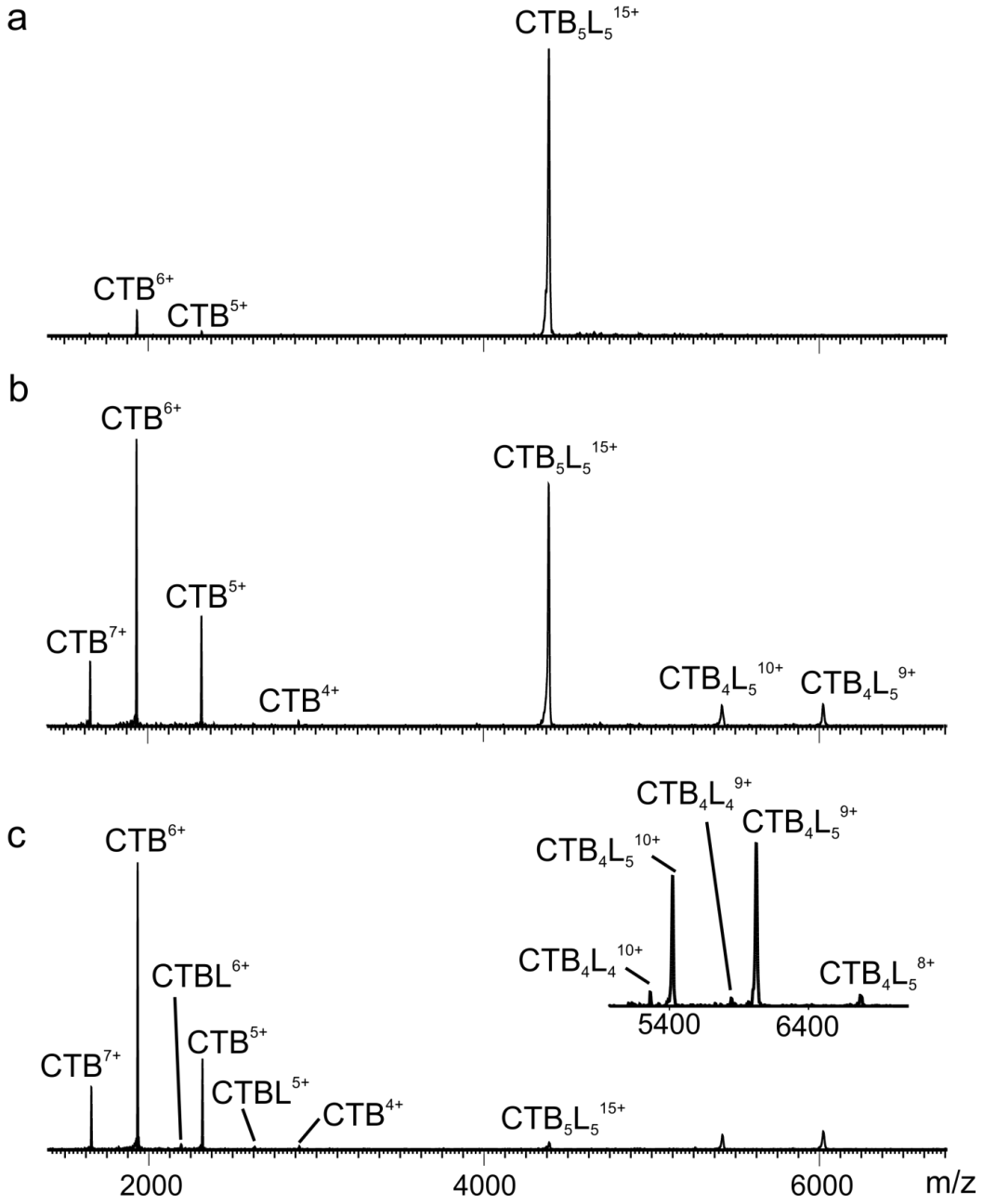

Figure 3.11 CID mass spectra in positive mode of the $(CTB_5 + 5L)^{15+}$ ion (where L = GM1-Cer) at a collision energy of (a) 20 V, (b) 40 V and (c) 50 V.

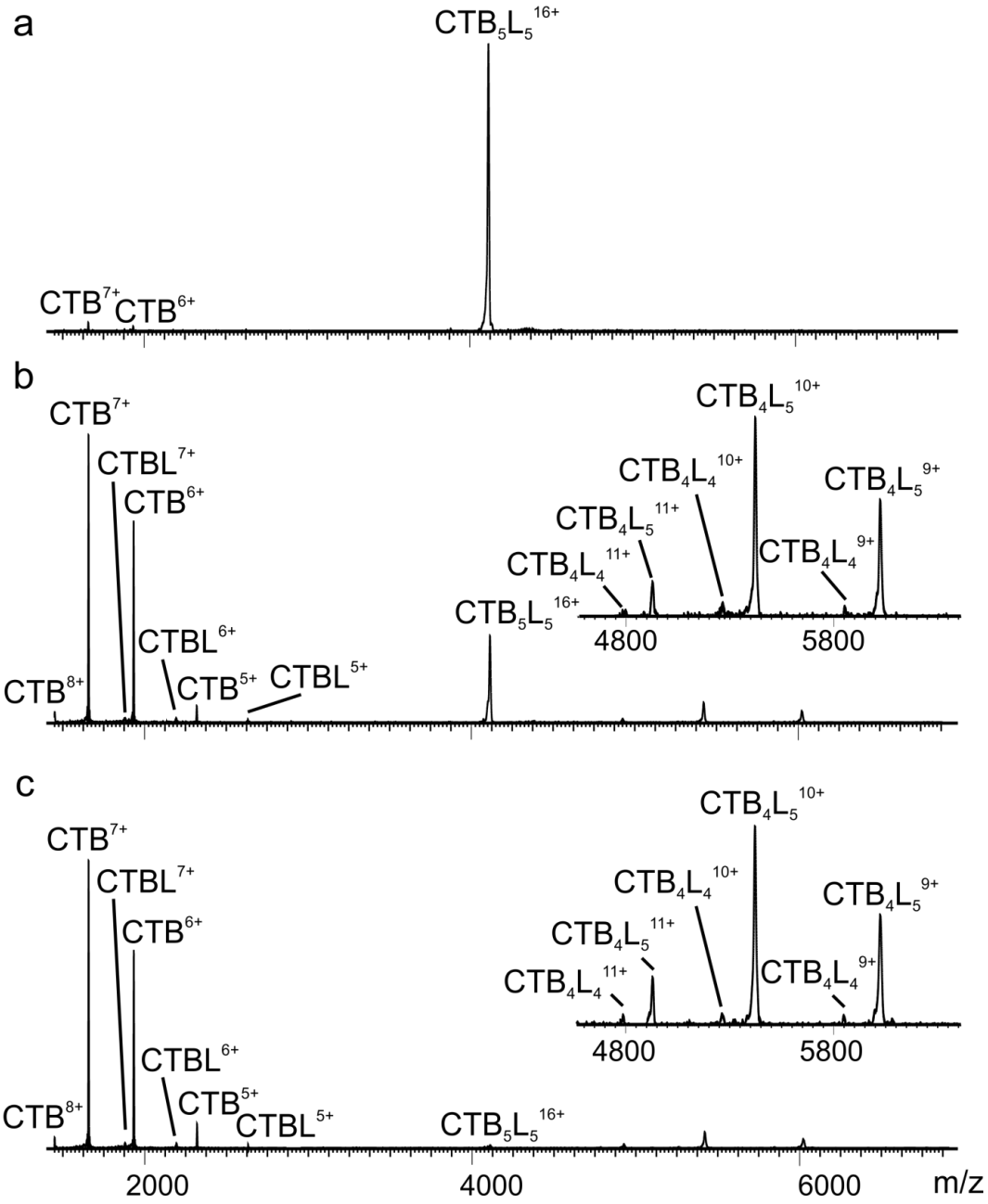

Figure 3.12 CID mass spectra in positive mode of the $(CTB_5 + 5L)^{16+}$ ion (where L = GM1-Cer) at a collision energy of (a) 20 V, (b) 40 V and (c) 50 V.

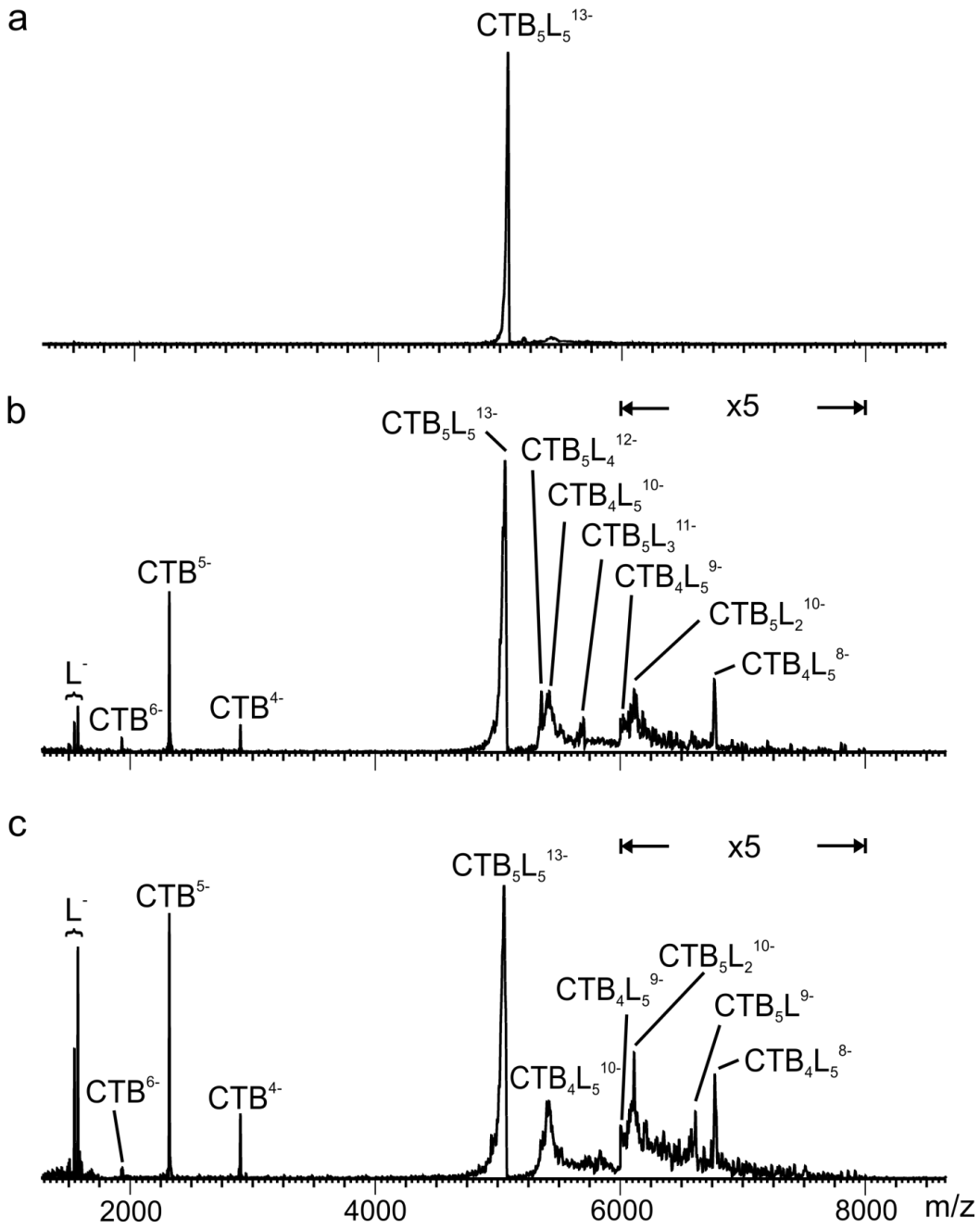

Figure 3.13 CID mass spectra in negative mode of the $(CTB_5 + 5L)^{13-}$ ion, ion (where L = GM1-Cer) at a collision energy of (a) 10 V, (b) 45 V and (c) 65 V. In (b) and (c) the intensities in the m/z range 6000 - 8000 were magnified x5.

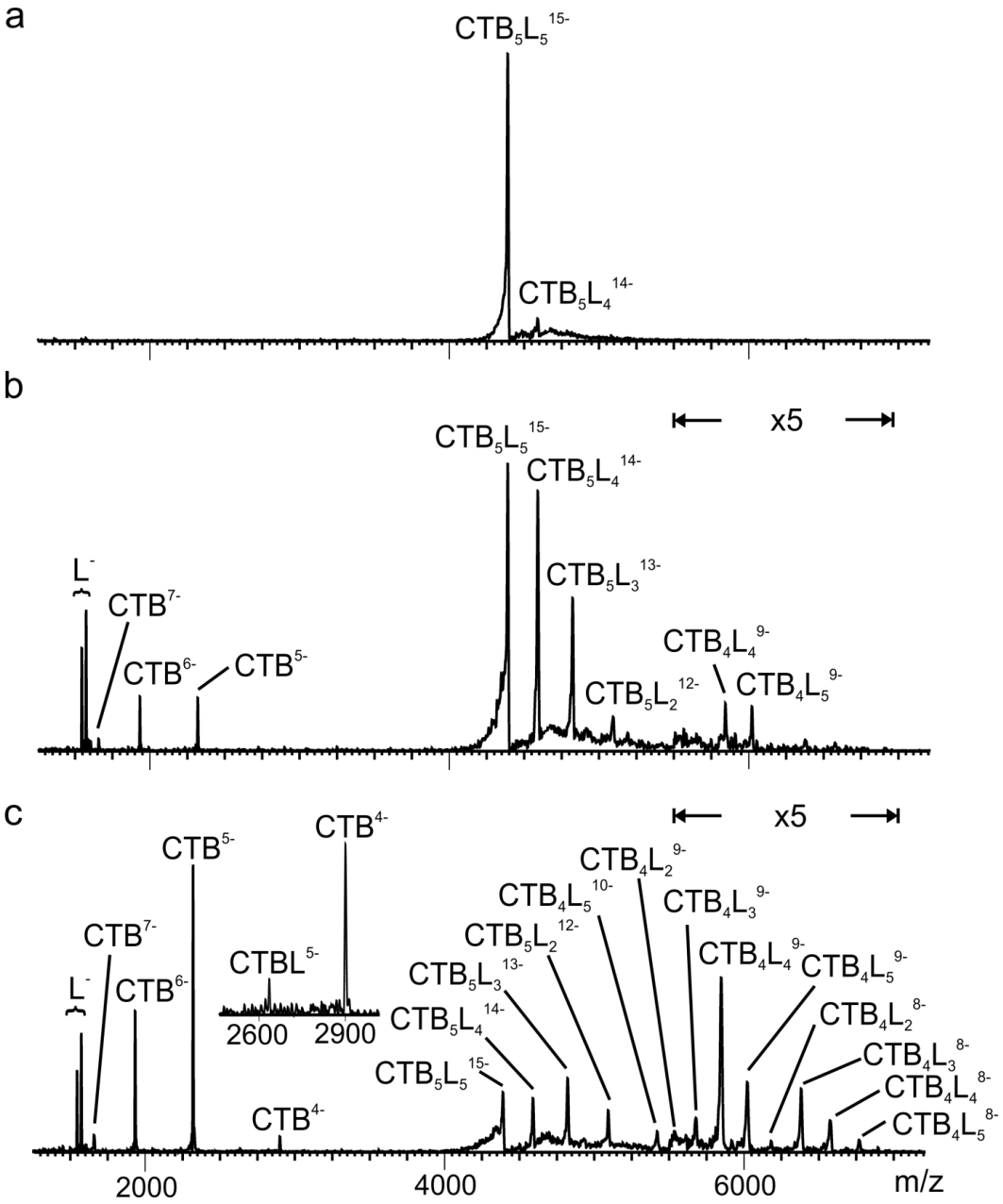

Figure 3.14 CID mass spectra in negative mode of the $(CTB_5 + 5L)^{15-}$ ion (where L = GM1-Cer) at a collision energy of (a) 10 V, (b) 30 V and (c) 40 V. In (b) and (c) the intensities in the m/z range 5500 - 7000 were magnified x5.

Table 3.2 Average charge states (*ACS*) of the CTB, (CTB + GM1) and (CTB + GM1-Cer) product ions observed by CID of protonated and deprotonated $(CTB_5 + 5GM1)^{n+/-}$, $(CTB_5 + 5GM1\text{-}Cer)^{n+/-}$ and $(CTB_5)^{n+/-}$ ions.

Parent ion	n (charge state of parent ion)	x (*ACS* of leaving CTB)	y (*ACS* of leaving (CTB+GM1))	(x/n) %	(y/n) %
$(CTB_5 + 5GM1)$	14+	(5.3 ±0.1)+	(4.8 ±0.1)+	38%	34%
	15+	(5.9 ±0.1)+	(5.6 ±0.1)+	39%	37%
	12-	(4.8 ±0.1)-	n/a	40%	n/a
	13-	(4.9 ±0.1)-	(5.3 ±0.3)- [a]	38%	41%
	14-	(5.2 ±0.1)-	(5.5 ±0.1)- [a]	37%	39%
$(CTB_5 + 5GM1\text{-}Cer)$	14+	(5.2 ±0.1)+	5+ [b]	37%	36%
	15+	(5.9 ±0.1)+	(5.7 ±0.1)+	39%	38%
	16+	(6.5 ±0.1)+	(6.4 ±0.1)+	41%	40%
	13-	(4.8 ±0.1)-	n/a	37%	n/a
	14-	(5.0 ±0.1)-	6- [a,b]	36%	43%
	15-	(5.4 ±0.2)-	(5.3 ±0.4)- [a]	36%	35%
CTB_5 [c]	14+	(5.3 ±0.1)+	n/a	38%	n/a
	15+	(5.9 ±0.1)+	n/a	39%	n/a
	16+	(6.3 ±0.1)+	n/a	39%	n/a
	12-	(5.0 ±0.1)-	n/a	42%	n/a
	13-	(5.1 ±0.1)-	n/a	39%	n/a
	14-	(5.5 ±0.1)-	n/a	39%	n/a

a. These product ions were observed only at higher collision energies (>40V).

b. Only a single charge state was observed.

c. CID mass spectra not shown.

bonds) with the subunit to which the ligand was originally bound is offset by the formation of new interactions with one or more of the other subunits. Moreover, that the presence of ceramide enhances the simultaneous loss of CTB subunit and GM1-Cer for the $(CTB_5 + 5GM1\text{-}Cer)^{n-}$ ions suggests that the long acyl chains of the ceramide moiety help to stabilize the nonspecific, nonpolar interactions with the subunit. The suggestion is supported by the results of recent studies of the dissociation kinetics of gaseous complexes of bovine β-lactoglobulin and long chain fatty acids, which revealed the gaseous complexes are stabilized predominantly by protein-lipid interactions.[64, 67, 71]

Equally intriguing is the observation of the simultaneous loss of a subunit bound to GM1. On its own, this finding would seem to suggest that ligand binding does not necessarily preclude subunit unfolding. Some insight into the degree of subunit unfolding can be gleaned from the *ACS* measured for the ejected subunits and subunit-ligand complexes from the $(CTB_5 + 5GM1)^{n+}$, $(CTB_5 + 5GM1\text{-}Cer)^{n+}$ ions (Table 3.2). For the protonated ions, it can be seen that the charge states of the $(CTB + GM1)^{y+}$ and $(CTB + GM1\text{-}Cer)^{y+}$ product ions are similar to those of the corresponding CTB^{x+} ions produced from the same reactant ion. Assuming that the *ACS* of the leaving subunit correlates with its surface area[22-24], these results suggest that ligand binding does not preclude unfolding.

That the deprotonated $(CTB_5 + 5GM1)^{n-}$ ions dissociate preferentially by the loss of deprotonated GM1, as opposed to subunit ejection, can be explained in terms of the relatively low gas phase acidities of carbohydrates and their ability to effectively compete for charge with the protein[63, 72] and the influence of

Coulombic repulsion on the dissociation kinetics. As discussed elsewhere[22, 34, 73], Coulombic repulsion between charged product ions produced from gaseous noncovalent protein complexes will lead to a reduction in the dissociation activation energy (E_a). Consequently, the E_a for the loss of deprotonated GM1 is expected to be significantly lower than for the loss of neutral GM1 and, presumably, lower than for GM1 migration to another subunit.

3.3.2 CID of $(S_4 + 4B)^{n+/-}$ and $(S_4 + 4Btl)^{n+/-}$ ions

The CID results obtained for the $(CTB_5 + 5GM1)^{n+/-}$ and $(CTB_5 + 5GM1\text{-}Cer)^{n+/-}$ ions provide evidence for the occurrence of ligand migration between subunits upon collisional activation. To test whether the phenomenon of ligand migration is general for multisubunit protein-ligand complexes in the gas phase, CID measurements were extended to the $(S_4 + 4B)^{n+/-}$ and $(S_4 + 4Btl)^{n+/-}$ ions. Shown in Figure 3.15 are ESI mass spectra acquired in both positive and negative ion mode for an aqueous ammonium acetate (200 mM) solution of S_4 (5 μM) and B (20 μM). The most abundant protein ions detected corresponded to protonated or deprotonated homotetramer bound to four B molecules, i.e.; $(S_4 + 4B)^{n+}$ at charge states +15 and +16 (Figure 3.15a) and $(S_4 + 4B)^{n-}$ ions at charge states -12, -13 and -14 (Figure 3.15b). Representative CID mass spectra obtained for the $(S_4 + 4B)^{15+}$ and $(S_4 + 4B)^{16+}$ ions are shown in Figures 3.16 and 3.17. The major dissociation pathway was the loss of B, either in its protonated or neutral forms. The loss of a single subunit, i.e.; S^{x+}, with an *ACS* of x = 6.8 ± 0.1 (+15) and 6.9 ± 0.1 (+16), was observed as a minor pathway (Table 3.3); the contribution of this pathway appeared to be enhanced at higher collision energies. Because substantial

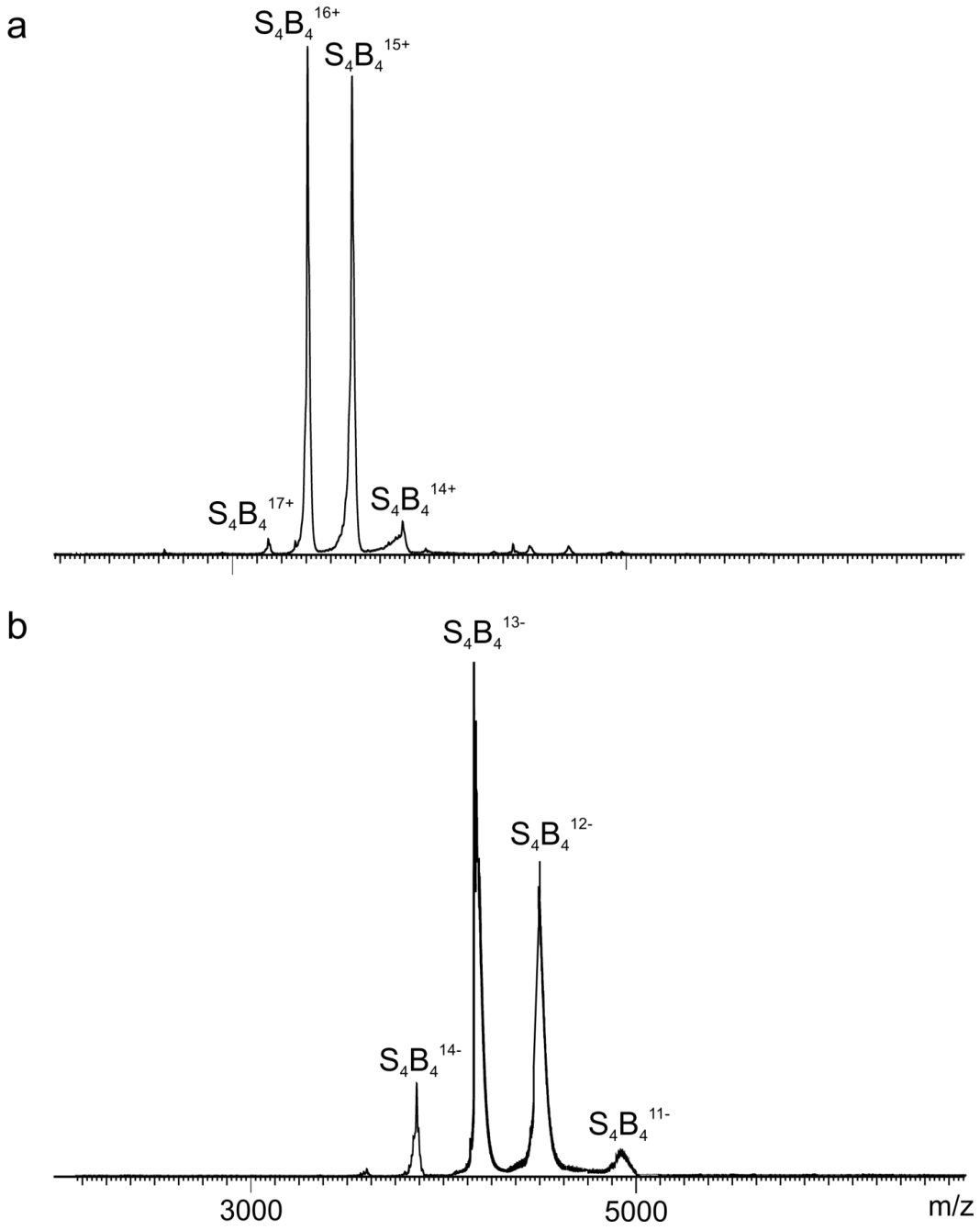

Figure 3.15 ESI mass spectra acquired in (a) positive and (b) negative ion mode for aqueous ammonium acetate (200 mM) solution of (5 μM) S_4 and (20 μM) B.

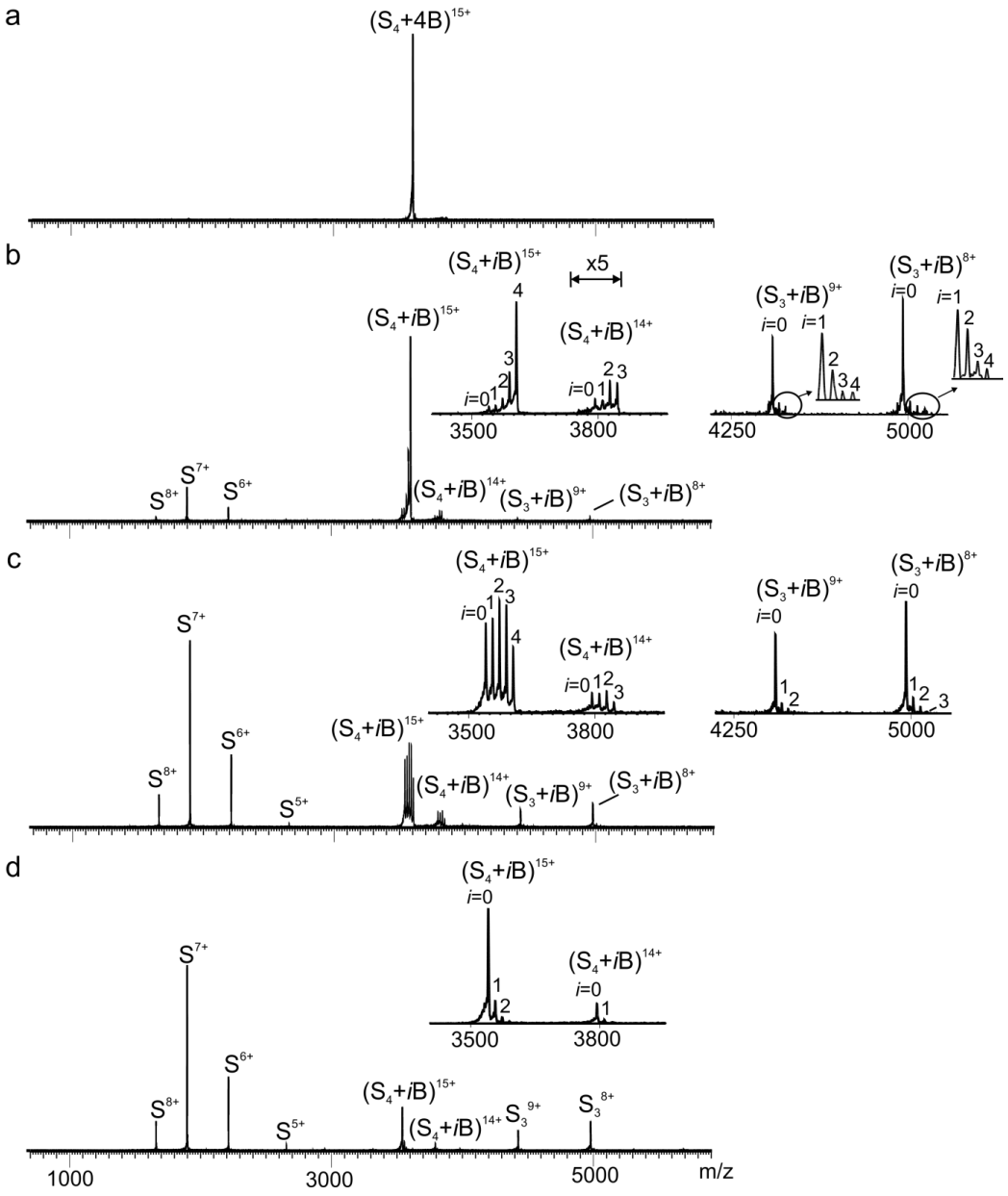

Figure 3.16 CID mass spectra in positive mode of the $(S_4 + 4B)^{15+}$ ion at a collision energy of (a) 3 V, (b) 26 V, (c) 32 V, and (d) 38 V. In the inset of (b), the intensities in the m/z range 3750 - 3850 were magnified x5.

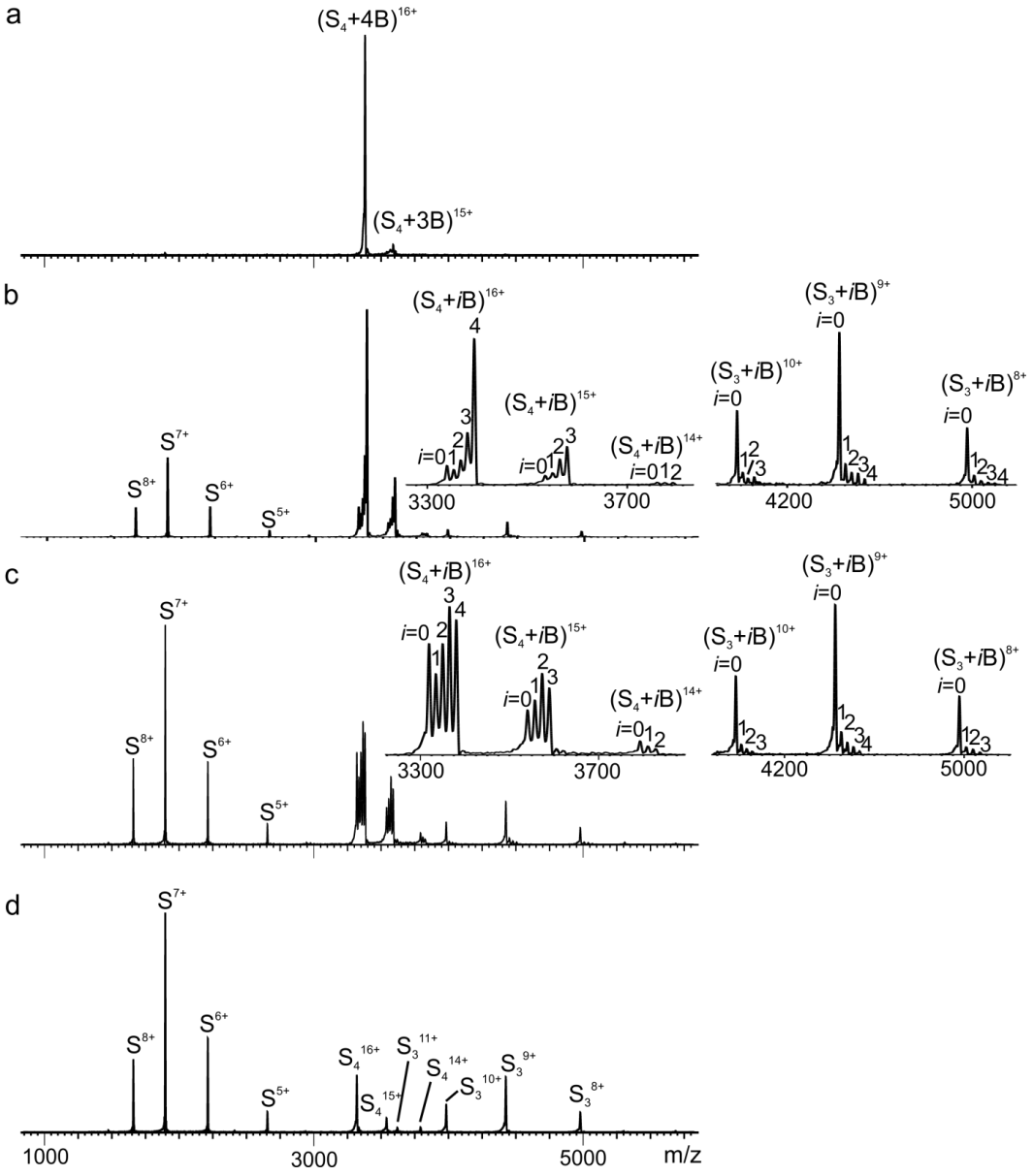

Figure 3.17 CID mass spectra in positive mode of the $(S_4 + 4B)^{16+}$ ion at a collision energy of (a) 3 V, (b) 24V, (c) 28 V and (d) 36 V.

loss of B was observed under the CID conditions used, it is not possible to conclude whether ligand migration take place prior to subunit ejection based solely on the appearance of S^{x+} ions. However, within a narrow range of collision energies (26-30V for +15 and 12 - 30 V for +16), $(S_3 + 4B)^{(n-x)+}$ ions could be detected, although at low abundance. These results confirm that collisional activation does promote ligand migration between subunits.

Representative CID mass spectra of the $(S_4 + 4Btl)^{15+}$ and $(S_4 + 4Btl)^{16+}$ ions are shown in Figures 3.18 and 3.19, respectively. Interestingly, the loss of a subunit (*ACS* of the S^{x+} product ions are 7.1 $\pm$ 0.1 for +15 and 7.3 $\pm$ 0.1 for +16, Table 3.3) was the major dissociation pathway observed at all collision energies investigated (this pathway is enhanced by 85% compared to the same pathway involving $(S_4 + 4B)^{n+}$); no ligand loss was detected. These results indicate that PE, much like does ceramide, promotes ligand migration between subunits, presumably through the formation of nonspecific interactions with subunits. A minor pathway involving the loss of $(S + Btl)^{y+}$ ions, y = 6.8 $\pm$ 0.1 (+15) and 6.9 $\pm$ 0.1 (+16), was also identified. Curiously, the *ACS* of the S^{x+} product ions produced from the $(S_4 + 4Btl)^{n+}$ ions are somewhat larger than for S^{x+} ions produced from the corresponding $(S_4 + 4B)^{n+}$ ions (Table 3.3). On its own, this suggests that Btl migration promotes additional unfolding of the subunits. The reason for this effect is not clear.

For the deprotonated $(S_4 + 4B)^{n-}$ ions, at charge states -12 and -13, the sequential loss of B (in its neutral or deprotonated forms) was the only dissociation pathway observed at all collision energies investigated (Figure 3.20

and Figure 3.21, respectively). Similar results were obtained for the $(S_4 + 4Btl)^{13-}$ and $(S_4 + 4Btl)^{12-}$ ions, except that only the loss of deprotonated Btl was observed (Figure 3.22 and Figure 3.23, respectively).

Table 3.3 Average charge states (*ACS*) of the S subunit and (S + Btl) product ions observed by CID of protonated and deprotonated $(S_4 + 4B)^{n+/-}$ and $(S_4 + 4Btl)^{n+/-}$ ions.

Parent ion	n (charge state of parent ion)	x (*ACS* of leaving S)	y (*ACS* of leaving (S+Btl))	(x/n)%	(y/n)%
$(S_4 + 4B)$	15+	(6.8 ±0.1)+	n/a	45%	n/a
	16+	(6.9 ±0.1)+	n/a	43%	n/a
	12-	n/a	n/a	n/a	n/a
	13-	n/a	n/a	n/a	n/a
$(S_4 + 4Btl)$	15+	(7.1 ±0.1)+	(6.8 ±0.1)+	47%	45%
	16+	(7.3 ±0.1)+	(6.9 ±0.1)+	46%	43%
	11-	n/a	n/a	n/a	n/a
	12-	n/a	n/a	n/a	n/a
	13-	n/a	n/a	n/a	n/a

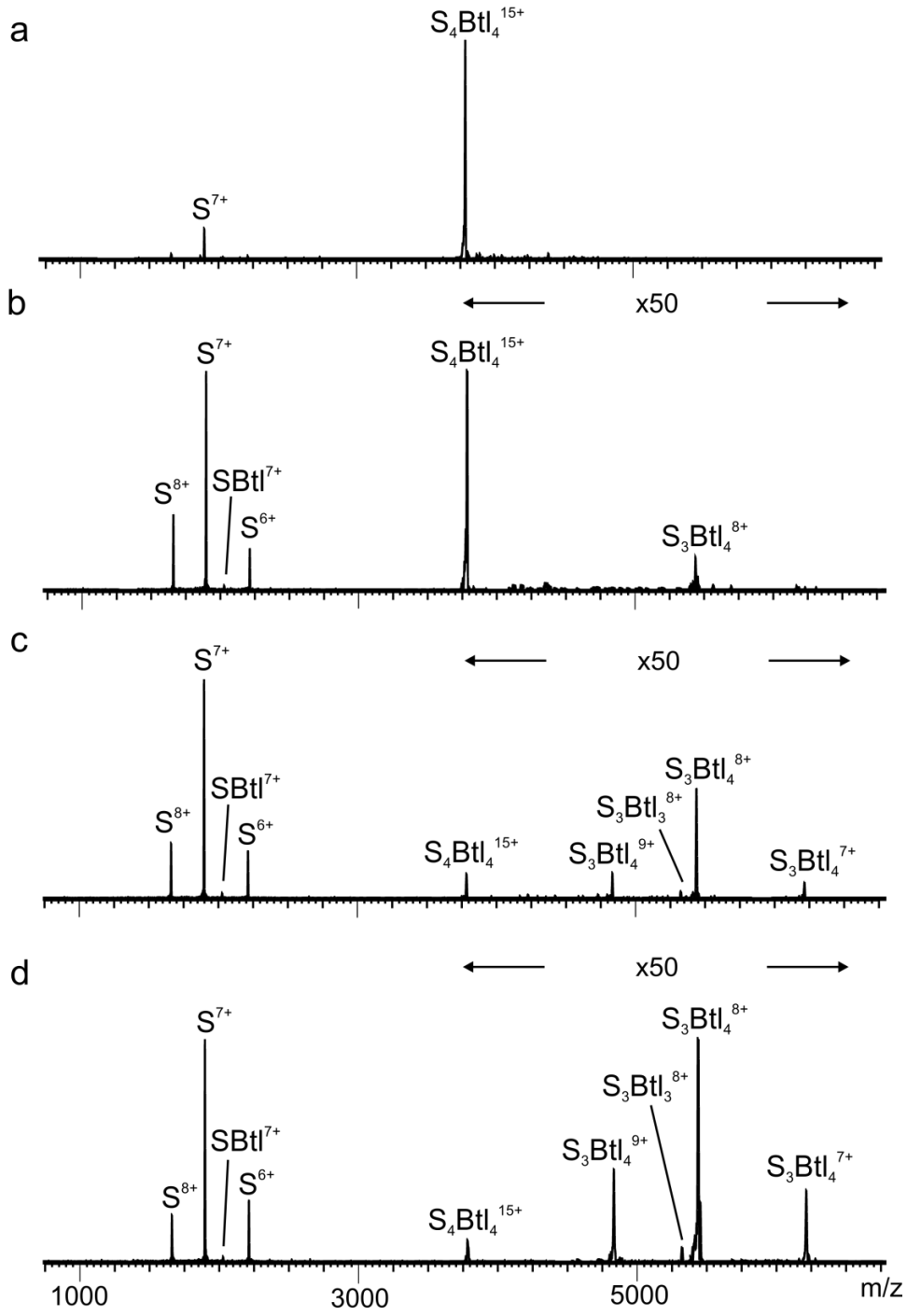

Figure 3.18 CID mass spectra in positive mode of the $(S4 + 4Btl)^{15+}$ ion at a collision energy of (a) 3 V, (b) 30 V, (c) 40 V, and (d) 50V. In (b), (c) and (d) the intensities in the m/z range 3700 - 6500 were magnified x50.

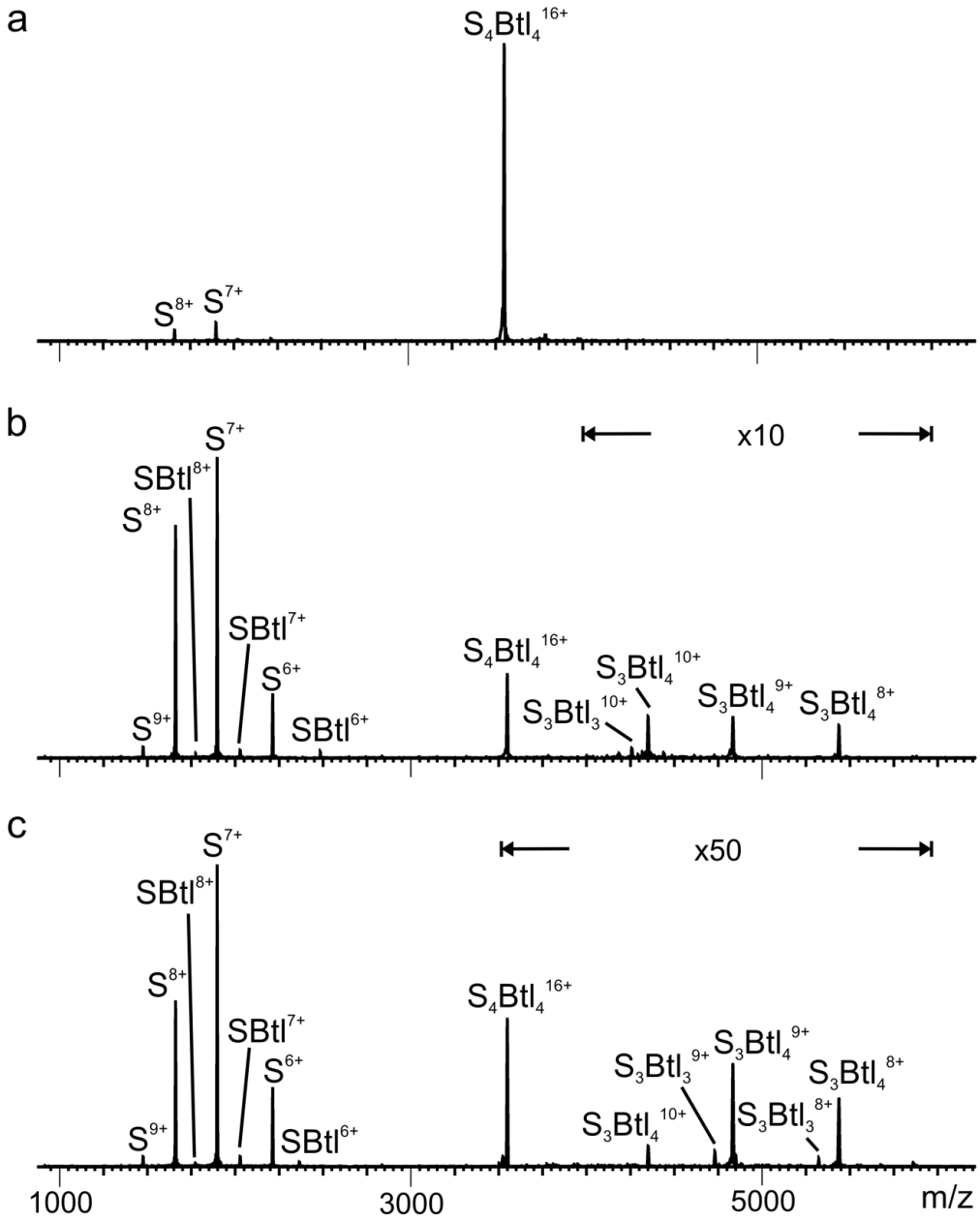

Figure 3.19 CID mass spectra in positive mode of the $(S_4 + 4Btl)^{16+}$ ion at a collision energy of (a) 3 V, (b) 25 V and (c) 40 V. In (b), the intensities in the m/z range 4000 - 6000 were magnified x10; in (c) the intensities in the m/z range 3500 - 6000 were magnified x50.

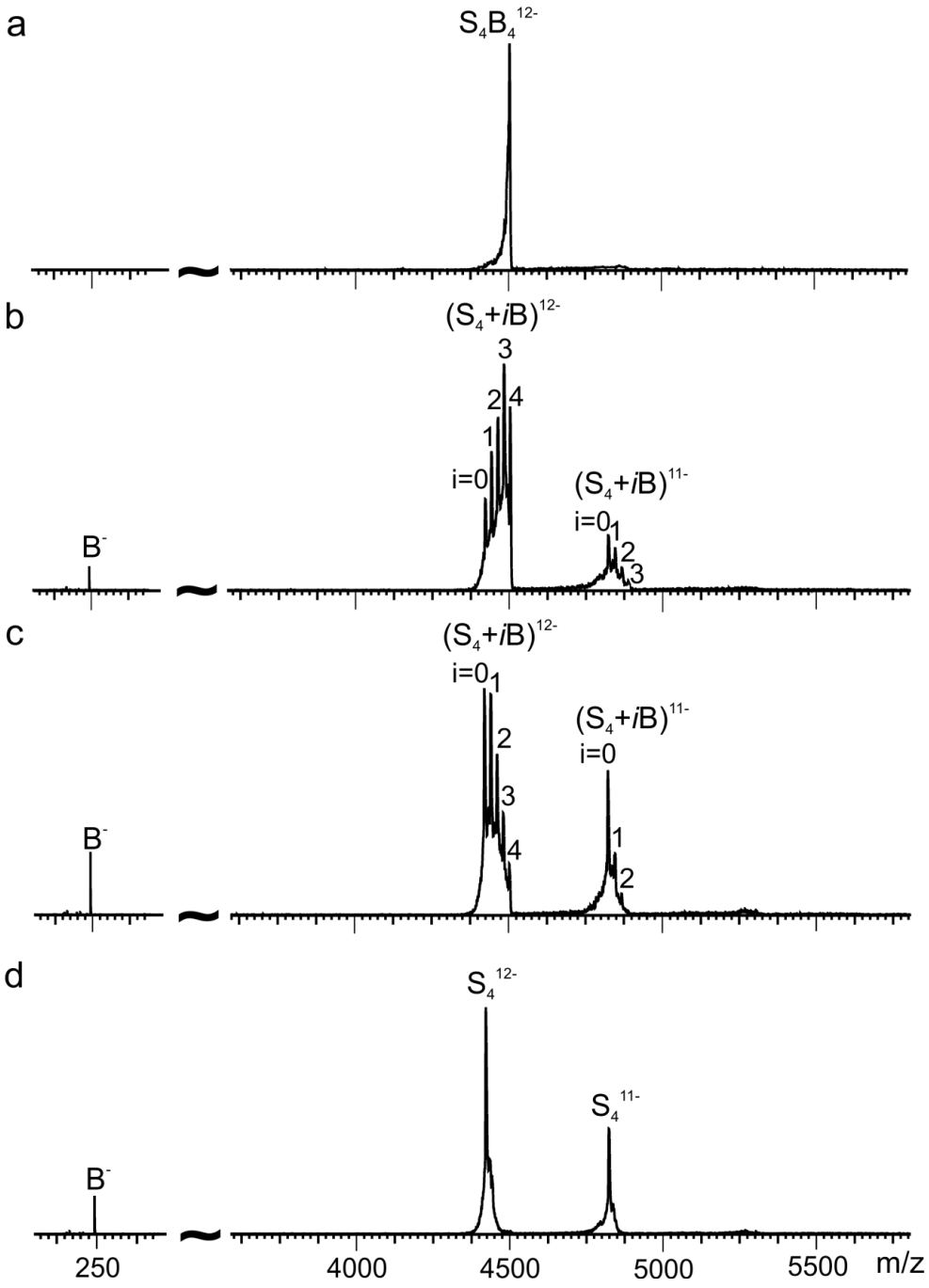

Figure 3.20 CID mass spectra in negative mode of the $(S_4 + 4B)^{12-}$ ion at a collision energy of (a) 3 V, (b) 28 V, (c) 32 V and (d) 40 V.

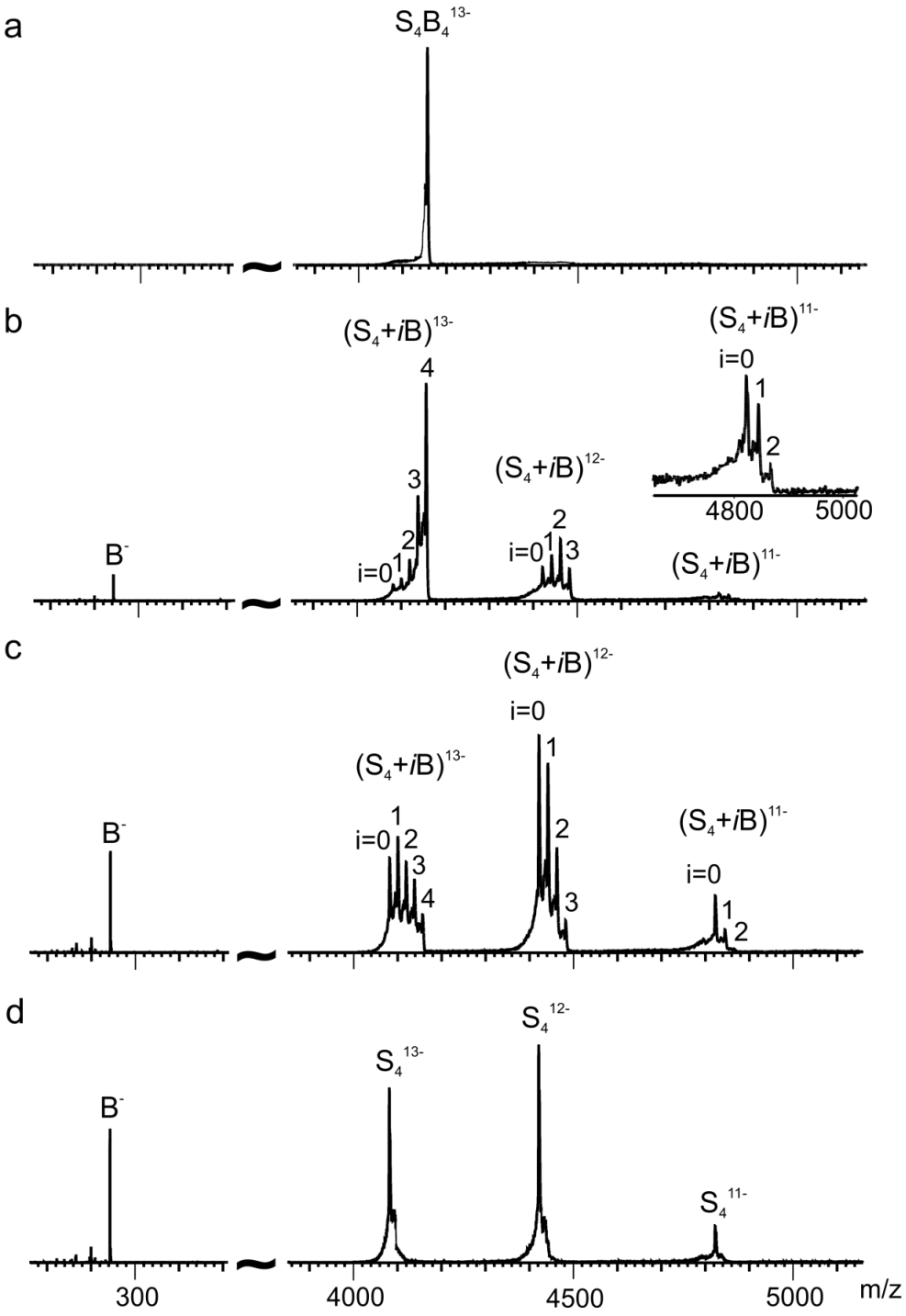

Figure 3.21 CID mass spectra in positive mode of the $(S_4 + 4B)^{13-}$ ion at a collision energy of (a) 3 V, (b) 20 V, (c) 26 V, and (d) 36 V.

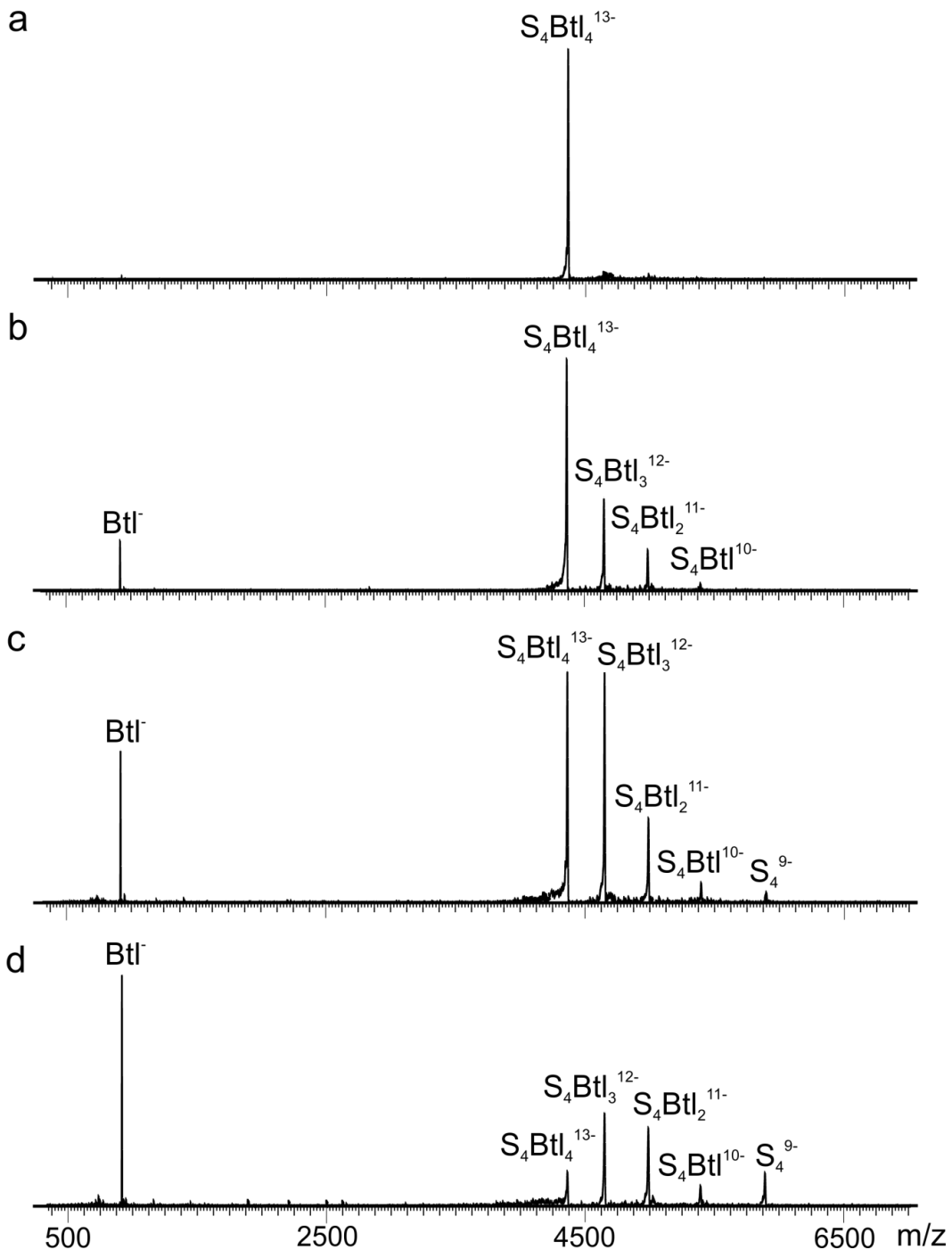

Figure 3.22 CID mass spectra in negative mode of the $(S_4 + 4Btl)^{13-}$ ion at a collision energy of (a) 3 V, (b) 20 V, (c) 40 V and (d) 60 V.

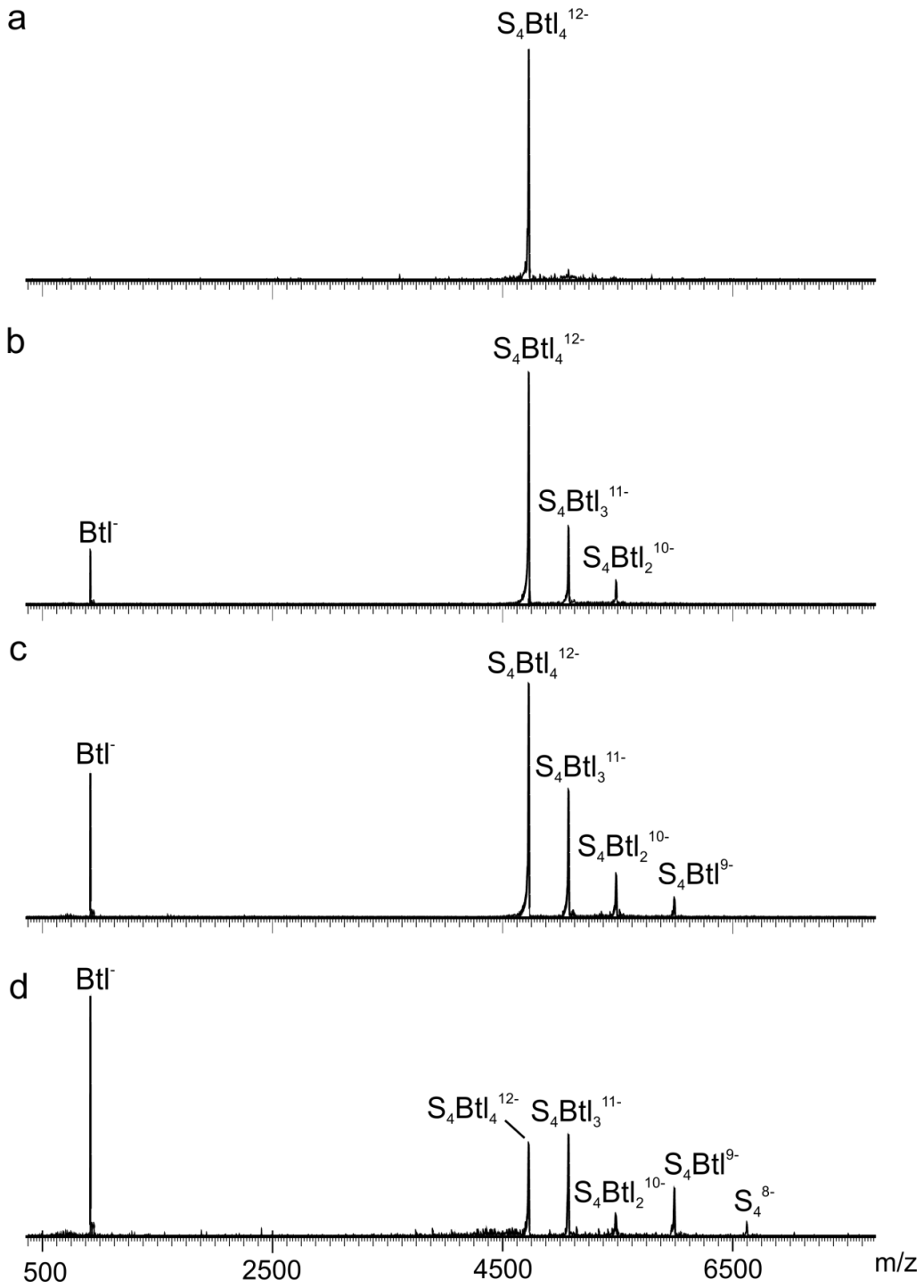

Figure 3.23 CID mass spectra in negative mode of the $(S_4 + 4Btl)^{12-}$ ion at a collision energy of (a) 3 V, (b) 20 V, (c) 40 V, and (d) 60V.

3.3.3 MD simulations

The aforementioned CID results confirm that ligand migration can generally occur upon collision activation of multiprotein-ligand complexes in the gas phase. However, on their own, they do not provide any insight into the underlying mechanisms. With the goal of elucidating the influence of charge on the ligand migration and subunit loss processes, MD simulations were performed on twelve different charge configurations of the $(CTB_5 + 5GM1)^{15+}$ ion in which seven charges were located on subunit D and two charges placed on each of other four subunits, E, F, G and H (Table 3.1). The GM1 ligands were assumed to be in their neutral form in all cases.

The initial structure of the $(CTB_5 + 5GM1)^{15+}$ ion used for the simulations is shown in Figure 3.24a. Shown in Figure 3.24b are plots of Rg measured along the trajectory for each of the twelve charge configurations considered. A common feature is a gradual increase in the magnitude of Rg of the ion with simulation time. This observation indicates that the overall size of the complex is increasing with time due to thermally-induced unfolding of the subunits. Interestingly though, all of the subunits, not just subunit D, exhibited significant unfolding. Analysis of the trajectories also reveals that, in all cases, the original interactions between GM1 and the CTB subunits were altered and the nature of the changes was strongly dependent on charge configuration. For nine (B15_1, B15_2, B15_3, B15_4, B15_6, B15_7, B15_10, B15_11 and B15_12) of the twelve configurations considered, ligand migration to another subunit was observed. However, the "donor" and "acceptor" subunits varied depending on configuration.

For charge configuration B15_12, GM1 migrated from subunit D to E (Figure 3.24c), from H to D for B15_3 (Figure 3.24d) and B15_7 (Figure 3.24e), from G to H for B15_1 (Figure 3.24f) and B15_6 (Figure 3.24g), from E to D for B15_4 (Figure 3.24h), and from F to G for B15_11 (Figure 3.24i). Interestingly, migration of more than one ligand was also observed for B15_2 (Figure 3.24j) and B15_10 (Figure 3.24k). For B15_2, GM1 molecules migrated from E to D and from G to H. In charge configuration B15_10, GM1 molecules originally bound to F and G migrated so as to bridge both subunits, similarly GM1 molecules on subunits D and E migrated so as to bridge both subunits and GM1 from subunit H migrated to the interface of D and H. For the three remaining charge state configurations, ligand migration within a subunit was observed. A representative structure from charge configuration B15_9 (at 1.5 ns) is shown in Figure 3.24l. GM1 located on the subunit D migrated from the original binding site to the N-terminus where it was stabilized by two ionic hydrogen bonds between charged N-terminal Thr and the branching Gal residue.

Although the results of the MD simulations must be viewed with caution, due to their inherent limitations (simulation time (ns) is much shorter compared to CID timescale (μs), charges cannot move, and uncertainty related to the simulation temperature), they do suggest that the migration of GM1 within and between subunits readily occurs upon heating of protonated $(CTB_5 + 5GM1)^{15+}$. These findings are consistent with the tendency of the $(CTB_5 + 5GM1)^{n+}$ ions to dissociate by the loss of subunit or subunit-ligand complex. The MD results also

suggest that the mechanism of ligand migration is highly dependent on the charge configuration.

For comparison purposes, MD simulations were also performed on the $(CTB_5 + 5GM1)^{14-}$ ion in which all five GM1 ligands were deprotonated (at the sialic acid residue); the other nine charges were distributed asymmetrically among the five subunits (five charges on subunit D and one charge on each of the other four subunits). Analysis of the MD trajectory reveals that sequential loss of deprotonated GM1; no ligand migration to other subunits was observed. These findings are consistent with the experimental observations. Interestingly, deprotonated GM1 was lost preferentially from subunits E and H, not from D; GM1 loss from D occurred only after the subunit underwent significant unfolding. The structure shown in Figure 3.24m was calculated at 1.5 ns, after the loss of four GM1 (initially on subunit D, E, F and H).

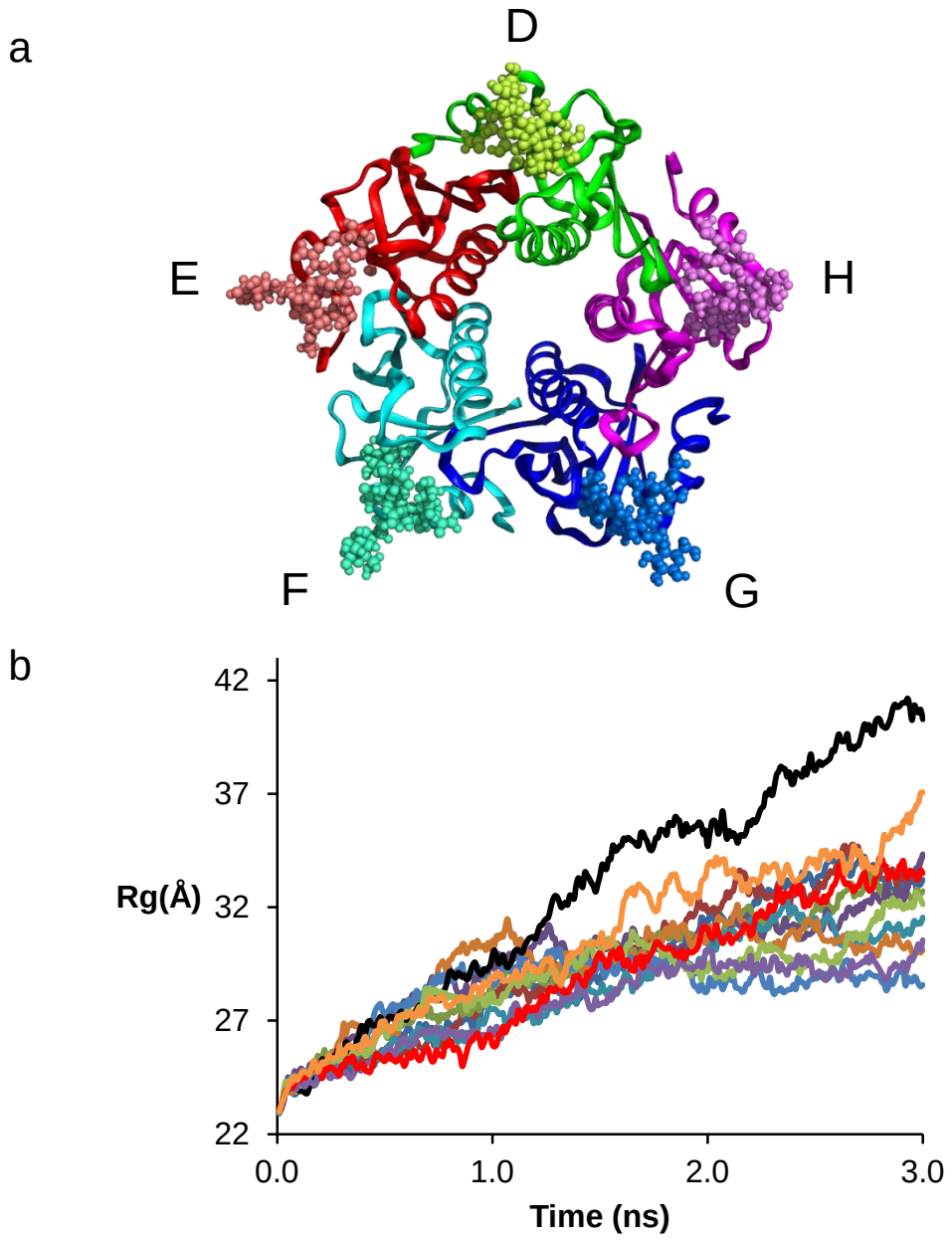

Figure 3.24 (a) Initial structure of the $(CTB_5 + 5GM1)^{15+}$ ion used for MD simulations. (b) Plots of Rg for 12 different charge configurations of $(CTB_5 + 5GM1)^{15+}$ ion calculated from the trajectories at 800 K. Charge configuration B15_1 (—), B15_2 (—), B15_3 (—), B15_4 (—), B15_5 (—), B15_6 (—), B15_7 (—), B15_8 (—), B15_9 (—), B15_10 (—), B15_11 (—), B15_12 (—).

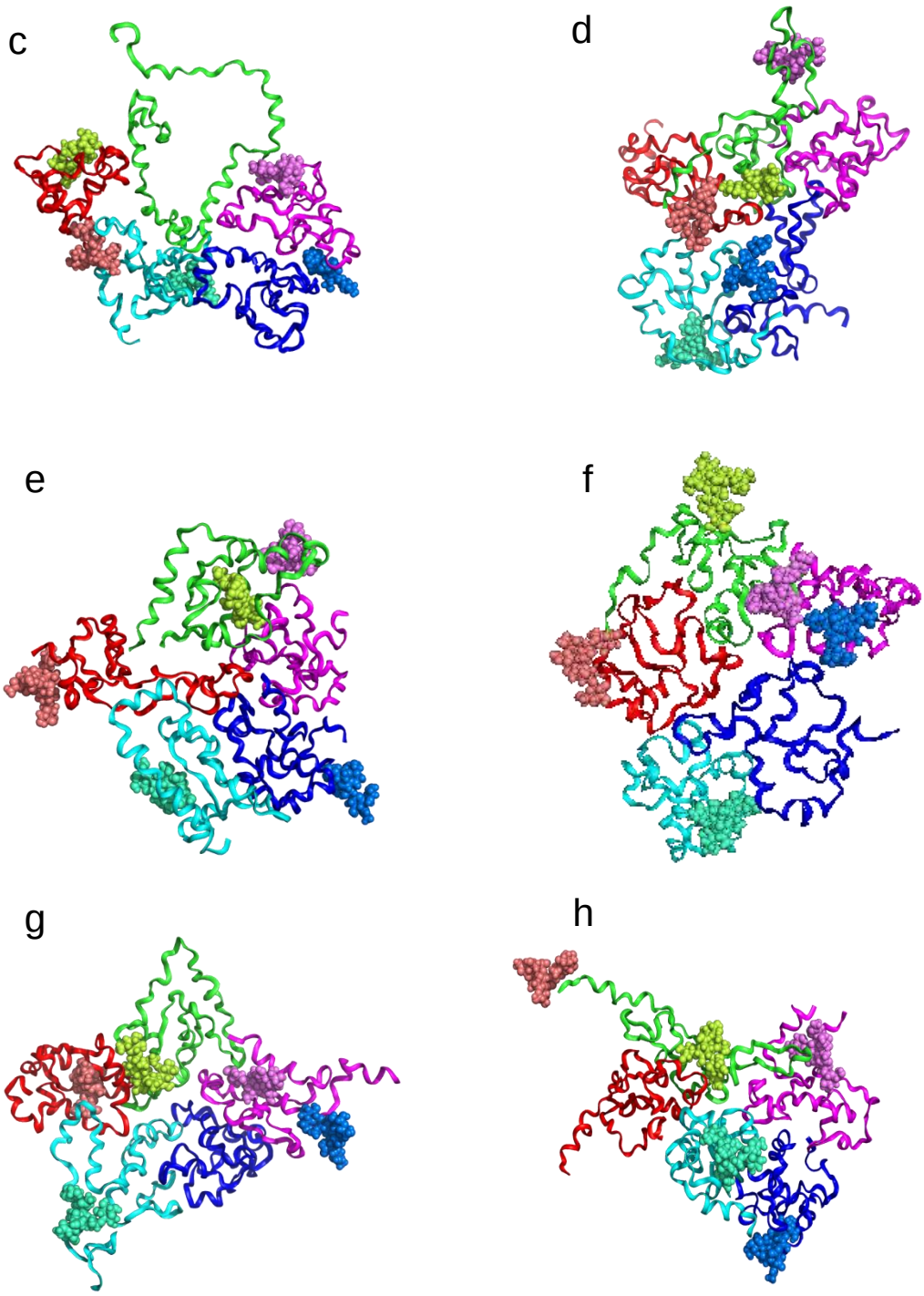

Figure 3.24 continued. (c)-(h) Representative structures taken at ~1.5 ns for charge configurations: (c) B15_12, (d) B15_3, (e) B15_7, (f) B15_1, (g) B15_6 and (h) B15_4.

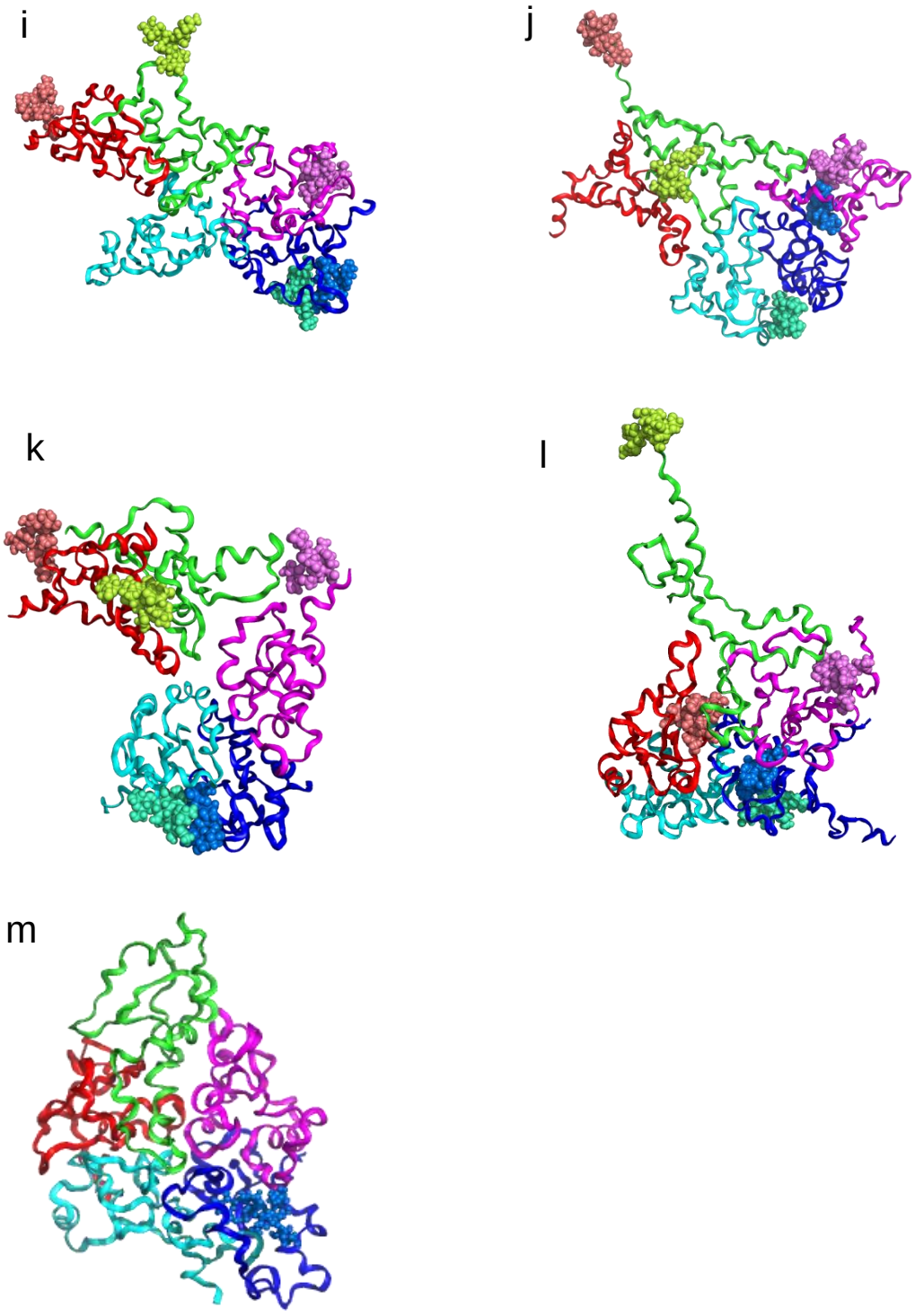

Figure 3.24 continued. (i)-(m) Representative structures taken at ~1.5 ns for charge configurations: (i) B15_11, (j) B15_2, (k) B15_10, (l) B15_9 and (m) B9_1. Subunit D is shown in *green*, subunit E in

red, subunit F in *light blue*, subunit G in *dark blue* and subunit H in *purple*. GM1 molecules are shown in the same colour as the subunit to which they are bound in the initial structure.

3.4 Conclusions

The results of CID measurements performed on the protonated and deprotonated ions of the (CTB_5 + 5GM1), (CTB_5 + 5GM1-Cer), (S_4 + 4B) and (S_4 + 4Btl) complexes reveal that multiple dissociation pathways are accessible to gaseous multisubunit protein-ligand complexes upon collisional activation. The relative contribution of the three dissociation pathways: (1) loss of the ligand-unbound protein subunit, (2) loss of subunit-ligand complex and (3) loss of ligand (neutral or charged), appears to reflect the strength of intermolecular protein-ligand interactions in gas phase. It is proposed that a high energetic barrier to ligand loss promotes ligand migration to other subunits, as well as the ejection of the ligand-subunit complex, upon collisional activation. The presence of ceramide or PE groups, which can participate in nonspecific interactions with subunits, enhances the loss of ligand-free and ligand-bound subunit. The results of MD simulations performed on the $(CTB_5 + 5GM1)^{15+}$ ion with different charge configurations reveal that ligands, when neutral, are highly mobile and readily migrate within and between subunits. Moreover, the mechanism of ligand migration appears to be highly dependent on charge configuration. In agreement with experiment, the loss of deprotonated ligand readily occurred in MD simulations performed on the $(CTB_5 + 5GM1)^{14-}$ ion. Taken together, the results

of this study suggest that collisional activation of multisubunit protein-ligand complexes in the gas phase is likely to induce significant changes to the nature of the protein-ligand interactions. Consequently, caution must be exercised when using MS and CID (or similar activation methods) to establish the location(s) of ligands bound to multiprotein complexes.

3.5 Literature cited

1. Rual, J.-F.; Venkatesan, K.; Hao, T.; Hirozane-Kishikawa, T.; Dricot, A.; Li, N.; Berriz, G. F.; Gibbons, F. D.; Dreze, M.; Ayivi-Guedehoussou, N.; Klitgord, N.; Simon, C.; Boxem, M.; Milstein, S.; Rosenberg, J.; Goldberg, D. S.; Zhang, L. V.; Wong, S. L.; Franklin, G.; Li, S.; Albala, J. S.; Lim, J.; Fraughton, C.; Llamosas, E.; Cevik, S.; Bex, C.; Lamesch, P.; Sikorski, R. S.; Vandenhaute, J.; Zoghbi, H. Y.; Smolyar, A.; Bosak, S.; Sequerra, R.; Doucette-Stamm, L.; Cusick, M. E.; Hill, D. E.; Roth, F. P.; Vidal, M. *Nature* **2005,** *437* (7062), 1173-1178.

2. Gavin, A.-C.; Aloy, P.; Grandi, P.; Krause, R.; Boesche, M.; Marzioch, M.; Rau, C.; Jensen, L. J.; Bastuck, S.; Dumpelfeld, B.; Edelmann, A.; Heurtier, M.-A.; Hoffman, V.; Hoefert, C.; Klein, K.; Hudak, M.; Michon, A.-M.; Schelder, M.; Schirle, M.; Remor, M.; Rudi, T.; Hooper, S.; Bauer, A.; Bouwmeester, T.; Casari, G.; Drewes, G.; Neubauer, G.; Rick, J. M.; Kuster, B.; Bork, P.; Russell, R. B.; Superti-Furga, G. *Nature* **2006,** *440* (7084), 631-636.

3. Robinson, C. V.; Sali, A.; Baumeister, W. *Nature* **2007,** *450* (7172), 973-982.

4. Ilari, A.; Savino, C. *Methods Mol. Biol.* **2008**, 452, 63-87.

5. Nietlispach, D.; Mott, H. R.; Stott, K. M.; Nielsen, P. R.; Thiru, A.; Laue, E. D. *Methods Mol. Biol.* **2004,** *278*, 255-288.

6. Jonic, S.; Vénien-Bryan, C. *Curr. Opin. Pharm.* **2009,** *9* (5), 636-642.

7. Mertens, H. D. T.; Svergun, D. I. *J. Struct. Biol.* **2010,** *172* (1), 128-141.

8. Greenfield, N. J. *Nat. Prot.* **2007,** *1* (6), 2876-2890.

9. Kelley, L. A.; Sternberg, M. J. E. *Nat. Prot.* **2009,** *4* (3), 363-371.

10. Loo, J. A. *Int. J. Mass Spectrom.* **2000,** *200* (1-3), 175-186.

11. Benesch, J. L.; Robinson, C. V. *Curr. Opin. Struct. Biol.* **2006,** *16* (2), 245-251.

12. Barrera, N. P.; Robinson, C. V. *Annu. Rev. Biochem.* **2011**, *80*, 247-271.

13. Uetrecht, C.; Heck, A. J. R. *Angew. Chem. Int. Ed.* **2011,** *50* (36), 8248-8262.

14. van den Heuvel, R. H.; Heck, A. J. R. *Curr. Opin. Chem. Biol.* **2004,** *8* (5), 519-526.

15. Hall, Z.; Politis, A.; Robinson, C. V. *Structure* **2012,** *20* (9), 1596-1609.

16. Taverner, T.; Hernandez, H.; Sharon, M.; Ruotolo, B. T.; Matak-Vinkovic, D.; Devos, D.; Russell, R. B.; Robinson, C. V. *Acc. Chem. Res.* **2008,** *41* (5), 617-627.

17. Benesch, J. L. P.; Ruotolo, B. T.; Simmons, D. A.; Robinson, C. V. *Chem. Rev.* **2007,** *107* (8), 3544-3567.

18. McLafferty, F. W.; Guan, Z. Q.; Haupts, U.; Wood, T. D.; Kelleher, N. L. *J. Am. Chem. Soc.* **1998,** *120* (19), 4732-4740.

19. Dunbar, R. C.; McMahon, T. B. *Science* **1998,** *279* (5348), 194-197.

20. Price, W. D.; Schnier, P. D.; Williams, E. R. *Anal. Chem.* **1996,** *68* (5), 859-866.

21. Dunbar, R. C. *Mass Spectrom. Rev.* **2004,** *23* (2), 127-158.

22. Wanasundara, S. N.; Thachuk, M. *J. Am. Soc. Mass Spectrom.* **2007,** *18* (12), 2242-2253.

23. Benesch, J. L. P.; Aquilina, J. A.; Ruotolo, B. T.; Sobott, F.; Robinson, C. V. *Chem. Biol.* **2006,** *13* (6), 597-605.

24. Jurchen, J. C.; Williams, E. R. *J. Am. Chem. Soc.* **2003,** *125* (9), 2817-2826.

25. Jones, C. M.; Beardsley, R. L.; Galhena, A. S.; Dagan, S.; Cheng, G. L.; Wysocki, V. H. *J. Am. Chem. Soc.* **2006,** *128* (47), 15044-15045.

26. Blackwell, A. E.; Dodds, E. D.; Bandarian, V.; Wysocki, V. H. *Anal. Chem.* **2011,** *83* (8), 2862-2865.

27. Rostom, A. A.; Fucini, P.; Benjamin, D. R.; Juenemann, R.; Nierhaus, K. H.; Hartl, F. U.; Dobson, C. M.; Robinson, C. V. *Proc. Natl. Acad. Sci. U. S. A.* **2000,** *97* (10), 5185-5190.

28. Lorenzen, K.; Vannini, A.; Crarner, P.; Heck, A. J. R. *Structure* **2007,** *15* (10), 1237-1245.

29. Sharon, M.; Taverner, T.; Ambroggio, X. I.; Deshaies, R. J.; Robinson, C. V. *PLoS. Biol.* **2006,** *4* (8), 1314-1323.

30. Damoc, E.; Fraser, C. S.; Zhou, M.; Videler, H.; Mayeur, G. L.; Hershey, J. W. B.; Doudna, J. A.; Robinson, C. V.; Leary, J. A. *Mol. Cell. Proteomics* **2007,** *6* (7), 1135-1146.

31. McCammon, M. G.; Hernandez, H.; Sobott, F.; Robinson, C. V. *J. Am. Chem. Soc.* **2004,** *126* (19), 5950-5951.

32. Beardsley, R. L.; Jones, C. M.; Galhena, A. S.; Wysocki, V. H. *Anal. Chem.* **2009,** *81* (4), 1347-1356.

33. Versluis, C.; Heck, A. J. R. *Int. J. Mass Spectrom.* **2001,** *210* (1-3), 637-649.

34. Felitsyn, N.; Kitova, E. N.; Klassen, J. S. *Anal. Chem.* **2001,** *73* (19), 4647-4661.

35. Hyung, S. J.; Robinson, C. V.; Ruotolo, B. T. *Chem. Biol.* **2009,** *16* (4), 382-390.

36. Turnbull, W. B.; Precious, B. L.; Homans, S. W. *J. Am. Chem. Soc.* **2004,** *126* (4), 1047-1054.

37. Lauer, S.; Goldstein, B.; Nolan, R. L.; Nolan, J. P. *Biochemistry* **2002,** *41* (6), 1742-1751.

38. Schafer, D. E.; Thakur, A. K. *Cell Biophys.* **1982,** *4* (1), 25-40.

39. Merritt, E. A.; Sarfaty, S.; Vandenakker, F.; Lhoir, C.; Martial, J. A.; Hol, W. G. J. *Prot. Sci.* **1994,** *3* (2), 166-175.

40. Chilkoti, A.; Stayton, P. S. *J. Am. Chem. Soc.* **1995,** *117* (43), 10622-10628.

41. Freitag, S.; LeTrong, I.; Klumb, L.; Stayton, P. S.; Stenkamp, R. E. *Prot. Sci.* **1997,** *6* (6), 1157-1166.

42. Chilkoti, A.; Tan, P. H.; Stayton, P. S. *Proc. Natl. Acad. Sci. U. S. A.* **1995,** *92* (5), 1754-1758.

43. Ritchie, T. K.; Grinkova, Y. V.; Bayburt, T. H.; Denisov, I. G.; Zolnerciks, J. K.; Atkins, W. M.; Sligar, S. G. *Methods Enzymol*. **2009**, *464*, 211-231.

44. Bayburt, T. H.; Grinkova, Y. V.; Sligar, S. G. *Nano Lett.* **2002,** *2* (8), 853-856.

45. Zhang, Y. X.; Liu, L.; Daneshfar, R.; Kitova, E. N.; Li, C. S.; Jia, F.; Cairo, C. W.; Klassen, J. S. *Anal. Chem.* **2012,** *84* (18), 7618-7621.

46. Case, D. A.; Darden, T. A.; Cheatham III, T. E.; Simmerling, C. L.; Wang, J.; Duke, R. E.; Luo, R.; Walker, R. C., Zhang, W.; Merz, K. M.; Roberts, B.; Wang, B.; Hayik, S.; Roitberg, A.; Seabra, G.; Kolossváry, I.; Wong, K. F.; Paesani, F.; Vanicek, J.; Liu, J.; Wu, X.; Brozell, S. R.; Steinbrecher, T.; Gohlke, H.; Cai, Q.; Ye, X.; Wang, J.; Hsieh, M.-J.; Cui, G.; Roe, D. R.; Mathews, D. H.; Seetin, M. G.; Sagui, C.; Babin, V.; Luchko, T.; Gusarov, S.; Kovalenko, A.; A., K. P. University of California, San Francisco, **2010**.

47. Deng, L.; Broom, A.; Kitova, E. N.; Richards, M. R.; Zheng, R. B.; Shoemaker, G. K.; Meiering, E. M.; Klassen, J. S. *J. Am. Chem. Soc.* **2012,** *134* (40), 16586-16596.

48. Vanquelef, E.; Simon, S.; Marquant, G.; Garcia, E.; Klimerak, G.; Delepine, J. C.; Cieplak, P.; Dupradeau, F. Y. *Nucleic Acids Res.* **2011,** *39*, W511-W517.

49. Dupradeau, F. Y.; Pigache, A.; Zaffran, T.; Savineau, C.; Lelong, R.; Grivel, N.; Lelong, D.; Rosanski, W.; Cieplak, P. *Phys. Chem. Chem. Phys.* **2010,** *12* (28), 7821-7839.

50. Frisch, M. J.; Trucks, G. W.; Schlegel, H. B.; Scuseria, G. E.; Robb, M. A.; Cheeseman, J. R.; Scalmani, G.; Barone, V.; Mennucci, B.; Petersson, G. A.; Nakatsuji, H.; Caricato, M.; Li, X.; Hratchian, H. P.; Izmaylov, A. F.; Bloino, J.; Zheng, G.; Sonnenberg, J. L.; Hada, M.; Ehara, M.; Toyota, K.; Fukuda, R.; Hasegawa, J.; Ishida, M.; Nakajima, T.; Honda, Y.; Kitao, O.; Nakai, H.; Vreven, T.; Montgomery, J. A.; Peralta, J. E.; Ogliaro, F.; Bearpark, M.; Heyd, J. J.; Brothers, E.; Kudin, K. N.; Staroverov, V. N.; Kobayashi, R.; Normand, J.; Raghavachari, K.; Rendell, A.; Burant, J. C.; Iyengar, S. S.; Tomasi, J.; Cossi, M.; Rega, N.; Millam, J. M.; Klene, M.; Knox, J. E.; Cross, J. B.; Bakken, V.; Adamo, C.; Jaramillo, J.; Gomperts, R.; Stratmann, R. E.; Yazyev, O.; Austin, A. J.; Cammi, R.; Pomelli, C.; Ochterski, J. W.; Martin, R. L.; Morokuma, K.; Zakrzewski, V. G.; Voth, G. A.; Salvador, P.; Dannenberg, J. J.; Dapprich, S.; Daniels, A. D.; Farkas, O.; Foresman, J. B.; Ortiz, J. V.; Cioslowski, J.; Fox, D. J. Gaussian, Inc. Wallingford, CT, **2009**.

51. Merritt, E. A.; Kuhn, P.; Sarfaty, S.; Erbe, J. L.; Holmes, R. K.; Ho, W. G. J. *J. Mol. Biol.* **1998,** *282* (5), 1043-1059.

52. O'Boyle, N. M.; Banck, M.; James, C. A.; Morley, C.; Vandermeersch, T.; Hutchison, G. R. *J. Cheminf.* **2011,** *3*, 33.

53. The Open Babel Package, version 2.3.1 http://openbabel.org.

54. Hall, Z.; Politis, A.; Bush, M. F.; Smith, L. J.; Robinson, C. V. *J. Am. Chem. Soc.* **2012,** *134* (7), 3429-3438.

55. Wang, J. M.; Wang, W.; Kollman, P. A.; Case, D. A. *J. Mol. Graph.* **2006,** *25* (2), 247-260.

56. Duan, Y.; Wu, C.; Chowdhury, S.; Lee, M. C.; Xiong, G. M.; Zhang, W.; Yang, R.; Cieplak, P.; Luo, R.; Lee, T.; Caldwell, J.; Wang, J. M.; Kollman, P. *J. Comput. Chem.* **2003,** *24* (16), 1999-2012.

57. Wang, J. M.; Wolf, R. M.; Caldwell, J. W.; Kollman, P. A.; Case, D. A. *J. Comput. Chem.* **2004,** *25* (9), 1157-1174.

58. Phillips, J. C.; Braun, R.; Wang, W.; Gumbart, J.; Tajkhorshid, E.; Villa, E.; Chipot, C.; Skeel, R. D.; Kale, L.; Schulten, K. *J. Comput. Chem.* **2005,** *26* (16), 1781-1802.

59. Sun, J. X.; Kitova, E. N.; Wang, W. J.; Klassen, J. S. *Anal. Chem.* **2006,** *78* (9), 3010-3018.

60. Wang, W. J.; Kitova, E. N.; Klassen, J. S. *Anal. Chem.* **2005,** *77* (10), 3060-3071.

61. Holmgren, J.; Lonnroth, I.; Mansson, J. E.; Svennerholm, L. *Proc. Natl. Acad. Sci.* **1975,** *72* (7), 2520-2524.

62. Kitova, E. N.; Bundle, D. R.; Klassen, J. S. *J. Am. Chem. Soc.* **2002,** *124* (20), 5902-5913.

63. Kitova, E. N.; Seo, M.; Roy, P. N.; Klassen, J. S. *J. Am. Chem. Soc.* **2008,** *130* (4), 1214-1226.

64. Liu, L.; Bagal, D.; Kitova, E. N.; Schnier, P. D.; Klassen, J. S. *J. Am. Chem. Soc.* **2009,** *131* (44), 15980-+.

65. Kitova, E. N.; Bundle, D. R.; Klassen, J. S. *Angew. Chem.-Int. Edit.* **2004,** *43* (32), 4183-4186.

66. Kitova, E. N.; Bundle, D. R.; Klassen, J. S. *J. Am. Chem. Soc.* **2002,** *124* (32), 9340-9341.

67. Liu, L.; Michelsen, K.; Kitova, E. N.; Schnier, P. D.; Klassen, J. S. *J. Am. Chem. Soc.* **2012,** *134* (6), 3054-3060.

68. Lightwahl, K. J.; Schwartz, B. L.; Smith, R. D. *J. Am. Chem. Soc.* **1994,** *116* (12), 5271-5278.

69. Jurchen, J. C.; Garcia, D. E.; Williams, E. R. *J. Am. Soc. Mass Spectrom.* **2004,** *15* (10), 1408-1415.

70. Pagel, K.; Hyung, S. J.; Ruotolo, B. T.; Robinson, C. V. *Anal. Chem.* **2010,** *82* (12), 5363-5372.

71. Liu, L.; Michelsen, K.; Kitova, E. N.; Schnier, P. D.; Klassen, J. S. *J. Am. Chem. Soc.* **2010,** *132* (50), 17658-17660.

72. Salpin, J. Y.; Tortajada, J. *Journal of Mass Spectrometry* **2004,** *39* (8), 930-941.

73. Sinelnikov, I.; Kitova, E. N.; Klassen, J. S. *J. Am. Soc. Mass Spectrom.* **2007,** *18* (4), 617-631.

Chapter 4

Conclusions and Future Work

This work describes the development and application of ESI-MS methods to study the interactions between water soluble proteins or protein complexes and insoluble GSL, and to investigate the changes of the nature of multisubunit protein-ligand complexes upon collisional activation in gas phase.

In Chapter 2, a novel assay, based on the CaR-ESI-MS assay and NDs, was developed to reveal the specific interactions between proteins or protein complexes and their cellular GSL receptors. The specificity and sensitivity of the assay was demonstrated for interactions involving CTB_5 and Stx2, and their native GSL receptors, the ganglioside GM1-Cer and the globotriaosylceramide Gb3-Cer, respectively. The success of this assay represents an important addition to the arsenal of tools available for identifying and characterizing protein-GSL receptor interactions. And the simultaneous detection of several isoforms of the receptor implies the utilization of this assay for detection of multiple receptors, and potentially, evaluation of relative affinities of different GSL. Proof-of-concept experiments will be performed on solutions of CTB_5 and ND containing mixtures of GSL which include the specific ganglioside receptors GM1-Cer, GM2-Cer and GM3-Cer.[1, 2] The relative abundances of released GSL may provide a simple readout of the relative affinities for different receptors present in the ND. The CaR-ESI-MS assay was also applied to detect the binding between CTB_5 and GM1-Cer within a mixture of lipids extracted from cell membranes. Under this

circumstance, ND served as a "surrogate cell". A clear application of this technique is the discovery of the native GSL receptors within the complex milieu of the plasma membrane and to characterize the biologically relevant protein-GSL interactions.

In Chapter 3, CID-MS was used to induce the dissociation of multiply charged ions of intact protein-ligand complexes in order to investigate their dissociation pathways. The results showed that the dissociation pathways of multisubunit protein-ligand complexes in the gas phase depend, not only on the native topology of the complex, but also on structural changes that occur upon collisional activation. However, besides CID, many other activation techniques are used to cause the dissociation of gaseous ions in MS. It would therefore be of interest to study the dissociation pathways of protein-ligand complexes using other activation techniques. For instance, blackbody infrared radiative dissociation (BIRD)[3, 4] is a dissociation technique which allows ions to undergo unimolecular dissociation at essentially zero pressure by the exchange of energy with an ambient blackbody radiation field. Unlike the neutral gas required for CID, ions are activated by the absorption of blackbody infrared photons emitted from the walls of the ion cell which is essentially a collision-free environment. The effects of different charge states, temperatures and the structure of ligand on the dissociation pathways can be assessed. Comparison between CID and BIRD results may provide insights about the influence of energy distribution of complex on the dissociation pathways. Moreover, using the BIRD dissociation technique, it is possible to probe unimolecular dissociation kinetics as a function of

temperature, which allows the construction of Arrhenius plots and the determination of activation energies (E_a) and pre-exponaional factors (A).[5]

Literature Cited:

1. Lauer, S.; Goldstein, B.; Nolan, R. L.; Nolan, J. P. *Biochemistry* **2002,** *41* (6), 1742-1751.

2. Turnbull, W. B.; Precious, B. L.; Homans, S. W. *J. Am. Chem. Soc.* **2004,** *126* (4), 1047-1054.

3. Kitova, E. N.; Seo, M.; Roy, P. N.; Klassen, J. S. *J. Am. Chem. Soc.* **2008,** *130* (4), 1214-1226.

4. Wang, W. J.; Kitova, E. N.; Sun, J. X.; Klassen, J. S. *J. Am. Soc. Mass Spectrom.* **2005,** *16* (10), 1583-1594.

5. Kitova, E. N.; Bundle, D. R.; Klassen, J. S. *J. Am. Chem. Soc.* **2002,** *124* (20), 5902-5913.